

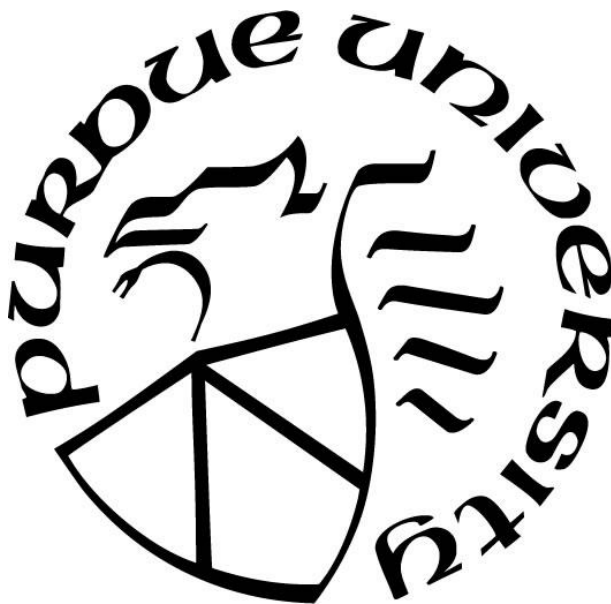
**STUDY FOR THE MECHANISM OF PROTEIN SEPARATION IN
REVERSED-PHASE LIQUID CHROMATOGRAPHY**

by
Yun Yang

A Dissertation

*Submitted to the Faculty of Purdue University
In Partial Fulfillment of the Requirements for the degree of*

Doctor of Philosophy



Department of Chemistry
West Lafayette, Indiana
August 2020

THE PURDUE UNIVERSITY GRADUATE SCHOOL
STATEMENT OF COMMITTEE APPROVAL

Dr. Mary J. Wirth, Chair

Department of Chemistry

Dr. Peter T. Kissinger

Department of Chemistry

Dr. Chittaranjan Das

Department of Chemistry

Dr. Scott McLuckey

Department of Chemistry

Approved by:

Dr. Christine A. Hrycyna

To my family and friends

ACKNOWLEDGMENTS

First, I would like to express my sincerest gratitude to my research advisor, Prof. Mary J Wirth, for her support and guidance throughout my graduate study. She has taught me how to come up with novel scientific ideas, how to design experiments rationally, and how to deliver the results efficiently, which turned me into an independent thinker. She has also kept me motivated by being a role model as a female scientist. I could not have imagined having a better advisor and mentor for my Ph.D. study.

Besides my advisor, I would like to thank my thesis committee members, Prof. Peter Kissinger, Prof. Chitta Das and Prof. Scott McLuckey for their support and encouragement for my graduate research.

I would like to give my acknowledgment to Dr. Zhaorui Zhang and Dr. Pamela Thompson from AbbVie for initiating the collaboration project and hosting me as an intern to provide me with exposure to the pharmaceutical industry.

I am also blessed to work with the members of Wirth's group. I am thankful to Dr. Yiyang Zhou and Dr. Tse-Hong Chen for their introduction to the scientific background and instruction on using the instruments at the beginning of my Ph.D. study. I have also enjoyed working with Cameron Schwartz, Dr. Edwin Alzate, Tyrel Wagner, Dr. Charlie Bupp, John Biechele-Speziale, Dr. Rachel Jacobson, and Dr. Jonathan Yasosky and am grateful for their help and all the fun we had in the last four years.

Finally, I would like to thank my mom and dad and all the other family members for their continued support and love.

TABLE OF CONTENTS

LIST OF TABLES	7
LIST OF FIGURES	8
LIST OF ABBREVIATIONS.....	12
ABSTRACT.....	14
CHAPTER 1. INTRODUCTION	15
1.1 Overview of biopharmaceutical drugs.....	15
1.2 Application for LC-MS on biopharmaceutical characterization	15
1.3 Research objectives and thesis overview	17
1.4 Reference.....	17
CHAPTER 2. POLYMER-SHELL ON SILICA TO IMPROVE RPLC RESOLUTION AND MS COMPATIBILITY FOR INTACT IGG1 CHARACTERIZATION.....	21
2.1 Introduction	21
2.2 Materials and methods.....	23
2.2.1 Materials.....	23
2.2.2 Silica particle and UHPLC column preparation.....	23
2.2.3 UHPLC-MS.....	25
2.3 Results and discussions	26
2.3.1 Silica particle characterization	26
2.3.2 Mobile phase condition optimization	27
2.3.3 Polymer thickness optimization and column comparison.....	29
2.4 Conclusion.....	31
2.5 Ongoing work.....	31
2.6 Reference.....	31
CHAPTER 3. NATIVE REVERSED-PHASE LIQUID CHROMATOGRAPHY: A TECHNIQUE FOR LCMS OF INTACT ANTIBODY-DRUG CONJUGATES	47
3.1 Introduction	47
3.2 Materials and methods.....	49
3.2.1 Materials.....	49
3.2.2 UHPLC column preparation.....	50

3.2.3	UHPLC.....	51
3.2.4	LC-MS.....	51
3.3	Results and discussions	53
3.3.1	ADC structure and DAR characterization.....	53
3.3.2	nRPLC bonded phase optimization.....	54
3.3.3	Mass spectrometry data.....	55
3.4	Conclusion.....	58
3.5	Future work	58
3.6	Reference.....	59
CHAPTER 4. MEASUREMENT AND SIMULATION OF TAILING ZONES OF PROTEIN IN REVERSED-PHASE LIQUID CHROMATOGRAPHY.....		77
4.1	Introduction	77
4.2	Materials and methods.....	78
4.2.1	Materials.....	78
4.2.2	Chromatographic conditions	79
4.2.3	Simulation	80
4.3	Results and discussions	80
4.3.1	Phase ratio measurement.....	81
4.3.2	Van Deemter plot	82
4.3.3	Optimization of the simulation parameters	82
4.4	Conclusion.....	87
4.5	Future work	87
4.6	Reference.....	88
CHAPTER 5. CONCLUSIONS AND FUTURE DIRECTIONS		108
5.1	Conclusions	108
5.2	Future directions.....	109
VITA.....		110
PUBLICATIONS.....		111

LIST OF TABLES

Table 3.1. Summary of HPLC columns and their applications	64
Table 4.1. Summary of the partition coefficient and the retention factor measured with the SPP C4 and FPP C4 columns	92
Table 4.2. Summary of the best-fit parameters for the simulation of the FPP C4 and SPP C4 columns	93
Table 4.3. Summary of best-fit parameters under different acidic modifier conditions	94
Table 4.4. Summary of the best-fit parameters under different organic solvent compositions	95
Table 4.5. Summary of HPLC columns and their applications	96

LIST OF FIGURES

- Figure 2.1. a) TEM image shows a 30 nm polymer layer coated on the silica surface. b) A plot of the polymer thickness as a function of polymer growth time. 36
- Figure 2.2. Structure for three major forms of the disulfide bond and free thiol variants of the IgG1. 37
- Figure 2.3. Chromatograms of IgG1 separation with different formic acid concentration in the mobile phase. Column: PMMA 60 min column; Gradient: 19-28% ACN in 30 min; Injection amount: 2 μg IgG1; Column temperature: 50 $^{\circ}\text{C}$; Flow rate: 100 $\mu\text{L}/\text{min}$ 38
- Figure 2.4. Chromatograms of IgG1 separation with different FA and TFA combination in the mobile phase at constant pH. Column: PMMA 60 min column; Gradient: 19-28% ACN in 30 min for the first three chromatograms, 19-34% ACN in 50 min for the last chromatogram; Injection amount: 2 μg IgG1; Column temperature: 50 $^{\circ}\text{C}$; Flow rate: 100 $\mu\text{L}/\text{min}$; pH = 2.46. 39
- Figure 2.5. Chromatograms of IgG1 separation with different column temperatures. Chromatograms are shifted to align the first peak. The dashed lines indicate the baseline and the distance between the major peaks. Column: PMMA 60 min column; Gradient: 19-28% ACN in 30 min; Injection amount: 2 μg IgG1; Column temperature shown in the figure; Flow rate: 100 $\mu\text{L}/\text{min}$ 40
- Figure 2.6. a) A plot of the normalized percentage recovery as a function of the column temperature b) Plot of the peak distance between the first two major peaks as a function of the column temperature. 41
- Figure 2.7. RPLC chromatogram for varying PMMA growth time, showing that the 60 min growth time is optimal with respect to resolution. Polymer growth time is labeled in each panel. The gradient for columns of 20, 40, 60, and 80 min PMMA growth time was 20-29% ACN with 0.5% FA in 30 min. 42
- Figure 2.8. Comparison for the RPLC chromatogram of IgG1 using PMMA, PBzMA and Diphenyl column with 0.5% FA in the mobile phase. Gradient: 15% change in 50 min; Flow rate: 100 $\mu\text{L}/\text{min}$. Column temperature optimized for each of the columns: 50 $^{\circ}\text{C}$ for PMMA and PBzMA column, 75 $^{\circ}\text{C}$ for the Diphenyl column. 43
- Figure 2.9. a) Overlaid graph of the pressure traces on the PMMA, PBzMA column and the viscosity data. The viscosity value is normalized to the pressure at 0% ACN. b) A plot of polymer thickness change as a function of the ACN percentage in the mobile phase for PMMA and PBzMA. 44
- Figure 2.10. Illustration of how swelling behavior could change the polymer structure and block the protein from interacting with the surface silanols. 45
- Figure 2.11. Chromatograms for NIST mAb separation using regular PMMA column and high-density PMMA column. Gradient: 25-34% ACN in 30 min with 0.1% TFA in the mobile phase; Injection amount: 0.75 μg NIST mAb; Column temperature: 80 $^{\circ}\text{C}$; Flow rate: 100 $\mu\text{L}/\text{min}$ 46

Figure 3.1. Chemical structures of linker-drug combination for a) the AbbVie model ADC, Ab095-PZ and b) brentuximab vedotin. Each drug or drug mimic part is in the red square, and its hydrophobicity is expressed by log P, where P represents the octanol/water partition coefficient. 65

Figure 3.2. a) Sketches explain abbreviations for peak assignments. b) RPLC of the model ADC after reduction with DTT. c) RPLC of the model ADC without DTT. d) HIC of the intact ADC with tentative peak assignments..... 66

Figure 3.3. Raw mass spectra (right) and deconvoluted mass spectra (left) for each peak in the chromatograms of Figure 3.2b..... 67

Figure 3.4. nRPLC of AbbVie model ADC with varying hydrophobicity of bonded phase, as denoted by the structures. Gradient conditions are A: 50 mM NH₄OAc, pH 7, B: 50 mM NH₄OAc, 50% IPA, pH 7, 0-100 %B /40 min, 100 %B /5 min, 100 μL/min, 30 °C. The same tentative labels as for the HIC chromatogram of Figure 3.2d are made due to the similarity. 68

Figure 3.5. a) nRPLC of the AbbVie model ADC Ab095-PZ, with peaks labeled based on the mass spectra. Gradient: 0 to 4.5% IPA/water over 3 min., then 4.5 to 50% IPA/water over 20 min. Detection at 280 nm. b) Raw mass spectra for peaks as labeled, with the molecular weight based on deconvoluted mass spectra for peak ID. The blue lines show that extra peaks are from the overlap..... 69

Figure 3.6. Evidence that light chain dissociates in MS source for AbbVie model ADC. a) Full-range raw mass spectra show large signals for light chain+drug, but no significant signals for ADC minus light chain+drug. b) Chromatogram with UV detection (top) and EIC based on light chain+drug (bottom). The blue arrows point to two peaks that changed intensities, and the inset depicts the structures for the isomers consistent with these intensity changes. 70

Figure 3.7. HIC separation of a) model ADC and b) commercial ADC Brentuximab vedotin. The dashed lines illustrate the greater hydrophobicity of the mAb itself for Brentuximab vedotin. Tosoh TSKgel Butyl-NPR, 4.6x35mm, 2.5 μm. MPA: 1.5M ammonium sulfate, 25 mM sodium phosphate pH 7.0; MPB: 25 mM sodium phosphate pH 7.0 with 25% IPA; Flow rate: 0.8 mL/min; Column temp: 25 °C 71

Figure 3.8. nRPLC and mass spectra for commercial ADC: brentuximab vedotin. a) nRPLC with detection at 280 nm. Conditions are the same as for Figure 2.6. b) Raw mass spectra for D2, D4(1,2,3), D6, D8, with the molecular weight based on deconvoluted mass spectra. 72

Figure 3.9. a) LCMS data for brentuximab vedotin, analogous to Figure 5. a) Full-range raw mass spectra show even stronger signals for light chain+drug than observed for the AbbVie model ADC. b) Chromatogram for UV detection (top) approximately tracks that of EIC for the signal of light chain+drug, again indicating light chain+drug dissociated after separation. Again, the blue arrows show two peaks that changed intensities, and the inset depicts the structures for the D4 isomers that are consistent with these changes. 73

Figure 3.10. Illustration of the surface charge density in RPLC and HIC..... 74

Figure 3.11. nRPLC chromatogram for varying PMMA growth time using the same non-denaturing conditions as in, showing that the 70 min growth time is optimal with respect to resolution and recovery. Polymer growth time is labeled in each panel. 75

Figure 3.12. nRPLC chromatograms of the AbbVie model ADC using PMMA and crosslinked PMMA column. Gradient conditions are A: 25 mM NH₄OAc, pH 7, B: 25 mM NH₄OAc, 50% IPA, pH 7, 0-100 %B /40 min, 100 %B /5 min, 100 μ L/min, 30 $^{\circ}$ C..... 76

Figure 4.1. Chromatograms of RNases A at five different concentration, 0.025, 0.05, 0.1, 0.25, 0.5 mg/mL. Column: Fully porous C4 column; Mobile phase: 24.8% ACN with 0.1% TFA; Flow rate: 0.1 mL/min; Column temperature: 30 $^{\circ}$ C..... 97

Figure 4.2. Chromatograms of RNases A at the concentration of 0.025 mg/mL. Column: Fully porous C4 column; Mobile phase: 24.8% ACN with 0.1% TFA; Flow rate: 0.1 mL/min; Column temperature: 30 $^{\circ}$ C. 98

Figure 4.3. Chromatograms of RNases A at five different concentration, 0.025, 0.05, 0.1, 0.25, 0.5 mg/mL. Column: Superficially porous C4 column; Mobile phase: 24.8% ACN with 0.1% TFA; Flow rate: 0.1 mL/min; Column temperature: 30 $^{\circ}$ C. 99

Figure 4.4. Van Deemter plot for RNase A on the SPP C4 column (top) and FPP C4 column (bottom). Mobile phase condition: 24.8% ACN with 0.1% TFA; Flow rate as shown in the plot; Column temperature: 30 $^{\circ}$ C..... 100

Figure 4.5. Overlaid graph of the simulated chromatograms (blue trace) with the experimental data (black trace) of the lowest concentration to show the effect of desorption rate on the peak retention. Column: Fully porous C4 column; Mobile phase: 24.8% ACN with 0.1% TFA; Flow rate: 0.1 mL/min; Column temperature: 30 $^{\circ}$ C..... 101

Figure 4.6. Overlaid graph of the simulated chromatograms with the experimental data of the overloading study to show the sets of the solutions for the best-fit parameters. The corresponding *Kstrong* value are labeled on the graph. The set of best-fit parameters are summarized in Table 4.2. Column: Fully porous C4 column; Mobile phase: 24.8% ACN with 0.1% TFA; Flow rate: 0.1 mL/min; Column temperature: 30 $^{\circ}$ C..... 102

Figure 4.7. Overlaid graph of the simulated chromatograms with the experimental data of the overloading study to show the effect of the acidic modifier on the peak retention. Column: Fully porous C4 column; Mobile phase as labeled in the figure; Flow rate: 0.1 mL/min; Column temperature: 30 $^{\circ}$ C. 103

Figure 4.8. Overlaid graph of the simulated chromatograms with the experimental data of the overloading study to show the effect of the organic solvent composition on the peak retention. Column: Fully porous C4 column; Mobile phase as labeled in the figure; Flow rate: 0.1 mL/min; Column temperature: 30 $^{\circ}$ C..... 104

Figure 4.9. A plot of the equilibrium constant of the strong sites and weak sites as a function of the organic solvent composition in the mobile phase. Fitted linear equations are labeled on the figure. 105

Figure 4.10. Overlaid graph of the simulated chromatograms with the experimental data for SPP C4 column (left) and FPP C4 column (right). Mobile phase condition: 24.8% ACN with 0.1% TFA; Flow rate: 0.1 mL/min; Column temperature: 30 $^{\circ}$ C. 106

Figure 4.11. RPLC chromatogram for varying PMMA thickness, showing that the retention and peak tailing depends on the polymer thickness. Polymer thickness is labeled in each panel. Gradient: 20-29% ACN with 0.5% FA in 30 min. 107

LIST OF ABBREVIATIONS

ACN	Acetonitrile
ADC	Antibody-drug conjugate
AGET	Activators Generated by Electron Transfer
ATRP	Atom Transfer Radical Polymerization
DAR	Drug-to-antibody ratio
DFA	Difluoroacetic acid
DTT	Dithiothreitol
EIC	Extracted ion chromatogram
FA	Formic acid
FWHM	Full width at half maximum
HDC	Hydrodynamic chromatography
HIC	Hydrophobic interaction liquid chromatography
IgG	Immunoglobulin G
IPA	Isopropanol
mAb	Monoclonal antibody
mBC	(Chloromethyl)phenyl)dimethylchlorosilane
mC1	Trimethylchlorosilane
mC4	n-Butyldimethylchlorosilane
NH ₄ OAc	Ammonium acetate
nRPLC	Native reversed-phase liquid chromatography
Me ₆ TREN	Tris 2-(dimethylamino) ethyl amine
MS	Mass Spectrometry
PBS	Phosphate-buffered saline
PEMA	Polyethylmethacrylate
PMMA	Polymethylmethacrylate
PPMA	Polypropylmethacrylate
PBMA	Polybutylmethacrylate
PBzMA	Polybenzylmethacrylate

RPLC	Reversed-phase liquid chromatography
TEM	Transmission electron microscope
TIC	Total ion chromatogram
TFA	Trifluoroacetic acid
UHPLC	Ultra-high performance liquid chromatography

ABSTRACT

Liquid chromatography coupling with mass spectrometry (LC/MS) plays an important role in pharmaceutical characterization because of its ability to separate, identify, and quantify individual compounds from the mixture. Polymer brush layer bonded to the silica surface is designed as a novel stationary phase to improve the LC resolution and MS compatibility. The polymer thickness can be controlled to shield the analyte from interacting with the active silanol on the surface and reduce peak tailing. The functional group of the polymer can be changed to tune the selectivity in different separation modes.

Two projects on LC/MS method development for biomolecule characterization using polymer-shell column are discussed in this work. In the first project, a polymer-shell column is used for disulfide bonds and free thiol subspecies identification, which is a major type of structural heterogeneities in IgG1. Compared with commercial columns, the polymer-shell column is able to resolve the free thiol variants without the presence of trifluoroacetic acid and greatly improve the MS signal. In the second project, a polymer-shell column is used for characterizing the drug-loading profile for antibody-drug-conjugates (ADC) via online LC/MS. The separation employs a mobile phase of 50 mM ammonium acetate to keep the ADC intact, and a gradient of water/isopropanol for ADC elution. MS data show that all ADC species remained intact and native on the column. Positional isomers can be separated and identified with the new method as well. Furthermore, to understand the surface chemistry and protein separation behavior quantitatively, a chromatographic simulation study is performed. The result shows that protein separation in RPLC can be described by a bi-Langmuir adsorption isotherm with mixed-mode retention of strong and weak sites. Smaller fractions and lower equilibrium constant of the strong site, which is the active silanol, give less tailing for protein separation.

CHAPTER 1. INTRODUCTION

1.1 Overview of biopharmaceutical drugs

Since the introduction of biopharmaceutical drugs in the 1980s, it has revolutionized the treatment for a broad range of diseases¹. The biopharmaceutical industry has become one of the most active fastest growing industries for the global market^{2, 3}. Biopharmaceuticals are defined as large molecules that are inherently biological in nature and extracted or manufactured by biotechnological methods including recombinant proteins, monoclonal antibodies, peptide, nucleic acid-based products^{4, 5}.

Among the different types of biopharmaceutical drugs, monoclonal antibodies (mAb) currently claim over 25% of the biopharmaceutical market and are expected to generate revenue of \$300 billion by 2025^{6, 7}. As of 2019, there are at least 79 therapeutic mAbs have been approved by the United States Food and Drug Administration and are currently on the markets⁸. Therapeutic mAbs have been used for the treatment of a variety of diseases including cancers^{9, 10}, and autoimmune diseases^{11, 12}. For example, Risankizumab is a humanized IgG1 monoclonal antibody that was approved to treat plaque psoriasis by inhabiting a cytokine involved in inflammatory processes¹³. Antibody-drug conjugates (ADCs) are another innovative class of therapeutics that consist of an antibody and small molecule drug that are covalently bonded to the antibody through a chemical linker¹⁴. ADCs demonstrated the ability to harness the specificity of the mAb and target the delivery of the cytotoxic agent to the tumor cell¹⁵, thus the majority of the ADCs currently in clinical trials are for treatment. Lysine amide coupling, cysteine coupling, and non-natural amino acid incorporation by genetic engineering are the commonly used method to install the payload to the antibody. This process typically leads to a mixture of ADCs with a different drug to antibody ratio (DAR) and tethering sites¹⁶. The broad distribution of the DAR could affect the stability and efficacy of the ADCs and needs to be tightly controlled^{17, 18}.

1.2 Application for LC-MS on biopharmaceutical characterization

Compared with traditional small molecule drug, biopharmaceutical drugs could provide excellent target specificity and lower off-target toxicity¹⁹. However, the characterization of

biopharmaceutical drugs is more challenging as well due to its structural complexities. Heterogeneities including post-translational modification, aggregation and degradation could be introduced during the production, purification, formulation and/or delivery process^{20, 21}. Various chromatographic, spectroscopic and electrophoretic methods are developed to characterize the structural heterogeneities of biopharmaceutical drugs. Among those, liquid chromatography coupled with mass spectrometry plays an important role in biopharmaceutical characterization because of its ability to separate, identify and quantify individual compounds from the mixture²². For instance, hydrophilic interaction chromatography (HILIC) combined with fluorescence detection is a standard technique for characterizing the N-glycans originating from biopharmaceuticals²³⁻²⁵. Ion-exchange chromatography (IEX) can separate protein based on the electrostatic interactions, therefore, it is used to characterize the charge variant of the protein^{26, 27}. Size-exclusion chromatography (SEC) a reference technique for quantitative evaluation of the fragmentation and aggregation of the proteins based on the different pore accessibility with different sizes of the analyte²⁸. Reversed-phase liquid chromatography (RPLC) is the valuable tool for separating protein by the difference in hydrophobicity. Moreover, two-dimensional liquid chromatography (2D-LC) has emerged as one of the most active areas for technology advancement²⁹⁻³¹. Peak capacity can be greatly enhanced with 2D-LC. Coupling liquid chromatography with mass spectrometry makes it an even powerful tool to identify the species that can be separated with the liquid chromatography. The development of the electrospray ionization technique allows for the online detection with the mass spectrometry and greatly reduced the time and effect required for offline fraction collection³².

Although LC-MS is one of the most sensitive and selective analytical techniques for biopharmaceutical characterization, the resolution of LC-MS often suffers from matrix effects, especially when ESI is used^{33, 34}. Matrix effects are often caused by the adducts in the mobile phase that could alter the ionization efficiency of the target analyte. For example, the most commonly used acidic modifier in RPLC, trifluoroacetic acid (TFA), causes ion suppression effect in MS because of the ion-pairing effect^{35, 36}. While for hydrophobic interaction chromatography (HIC), a salt gradient is employed to separate the protein based on its surface hydrophobicity³⁷. Sodium, potassium, and ammonium adducts are often encountered when salt is present in the mobile phase³⁸. In order to improve the online LC-MS performance, a better instrumental design³⁹ and better

separation materials are needed^{40, 41}. In this thesis, a strategy of developing better bonded phase materials is introduced to increase both the LC resolution and the MS sensitivity.

Polymer brush layers have been successfully applied as the bonded phase material for HILIC separation⁴². The polymer brushed layer can be grafted onto the silica surface using activators generated by electron transfer for atom transfer radical polymerization (AGET-ARTP). The high-density and thick layer of the polymer brush sterically pushes analyte further away from the isolated silanols and shields the electrostatic interaction. The availability of monomers with different functional groups allows the fine-tuning of the selectivity of the bonded phase for separation in different modes.

1.3 Research objectives and thesis overview

The objective of this research is to develop bonded phase material based on a polymer brush layer to improve the online LC-MS analysis for biopharmaceuticals including protein, monoclonal antibody and antibody-drug conjugates. Furthermore, the retention mechanism of protein in RPLC and the surface chemistry of the bonded phase are studied with chromatographic simulation.

In Chapter 2, a polymer brush layer is introduced as the bonded phase for characterizing the disulfide bonds and free thiols variants for IgG1. In Chapter 3, an online LC-MS method is developed to characterize the drug loading profile for intact ADCs under non-denaturing conditions. In chapter 4, chromatographic simulations are performed on two commercial RPLC columns under different conditions. Physical parameters including equilibrium constants, surface coverages, and desorption rate constants can be calculated from the simulation.

1.4 Reference

1. Kesik-Brodacka, M., Progress in biopharmaceutical development. *Biotechnology and applied biochemistry* **2018**, *65* (3), 306-322.
2. Jagschies, G., Brief Review of the Biopharmaceutical and Vaccine Industry. In *Biopharmaceutical Processing*, Elsevier: 2018; pp 33-58.
3. Farid, S. S., Integrated Continuous Biomanufacturing: Industrialization on the Horizon. *Biotechnology journal* **2019**, *14* (2), 1800722.

4. Rader, R. A., (Re) defining biopharmaceutical. *Nature biotechnology* **2008**, 26 (7), 743-751.
5. Rader, R. A., What is a biopharmaceutical. *Part* **2005**, 1, 60-65.
6. Chung, J., Special issue on therapeutic antibodies and biopharmaceuticals. *Experimental & molecular medicine* **2017**, 49 (3), e304-e304.
7. Lu, R.-M.; Hwang, Y.-C.; Liu, I.-J.; Lee, C.-C.; Tsai, H.-Z.; Li, H.-J.; Wu, H.-C., Development of therapeutic antibodies for the treatment of diseases. *Journal of Biomedical Science* **2020**, 27 (1), 1-30.
8. Kaplon, H.; Muralidharan, M.; Schneider, Z.; Reichert, J. M. In *Antibodies to watch in 2020*, MAbs, Taylor & Francis: 2020; p 1703531.
9. Scott, A. M.; Allison, J. P.; Wolchok, J. D., Monoclonal antibodies in cancer therapy. *Cancer Immunity Archive* **2012**, 12 (1), 14.
10. Stern, M.; Herrmann, R., Overview of monoclonal antibodies in cancer therapy: present and promise. *Critical reviews in oncology/hematology* **2005**, 54 (1), 11-29.
11. Macisaac, J.; Sidiqqi, R.; Jamula, E.; Li, N.; Baker, S.; Webert, K. E.; Heddle, N.; Arnold, D. M., Anti-CD20 monoclonal antibody therapy for immune modulation across a range of autoimmune diseases. *Blood* **2017**, 130 (Supplement 1), 4936-4936.
12. Randall, K. L., Rituximab in autoimmune diseases. *Australian prescriber* **2016**, 39 (4), 131.
13. Papp, K. A.; Blauvelt, A.; Bukhalo, M.; Gooderham, M.; Krueger, J. G.; Lacour, J.-P.; Menter, A.; Philipp, S.; Sofen, H.; Tyring, S., Risankizumab versus ustekinumab for moderate-to-severe plaque psoriasis. *New England Journal of Medicine* **2017**, 376 (16), 1551-1560.
14. de Goeij, B. E.; Lambert, J. M., New developments for antibody-drug conjugate-based therapeutic approaches. *Current opinion in immunology* **2016**, 40, 14-23.
15. Alley, S. C.; Okeley, N. M.; Senter, P. D., Antibody–drug conjugates: targeted drug delivery for cancer. *Current opinion in chemical biology* **2010**, 14 (4), 529-537.
16. Tsuchikama, K.; An, Z., Antibody-drug conjugates: recent advances in conjugation and linker chemistries. *Protein & cell* **2018**, 9 (1), 33-46.
17. Hamblett, K. J.; Senter, P. D.; Chace, D. F.; Sun, M. M.; Lenox, J.; Cerveny, C. G.; Kissler, K. M.; Bernhardt, S. X.; Kopcha, A. K.; Zabinski, R. F., Effects of drug loading on the antitumor activity of a monoclonal antibody drug conjugate. *Clinical cancer research* **2004**, 10 (20), 7063-7070.
18. Behrens, C. R.; Liu, B. In *Methods for site-specific drug conjugation to antibodies*, MAbs, Taylor & Francis: 2014; pp 46-53.

19. Wan, H., An overall comparison of small molecules and large biologics in ADME testing. *ADMET and DMPK* **2016**, 4 (1), 1-22.
20. Jefferis, R., Protein heterogeneity and the immunogenicity of biotherapeutics. *J Biochem Biotech.* 2018; 1 (1): 55-62. 56 *J Biochem Biotech.* 2018 Volume 1 Issue **2018**, 1, 3.
21. Sharma, B., Immunogenicity of therapeutic proteins. Part 3: impact of manufacturing changes. *Biotechnology advances* **2007**, 25 (3), 325-331.
22. Berkowitz, S. A.; Engen, J. R.; Mazzeo, J. R.; Jones, G. B., Analytical tools for characterizing biopharmaceuticals and the implications for biosimilars. *Nature Reviews Drug Discovery* **2012**, 11 (7), 527-540.
23. Melmer, M.; Stangler, T.; Schiefermeier, M.; Brunner, W.; Toll, H.; Ruppachter, A.; Lindner, W.; Premstaller, A., HILIC analysis of fluorescence-labeled N-glycans from recombinant biopharmaceuticals. *Analytical and bioanalytical chemistry* **2010**, 398 (2), 905-914.
24. Ahn, J.; Bones, J.; Yu, Y. Q.; Rudd, P. M.; Gilar, M., Separation of 2-aminobenzamide labeled glycans using hydrophilic interaction chromatography columns packed with 1.7 μm sorbent. *Journal of Chromatography B* **2010**, 878 (3-4), 403-408.
25. Melmer, M.; Stangler, T.; Premstaller, A.; Lindner, W., Comparison of hydrophilic-interaction, reversed-phase and porous graphitic carbon chromatography for glycan analysis. *Journal of chromatography A* **2011**, 1218 (1), 118-123.
26. Fekete, S.; Beck, A.; Veuthey, J.-L.; Guillaume, D., Ion-exchange chromatography for the characterization of biopharmaceuticals. *Journal of pharmaceutical and biomedical analysis* **2015**, 113, 43-55.
27. Amartely, H.; Some, D.; Tsadok, A.; Lebendiker, M., Ion Exchange Chromatography (IEX) Coupled to Multi-angle Light Scattering (MALS) for Protein Separation and Characterization. *JoVE (Journal of Visualized Experiments)* **2019**, (146), e59408.
28. Berkowitz, S. A.; Houde, D. J., Size-exclusion chromatography (SEC) in biopharmaceutical process development. In *Biophysical characterization of proteins in developing biopharmaceuticals*, Elsevier: 2020; pp 153-184.
29. Sandra, K.; Sandra, P., The opportunities of 2D-LC in the analysis of monoclonal antibodies. Future Science: 2015.
30. Stoll, D.; Danforth, J.; Zhang, K.; Beck, A., Characterization of therapeutic antibodies and related products by two-dimensional liquid chromatography coupled with UV absorbance and mass spectrometric detection. *Journal of Chromatography B* **2016**, 1032, 51-60.
31. Delahunty, C.; Yates Iii, J. R., Protein identification using 2d-lc-ms/ms. *Methods* **2005**, 35 (3), 248-255.

32. Angel, T. E.; Aryal, U. K.; Hengel, S. M.; Baker, E. S.; Kelly, R. T.; Robinson, E. W.; Smith, R. D., Mass spectrometry-based proteomics: existing capabilities and future directions. *Chemical Society Reviews* **2012**, *41* (10), 3912-3928.
33. Matuszewski, B.; Constanzer, M.; Chavez-Eng, C., Matrix effect in quantitative LC/MS/MS analyses of biological fluids: a method for determination of finasteride in human plasma at picogram per milliliter concentrations. *Analytical chemistry* **1998**, *70* (5), 882-889.
34. Cappiello, A.; Famigliani, G.; Palma, P.; Trufelli, H., Matrix effects in liquid chromatography-mass spectrometry. *Journal of liquid chromatography & related technologies* **2010**, *33* (9-12), 1067-1081.
35. Annesley, T. M., Ion suppression in mass spectrometry. *Clinical chemistry* **2003**, *49* (7), 1041-1044.
36. Furey, A.; Moriarty, M.; Bane, V.; Kinsella, B.; Lehane, M., Ion suppression; a critical review on causes, evaluation, prevention and applications. *Talanta* **2013**, *115*, 104-122.
37. Fekete, S.; Veuthey, J.-L.; Beck, A.; Guillarme, D., Hydrophobic interaction chromatography for the characterization of monoclonal antibodies and related products. *Journal of pharmaceutical and biomedical analysis* **2016**, *130*, 3-18.
38. Kruve, A.; Kaupmees, K., Adduct formation in ESI/MS by mobile phase additives. *Journal of the American Society for Mass Spectrometry* **2017**, *28* (5), 887-894.
39. Chen, J.; Liu, Z.; Wang, F.; Mao, J.; Zhou, Y.; Liu, J.; Zou, H.; Zhang, Y., Enhancing the performance of LC-MS for intact protein analysis by counteracting the signal suppression effects of trifluoroacetic acid during electrospray. *Chemical Communications* **2015**, *51* (79), 14758-14760.
40. Sanchez, A. C.; Friedlander, G.; Fekete, S.; Anspach, J.; Guillarme, D.; Chitty, M.; Farkas, T., Pushing the performance limits of reversed-phase ultra high performance liquid chromatography with 1.3 μm core-shell particles. *Journal of Chromatography A* **2013**, *1311*, 90-97.
41. Schuster, S. A.; Wagner, B. M.; Boyes, B. E.; Kirkland, J. J., Optimized superficially porous particles for protein separations. *Journal of Chromatography A* **2013**, *1315*, 118-126.
42. Huckabee, A. G.; Yerneni, C.; Jacobson, R. E.; Alzate, E. J.; Chen, T. H.; Wirth, M. J., In-column bonded phase polymerization for improved packing uniformity. *Journal of separation science* **2017**, *40* (10), 2170-2177.

CHAPTER 2. POLYMER-SHELL ON SILICA TO IMPROVE RPLC RESOLUTION AND MS COMPATIBILITY FOR INTACT IGG1 CHARACTERIZATION

2.1 Introduction

Recombinant monoclonal antibody (mAb) continues to be a productive growth area for the pharmaceutical industry¹. The ability to target a cognate antigen and triggering of the antigenic expression by malignant cells led to the development of mAb-based drugs². Comparing with the small molecule drug, mAb-based drugs show higher target specificity and lower toxicity to the biological system^{3, 4}. Currently, there are more than 40 mAb-based drugs in the market that have been approved by the FDA and more than 300 mAb-based drug candidates in the clinical pipelines^{5, 6}. Identification of new targets with improved efficacy makes it possible for the wide application of mAb on the treatment of various diseases including infectious disease, auto-immune disease, metabolic disorder, and cancer therapy⁷. For example, Adalimumab was approved in 2002 as an immunosuppressive medication to treat rheumatoid arthritis. Cetuximab is another mAb-drug used for the treatment of a certain type of breast cancer and lymphomas by blocking HER-1⁸. Among the sub-class of monoclonal antibodies, immunoglobulin G1 (IgG1) is the most prevalent due to its stability, lower aggregate formation and greater affinity to the Fc receptor^{9, 10}.

Structure heterogeneity can be inadvertently introduced to monoclonal antibodies during the production, storage, and transportation process. Unpairing of disulfide linkages is a common post-translational modification (PTM) of IgG1 that has been routinely detected¹¹⁻¹³. Typically, IgG1 consists of a total of 32 cysteine residues with 10 residues on the light chain and 22 residues on the heavy chain. Other than the interchain or intrachain disulfide bonds, scrambling of disulfide bonds and cysteinylations also occur¹⁴. These can affect the biological affinity, activity and stability if the bonding cysteines are unpaired or shuffled^{15, 16}. Various approaches have been developed and reported for the disulfide bond and free thiol variants characterization including fluorescent labeling¹⁷, alkylation^{11, 18}, and Ellman assay¹⁹. The additional sample preparation step is needed for the previous method and it could alter the original protein structure and is time-consuming and labor-intensive. Ion exchange chromatography (IEX)¹², hydrophobic interaction chromatography (HIC)²⁰, and reversed-phase liquid chromatography (RPLC) have been developed to eliminate the

sample preparation step and provide information on intact molecule level, among which RPLC offers the advantage for online coupling with mass spectrometry. Changes in the disulfide bond structure change the hydrophobicity of the protein because of induced changes in the protein folding and conformation, thus these variants can be identified and quantified using reversed-phase chromatographic separation²¹⁻²³. Reverse phase liquid chromatography coupling with mass spectrometry (RPLC-MS) is now the prevailing technique for the direct characterization method for the disulfide bond and free thiol variants^{12, 18, 21}. The Protein Analytical Chemistry group at Genentech recently reported an online RPLC-MS method for IgG1 characterization²¹. Chromatographic method optimization was done using a commercial Zorbax Stablebond Diphenyl UHPLC columns (100 × 2.1 mm with a particle size of 1.7 μm and pore size of 300 Å). Results show that 0.1% trifluoroacetic acid (TFA) gives the best resolution among all the different acidic modifier combinations. Five peaks including three major thiol forms on complementarity determining regions (CDR) and two minor thiol forms on other positions were separated. TFA reduces the surface charge density and ion pair with the positively charged protein to minimize the electrostatic interaction with the stationary phase. Nonetheless, TFA is not MS-friendly because the strong ion pairing effect suppresses the electrospray ionization efficiency^{24, 25}. Formic acid (FA) is considered as an MS-friendly acidic modifier that increases the MS sensitivity^{26, 27}. However, the high pKa and weak ion pairing effect of FA allows more peak tailing with the commercial RPLC column, as shown in the published result. There is a need for developing a label-free RPLC-MS method for characterizing the disulfide bond and free thiol variants of IgG1 that can provide both high LC resolution and MS sensitivity.

In this work, an RPLC-MS method using a polymer-shell bonded phase column to separate the IgG1 disulfide bond and free thiol variants is reported. The polymer shell is coated onto the silica surface using a previously reported AGET-ATRP method developed by our group^{28, 29}. Compared with traditional RPLC columns, a thick polymer layer as the bonded phase can shield the electrostatic interaction between the analyte and the silanols. Baseline separation of the three major species and improved resolution of the minor species are observed with the polymer-shell column using 0.5% FA and MS signal intensity increases 10 times. The mobile phase condition, column temperature, and polymer choice are optimized to evaluate the column performance.

2.2 Materials and methods

2.2.1 Materials

Nonporous silica particles (1.5 μm) were purchased from Superior Silica (Tempe, AZ). Empty stainless-steel columns (2.1 mm I.D., 50 mm length), reservoirs (4.6 mm I.D., 150 mm), and frits (0.5 μm pore diameter) were purchased from Isolation Technologies (Middleboro, MA). Stainless-steel tubing, ferrules, and internal nuts were all purchased from Valco Instruments (Houston, TX). Silanes, i.e., (chloromethyl)phenyldimethylchlorosilane (+99%) and trimethylchlorosilane (+99%), were purchased from Gelest (Morrisville, PA). Methyl methacrylate (MMA, 99%), benzyl methacrylate (BzMA, 98%) sodium ascorbate ($\geq 99\%$), butylamine (99.5%), and ammonium hydroxide were purchased from Sigma–Aldrich (St. Louis, MO). Formic acid (FA, 96%), difluoroacetic acid (DFA, 98%), trifluoroacetic acid (TFA, 99%), and copper(II) chloride (CuCl_2 , 99%) from Acros Organics (Morris Plains, NJ), tris(2-dimethylaminoethyl)amine (Me_6TREN , +99%) from Alfa Aesar (Haverhill, MA), isopropanol (IPA), and acetonitrile (ACN) from Fisher Scientific (Hampton, NH) were used as well. Ultrapure water was obtained from a Milli-Q system (MilliporeSigma, Darmstadt, Germany.)

The IgG1 sample was obtained by courtesy of Genentech, Inc. Before injection onto the column, the original 30 mg/mL IgG1 sample was diluted to 1 mg/mL with PBS 1x buffer (pH 7.2). NISTmAb, a humanized IgG1, was purchased from Sigma Aldrich (St. Louis, MO). The original 10 mg/mL sample was diluted to 1 mg/mL with PBS 1x buffer (pH 7.2) and used for injection.

2.2.2 Silica particle and UHPLC column preparation

The silica particles were modified as described earlier³⁰. Briefly, the 1.5 μm silica particles were calcined at 600 $^\circ\text{C}$ for 12 h, repeated three times, then annealed at 1050 $^\circ\text{C}$ for 3 h. SEM showed that the particles decreased in diameter to 1.2 μm from the calcining and annealing steps. The silica particles were rehydroxylated overnight in 10% HNO_3 after heat treatment, and then rinsed with ultrapure water and dried in a 60 $^\circ\text{C}$ vacuum oven. Freshly rehydroxylated silica particles were suspended in a dry toluene solution containing 2% (v/v) of ((chloromethyl)phenyl)-dimethylchlorosilane and 0.1% (v/v) of butylamine. The solution was refluxed for 3 h and then 2% (v/v) of trimethylchlorosilane was added for end-capping and refluxed for 3 h. The silylated, end-

capped particles were then rinsed with dry toluene and allowed to dry in a 60 °C vacuum oven for 2 h.

For packing a column, 0.26 g of the silylated, end-capped particles were suspended in acetonitrile, then loaded onto an empty column as reservoir (4.6 mm × 150 mm), which was connected in series with the column to be packed (2.1 mm × 50 mm). The column was packed under sonication using a high-pressure pump (Laboratory Alliance of Central New York, LLC, Syracuse, NY). For in-situ modification, methylmethacrylate monomer was dissolved in 40:60 H₂O/IPA (v/v) in a 50 mL centrifuge tube for a final concentration of 2.5 M. Two other solutions were made in 2.0 mL of 40:60 H₂O/IPA: 1) a solution containing 40 mg of CuCl₂ and 80 μL Me₆TREN, and 2) a solution containing 20 mg sodium ascorbate. Afterward, the Cu/Me₆TREN solution was added to the centrifuge tube, followed by the sodium ascorbate solution. The reaction mixture was loaded into a plugged reservoir. The reaction solution from the reservoir was pumped into the column starting at 200 μL/min until five minutes after the reaction mixture dripped from the end of the column. The polymerization reaction was allowed to proceed for a range of reaction times from 0, 20, 40, 60 and 80 min for optimization. After the reaction, the freshly packed column PMMA was rinsed with ACN/water and IPA/water for 20 min at 100 μL/min.

For higher density polymer, an adjustment was made to the method described above. In solution 2 which contains 20 mg sodium ascorbate, 29 μL of the acetic acid is added to the solution to adjust the pH value. Afterward, the polymerization reaction was carried out with the same protocol.

For the ex-situ polymerization reaction, a modified version of a previously reported method was used²⁸. In a 50 mL round bottom flask, 0.5 g of the silylated particles and methylmethacrylate monomer was dissolved in 20 mL 40:60 H₂O/IPA (v/v). Two other solutions containing CuCl₂, Me₆TREN and sodium ascorbate were prepared as described above and added to the suspension. This vessel was left to react for 60 min under stirring. The particles were rinsed with 40:60 H₂O/IPA (v/v) and ACN, then dried in a vacuum desiccator at room temperature.

For another bonded phase, the polymerization of benzyl methacrylate was conducted with 20:80 H₂O/IPA (v/v) in a 50 mL centrifuge tube for a final concentration of 1.0 M and polymer growth time was 90 min or otherwise noted.

2.2.3 UHPLC-MS

The UHPLC-MS instrumentation was described before³¹. The RPLC separation was performed on a Waters Acquity UPLC I-Class (Waters, Milford, MA). Lab-made RPLC columns (2.1 × 50 mm, 1.2 μm nonporous silica particles coated with polymerization time varied PMMA and PBenzylMA) were used as the analytical columns. Mobile phase A (MPA) and B (MPB) were water and acetonitrile, with different percentages of TFA, DFA, and FA as acidic modifiers. The acidic modifiers and gradients used for elution are detailed along with the results. UV absorbance wavelength was set to 280 nm. The optimal flow rate and injection amount were 0.1 mL/min and 2 μg. The optimal column temperature was discussed later in the chapter.

A commercially available AdvancedBio RP-mAb Diphenyl column (2.1 × 50 mm, 3.5 μm, 450 Å, Agilent, Santa, Clara, CA, USA) was used for comparison. Mobile phase A (MPA) and B (MPB) were water and acetonitrile, with different percentages of FA as an acidic modifier. The acidic modifiers and gradients used for elution are detailed along with the results. The optimized flow rate was 100 μl/min and the column temperature was 75 °C. The injection amount of IgG1 was 2 μg. The UV detection was 280 nm.

For online RPLC-MS, Waters Acquity UPLC I-Class was coupled directly to a Thermo LTQ Velos mass spectrometer with an electrospray interface. The electrospray ionization (ESI) spray voltage was set in positive mode at 3.8 kV. Sheath and auxiliary gas pressure was 40 arb and 10 arb, respectively. All spectra were obtained in the m/z range of 1000 – 3800, which included nearly all of the intact IgG1 charge envelope while excluding low m/z noise. The gradients and acidic modifiers used for elution are detailed along with the results.

2.3 Results and discussions

2.3.1 Silica particle characterization

The silica particles were modified using the activator generated by electron transfer atom transfer radical polymerization reaction as described before. The copper (II) concentration, ligand choice, reducing agent choice, solvent composition, and temperature, which affect the polymer growth rate and surface coverage, were first optimized. Then the modified silica particles were characterized using transmission electron microscopy (TEM). Figure 2.1a shows a 30 nm polymer layer grown onto the silica surface. The darker core shows the non-porous silica particle and the grey shell is from the polymer coating. The image was taken from the particle modified with PMMA for 60 min using the ex-situ method. For the in-situ polymerization reaction, the thickness of the polymer layer is estimated from the Kozeny-Carman equation, which relates the measured back-pressure, P , to porosity, ε .

$$\frac{P}{L} = \frac{180 \cdot \eta}{d_p^2} \cdot \frac{(1 - \varepsilon)^2}{\varepsilon^3} \cdot \frac{Q}{\pi r^2}$$

The volume flow rate is Q , the column radius is r , and all other variables have their usual meanings. The injection time and pressure were measured for the same column before and after the polymerization reaction. The porosity could be calculated based on the injection time. d_p can be generated from the equation as all other variables are known. The increase in d_p and decrease in ε after the polymerization reaction is attributed to the polymer growth. The polymer thickness is then calculated from the hydrodynamic radius of the fluid channel with known particle size and measured porosity.

$$r_{hyd} = \frac{d_p}{3} \cdot \frac{\varepsilon}{1 - \varepsilon}$$

The difference of the hydrodynamic radius before and after the reaction is the polymer thickness. Thickness data measured with TEM and the pressure trace shows a good agreement. By controlling the initial monomer concentration in the solution and the polymer growth time, the thickness can be controlled. Figure 2.1b shows a linear trend of the polymer thickness vs the growth time. This is a well-controlled method for growing polymers onto the silica surface.

2.3.2 Mobile phase condition optimization

For developing the mobile phase condition, a PMMA column of 60 min polymer growth time is used. The discussion for the stationary phase choice and optimization for the polymer thickness will be detailed in section 3.3

Figure 2.2 shows the structure of three major forms of the disulfide bond variants of the Genentech IgG1. The molecular weight difference between each species is 2 Da out of a total molecular weight of 150 kDa. To distinguish the subtle structure change in the different species, separation with baseline resolution, and a clear mass spectrum are required. A previous study has been done on 0.1% TFA gives the best separation resolution. The reason that TFA is commonly used as the acidic modifier that can reduce the surface charge density and shield the electrostatic interaction between the analyte and the negatively charged surface silanol. Gouy-Chapman theory of the electrical double layer provides a good understanding of the electrostatic interaction.

$$\phi = \phi_0 e^{-\frac{x}{\lambda}}$$

ϕ is the potential at any distance, x , away from the charged surface and ϕ_0 is the surface potential. λ is the Debye length. Based on Gouy-Chapman theory, the interaction does not only depend on the surface charge density, which is related to ϕ_0 , but also depends on the distance between the positive charge and negative charge. The proposed strategy for using a polymer brush layer is the stationary phase increases the distance and could eliminate the need for TFA in the mobile phase.

FA is considered as an MS friendly acidic modifier to replace TFA, however, the drawback for using FA is that it has a higher pKa and low ion pairing effect. First, the effect of pH on the separation was investigated, which is related to the charge density on the surface and has a great impact on the performance of column efficiency^{32, 33}. Figure 2.3 shows the chromatogram of IgG1 separation with FA concentration varying from 0.1% to 0.75% using the optimized PMMA column. The pH for the corresponding mobile phase decreases from 2.37 to 2.81 with increasing FA concentration. Peak tailing and broadening are observed for pH higher than 2.46 due to the strong electrostatic interactions between IgG1 and silica surface. When pH is below 2.46, the peak width and selectivity don't change significantly. This shows that 0.5% FA is sufficient to provide a shielding effect of the electrostatic interaction. Compared with the result published previously using the Agilent Diphenyl column³¹, the PMMA column still resolves the three major disulfide

variants with the information loss on the minor species under 0.1% FA condition. It supports the idea that the polymer-shell bonded phase is capable of shielding charge interactions better and keeping the protein away from directly interacting with the silica surface.

Other than the mobile phase pH, the ion-pairing effect by acidic modifier is another vital factor affecting RPLC separation as well, hence it needs to be studied. Figure 2.4 shows the chromatogram of IgG1 separation with a varying combination of FA and TFA as the acidic modifier in the mobile phase. The pH of the mobile phase was kept constant at 2.46 while the concentration of the FA and TFA was changing as listed in the figure. The running gradient was the same for figure 2.4a-d, 19-28% ACN. However, for 0.031% TFA, a different gradient with a higher ACN percentage is needed as the ion-pairing effect of TFA makes the protein more hydrophobic. Blue double-headed arrows and yellow rectangular boxes are labeled on chromatograms for peak selectivity measurement. The distances between the three major peaks measured from the double-headed arrows were the same for all the chromatogram shown in Figure 2.4, which suggests that TFA have a negligible impact on the selectivity at constant pH. Noteworthy, the first minor peak moves closer to the first major peak with more TFA present in the mobile phase as illustrated by the brown rectangular boxes. This result reveals TFA possibly masks the intrinsic hydrophobicity differences between peaks by because of the ion-pairing effect. The TIC chromatogram is shown in the right column of Figure 2.4. The MS signal intensity decreased by 90% when FA is replaced by TFA in the mobile phase, which demonstrates the strong ion suppression effect of TFA. In this study, the RPLC resolution maintains the same at the constant pH, regardless of the presence of the TFA.

Temperature plays a critical role for the protein separation, affecting the resolution and recovery³⁴. Studies have shown that higher temperature assist mass transfer between the mobile phase and the stationary phase, which is a major contribution to the protein peak broadening^{35, 36}. Here the column temperature is varied from 30 °C to 70 °C, with other conditions being the same as detailed in Figure 2.5. Two vertical dashed lines indicate the distance between the two largest peaks in 30 °C chromatogram and horizontal dashed line on each chromatogram points out the baseline shift before and after IgG1 elution. The baseline shift after the separation is not observed with the PMMA column even at 30 °C. The higher recovery indicated by the flat baseline can be attributed

to the thicker stationary phase. Figure 2.6a shows the protein recovery vs the column temperature. The recovery is calculated by integrating all the peaks and normalized by the highest integral value, 50 °C. The figure shows that peak recovery increase with temperature and levels-off after 50 °C. The distance between the major peaks, which represents the selectivity of the column, is shown in Figure 2.6b. Obviously, the distance is narrower, decreasing from 2.92 min (30 °C) to 2.00 min (70 °C). This suggests that the higher temperature decreases the relative hydrophobicity difference between the disulfide bond variants. Taking both the protein recovery and peak selectivity into consideration, 50 °C is chosen as the optimal column temperature which can provide maximum recovery and acceptable selectivity.

2.3.3 Polymer thickness optimization and column comparison

As discussed in section 3.1, ATRP is a well-controlled method for coating polymer layer onto the silica surface. The RPLC chromatogram of IgG1 separation with varying PMMA growth time is presented in Figure 2.7. The resolution increases when the polymer growth time increases from 0 min to 60 min. No virtual elution of the IgG1 is observed on the silica surface with no polymer coating. IgG1 is trapped on column since strong interaction between analyte and silanols. As the polymer layer becomes thicker, the peak width, peak shape, selectivity, and recovery increases accordingly. This shows a good agreement with the theory discussed before, which is using a thick polymer layer to shield the electrostatic interaction between the stationary phase and the negatively charged surface. However, further increasing the polymer growth time to 80 min causes peak broadening and reduced resolution. This could partially be attributed to the increased polydispersity with longer polymer chains. In addition, the free long polymer chain could cause tangling among analyte and polymers. For the PMMA column, 60 min is the optimized reaction time. For the PBzMA column, a similar study on the polymer thickness was done in which the reaction time is optimized to be 150 min. Agilent AdvancedBio RP-mAb Diphenyl column (2.1 × 50 mm, 3.5 μm, 450 Å) has been selected as the commercial column for comparison because of the unique π - π interaction provided by the diphenyl group have shown great resolution for mAb characterization³⁷. The monoclonal antibody is a relatively large protein, which has around 11 nm in diameter. By running the same condition (6% ACN/ 3 min, 0.6 mL/min at 75 °C), 450 Å pore size exhibits better chromatographic resolution than 300 Å pore size used in Liu's article.²¹ The temperature is optimized for the new Diphenyl column as well. Figure 2.8 shows the comparison

for the PMMA, PBzMA, and Diphenyl columns under the MS compatible condition, which is 0.5% FA in the mobile phase instead of TFA. The PMMA column provides the best peak resolution among the three columns. Compared with the best-reported results for separation of five different disulfide variants²¹, three additional peaks can be identified with the PMMA column.

One thing to notice with the PMMA column is that the pressure trace is different from other columns during the water/ACN gradient. Typically, viscosity change in the mobile phase causes the pressure change. Pressure traces were obtained by running a gradient of 0-70% ACN over 84 min was run using the PMMA 60 min column and PBzMA 150 min column for comparison. The overlaid graph of the pressure trace vs. viscosity of the water/ACN mixture is shown in Figure 2.9a. The viscosity values are normalized to the pressure at 0% ACN. The trend of the pressure on the PBzMA column matches the viscosity change, while the pressure on the PMMA column is increasing with a higher percentage of the ACN in the mobile phase. Our interpretation is that the PMMA polymer is swelling with an increasing percentage of the ACN. Previous studies have shown swelling is observed for PMMA polymer brush with different solvent compositions^{38, 39}. As the polymer layer becomes thicker, the pressure will increase based on the Kozeny-Carman equation. The swelling behavior of the polymer can be studied quantitatively by calculating the polymer thickness change with the ACN percentage, as shown in Figure 2.9b. Similar to the calculation of the polymer thickness, the pressure and injection time were recorded for the column at different mobile phase conditions. The change in the thickness is the difference between the hydrodynamic radius at 20% ACN, 40% ACN, 60% ACN with the hydrodynamic radius measured at 0% ACN. The thickness of PMMA increases by 40 nm when the ACN percentage increases from 0% to 60%. This doubles the initial thickness measured under dry conditions. While in the PBzMA column, the thickness only increases by 10 nm. Our hypothesis on how swelling could help the separation is to block the protein from penetrating the polymer layer. Observation has shown that there could be areas with low surface coverage, which is resulted from the initiator loss during the ATRP reaction condition. Protein could penetrate through the gap and interact with the surface charge. When the surface is wetted, the swelling behavior would close up the gaps and minimize the unwanted interactions as presented in Figure 2.10.

2.4 Conclusion

Polymer-shell on silica can shield the electrostatic interaction from the charged surface silanols to limit the need for TFA. Compared with commercial columns, the in-house polymer-shell bonded phase performs exceptionally well with online RPLC-MS analysis for IgG1 free thiols using 0.5% FA with good LC resolution and MS sensitivity. Polymer swelling improves the LC resolution in an MS friendly condition by blocking the protein from penetrating the bonded phase.

2.5 Ongoing work

Recently, a method for growing high-density polymer onto the silica surface is developed as described in the method section. Previously, the ATRP reaction mixture is conducted at pH 8 to prevent catalyst protonation at low pH and formation of hydroxy complexes at high pH⁴⁰. The introduction of acetic acid to the reaction mixture lowers the pH of the reaction mixture to prevent the loss of the initiator. This could potentially increase the polymer density on the silica surface. For the preliminary study on the high-density polymer, NIST mAb is used as a model protein for simplicity. Figure 2.11 shows the comparison for the RPLC chromatogram using the regular PMMA 60 min column and the high-density PMMA 60 min column. FWHM of the major peak is narrower with the high-density polymer column. This is a promising start for the project. In the meantime, a change in the polymer growth rate is observed for the high-density polymer, therefore, the growth time can be further optimized. The actual carbon load on the silica surface can be measured using the total carbon analysis to confirm a denser layer of polymer is grown onto the surface⁴¹. The high-density polymer shell bonded phase can be then applied to the characterization of the disulfide bond and free thiol variants of IgG1.

2.6 Reference

1. Beck, A.; Wurch, T.; Bailly, C.; Corvaia, N., Strategies and challenges for the next generation of therapeutic antibodies. *Nature reviews immunology* **2010**, *10* (5), 345.
2. Teo, E. C.-y.; Chew, Y.; Phipps, C., A review of monoclonal antibody therapies in lymphoma. *Critical reviews in oncology/hematology* **2016**, *97*, 72-84.
3. Morrow, T.; Felcone, L. H., Defining the difference: What makes biologics unique. *BIOTECHNOLOGY HEALTHCARE* **2004**, *1*, 24-26, 28-29.

4. Imai, K.; Takaoka, A., Comparing antibody and small-molecule therapies for cancer. *Nature Reviews Cancer* **2006**, *6* (9), 714-727.
5. Shen, B., A review of monoclonal antibody therapy for cancer and prospects. *Chinese Journal of Pharmacology and Toxicology* **2016**, (1), 1-6.
6. Ecker, D. M.; Jones, S. D.; Levine, H. L., The therapeutic monoclonal antibody market. *MAbs* **2015**, *7* (1), 9-14.
7. Mahmuda, A.; Bande, F.; Al-Zihiry, K. J. K.; Abdulhaleem, N.; Majid, R. A.; Hamat, R. A.; Abdullah, W. O.; Unyah, Z., Monoclonal antibodies: A review of therapeutic applications and future prospects. *Tropical Journal of Pharmaceutical Research* **2017**, *16* (3), 713-722.
8. Lambert, J. M.; Chari, R. V., Ado-trastuzumab Emtansine (T-DM1): an antibody–drug conjugate (ADC) for HER2-positive breast cancer. ACS Publications: 2014.
9. Salfeld, J. G., Isotype selection in antibody engineering. *Nature biotechnology* **2007**, *25* (12), 1369-1372.
10. Correia, I. In *Stability of IgG isotypes in serum*, MAbs, Taylor & Francis: 2010; pp 221-232.
11. Xiang, T.; Chumsae, C.; Liu, H., Localization and Quantitation of Free Sulfhydryl in Recombinant Monoclonal Antibodies by Differential Labeling with ¹²C and ¹³C Iodoacetic Acid and LC-MS Analysis. *Analytical Chemistry* **2009**, *81*, 8101-8108.
12. Zhang, T.; Zhang, J.; Hewitt, D.; Tran, B.; Gao, X.; Qiu, Z. J.; Tejada, M.; Gazzano-Santoro, H.; Kao, Y.-H., Identification and characterization of buried unpaired cysteines in a recombinant monoclonal IgG1 antibody. *Analytical chemistry* **2012**, *84* (16), 7112-7123.
13. Harris, R., Heterogeneity of Recombinant Antibodies: linking Structure to Function. **2005**.
14. Liu, H.; May, K. In *Disulfide bond structures of IgG molecules: structural variations, chemical modifications and possible impacts to stability and biological function*, MAbs, Taylor & Francis: 2012; pp 17-23.
15. Hagihara, Y.; Mine, S.; Uegaki, K., Stabilization of an immunoglobulin fold domain by an engineered disulfide bond at the buried hydrophobic region. *Journal of Biological Chemistry* **2007**, *282* (50), 36489-36495.
16. Mcauley, A.; Jacob, J.; Kolvenbach, C. G.; Westland, K.; Lee, H. J.; Brych, S. R.; Rehder, D.; Kleemann, G. R.; Brems, D. N.; Matsumura, M., Contributions of a disulfide bond to the structure, stability, and dimerization of human IgG1 antibody CH3 domain. *Protein Science* **2008**, *17* (1), 95-106.
17. Wu, C.-W.; Yarbrough, L. R.; Wu, F. Y., N-(1-pyrene) maleimide: a fluorescent crosslinking reagent. *Biochemistry* **1976**, *15* (13), 2863-2868.

18. Cheng, Y.; Chen, M. T.; Patterson, L. C.; Yu, X. C.; Zhang, Y. T.; Burgess, B. L.; Chen, Y., Domain-specific free thiol variant characterization of an IgG1 by reversed-phase high-performance liquid chromatography mass spectrometry. *Analytical biochemistry* **2017**, *519*, 8-14.
19. Riener, C. K.; Kada, G.; Gruber, H. J., Quick measurement of protein sulfhydryls with Ellman's reagent and with 4, 4'-dithiodipyridine. *Analytical and bioanalytical chemistry* **2002**, *373* (4-5), 266-276.
20. Chaderjian, W. B.; Chin, E. T.; Harris, R. J.; Etcheverry, T. M., Effect of copper sulfate on performance of a serum-free CHO cell culture process and the level of free thiol in the recombinant antibody expressed. *Biotechnology progress* **2005**, *21* (2), 550-553.
21. Liu, H.; Jeong, J.; Kao, Y.-H.; Zhang, Y. T., Characterization of free thiol variants of an IgG1 by reversed phase ultra high pressure liquid chromatography coupled with mass spectrometry. *Journal of pharmaceutical and biomedical analysis* **2015**, *109*, 142-149.
22. Dillon, T. M.; Ricci, M. S.; Vezina, C.; Flynn, G. C.; Liu, Y. D.; Rehder, D. S.; Plant, M.; Henkle, B.; Li, Y.; Deechongkit, S., Structural and functional characterization of disulfide isoforms of the human IgG2 subclass. *Journal of Biological Chemistry* **2008**, *283* (23), 16206-16215.
23. Wypych, J.; Li, M.; Guo, A.; Zhang, Z.; Martinez, T.; Allen, M. J.; Fodor, S.; Kelner, D. N.; Flynn, G. C.; Liu, Y. D., Human IgG2 antibodies display disulfide-mediated structural isoforms. *Journal of Biological Chemistry* **2008**, *283* (23), 16194-16205.
24. Annesley, T. M., Ion suppression in mass spectrometry. *Clinical chemistry* **2003**, *49* (7), 1041-1044.
25. Chen, J.; Liu, Z.; Wang, F.; Mao, J.; Zhou, Y.; Liu, J.; Zou, H.; Zhang, Y., Enhancing the performance of LC-MS for intact protein analysis by counteracting the signal suppression effects of trifluoroacetic acid during electrospray. *Chemical Communications* **2015**, *51* (79), 14758-14760.
26. Chakraborty, A. B.; Berger, S. J., Optimization of reversed-phase peptide liquid chromatography ultraviolet mass spectrometry analyses using an automated blending methodology. *Journal of biomolecular techniques: JBT* **2005**, *16* (4), 327.
27. Peri-Okonny, U. L., Effects of Eluent pH and Different Types of Acidic Modifiers on the Retention and Electrospray Ionization Efficiency of Basic Analytes in LC-ESI-MS. **2001**.
28. Huckabee, A. G.; Yerneni, C.; Jacobson, R. E.; Alzate, E. J.; Chen, T. H.; Wirth, M. J., In-column bonded phase polymerization for improved packing uniformity. *Journal of separation science* **2017**, *40* (10), 2170-2177.

29. Zhang, Z.; Wu, Z.; Wirth, M. J., Polyacrylamide brush layer for hydrophilic interaction liquid chromatography of intact glycoproteins. *Journal of Chromatography A* **2013**, *1301*, 156-161.
30. Chen, T. H.; Yang, Y.; Zhang, Z.; Fu, C.; Zhang, Q.; Williams, J. D.; Wirth, M. J., Native Reversed-Phase Liquid Chromatography: A Technique for LCMS of Intact Antibody-Drug Conjugates. *Anal Chem* **2019**, *91* (4), 2805-2812.
31. Chen, T.-H. Polymer-Shell Bonded Phase for Improving Online LC-MS Analysis of Intact Proteins, mAbs, and ADCs. Purdue University Graduate School, 2019.
32. Heinisch, S.; D'Attoma, A.; Grivel, C., Effect of pH additive and column temperature on kinetic performance of two different sub-2 μ m stationary phases for ultrafast separation of charged analytes. *J Chromatogr A* **2012**, *1228*, 135-47.
33. McCalley, D. V., Effect of buffer on peak shape of peptides in reversed-phase high performance liquid chromatography. *Journal of Chromatography A* **2004**, *1038* (1-2), 77-84.
34. Blackler, A. R.; Speers, A. E.; Wu, C. C., Chromatographic benefits of elevated temperature for the proteomic analysis of membrane proteins. *Proteomics* **2008**, *8* (19), 3956-3964.
35. Chen, L. C., High-Temperature Liquid Chromatography and the Hyphenation with Mass Spectrometry Using High-Pressure Electrospray Ionization. *Mass Spectrometry* **2019**, *8* (2), S0079-S0079.
36. McNeff, C. V.; Yan, B.; Stoll, D. R.; Henry, R. A., Practice and theory of high temperature liquid chromatography. *Journal of separation science* **2007**, *30* (11), 1672-1685.
37. Ren, D.; Pipes, G. D.; Hambly, D. M.; Bondarenko, P. V.; Treuheit, M. J.; Brems, D. N.; Gadgil, H. S., Reversed-phase liquid chromatography of immunoglobulin G molecules and their fragments with the diphenyl column. *Journal of Chromatography A* **2007**, *1175* (1), 63-68.
38. Orski, S. V.; Sheridan, R. J.; Chan, E. P.; Beers, K. L., Utilizing vapor swelling of surface-initiated polymer brushes to develop quantitative measurements of brush thermodynamics and grafting density. *Polymer* **2015**, *72*, 471-478.
39. Papanu, J.; Hess, D.; Soane, D.; Bell, A., Swelling of poly (methyl methacrylate) thin films in low molecular weight alcohols. *Journal of applied polymer science* **1990**, *39* (4), 803-823.
40. Mincheva, R.; Paneva, D.; Mespouille, L.; Manolova, N.; Rashkov, I.; Dubois, P., Optimized water-based ATRP of an anionic monomer: Comprehension and properties characterization. *Journal of Polymer Science Part A: Polymer Chemistry* **2009**, *47* (4), 1108-1119.

41. Young, C. S.; Weigand, R. J., An efficient approach to column selection in HPLC method development. *LC GC NORTH AMERICA* **2002**, 20 (5), 464-473.

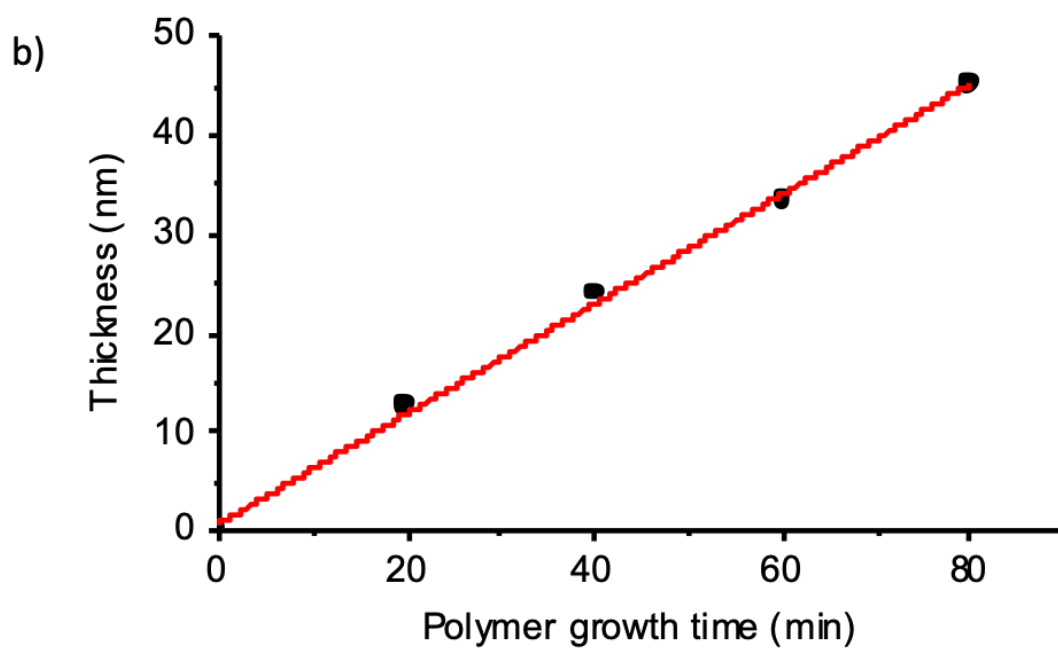
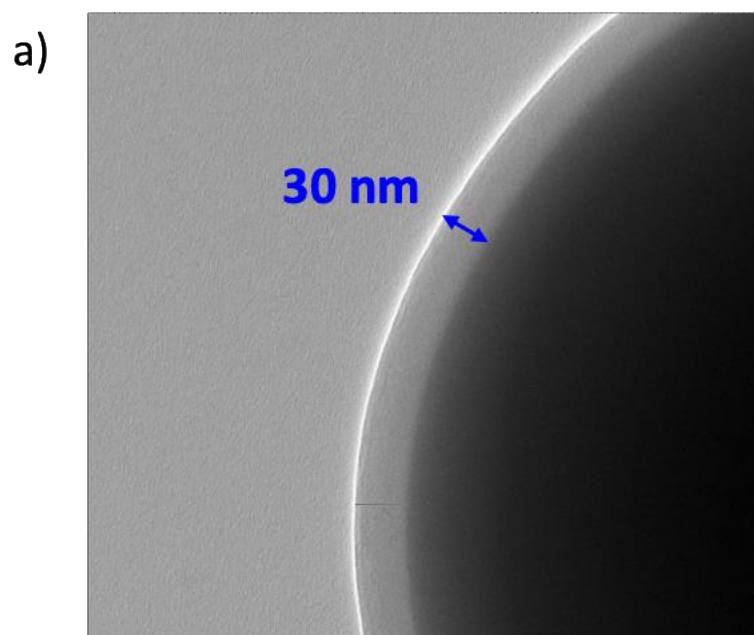


Figure 2.1. a) TEM image shows a 30 nm polymer layer coated on the silica surface. b) A plot of the polymer thickness as a function of polymer growth time.

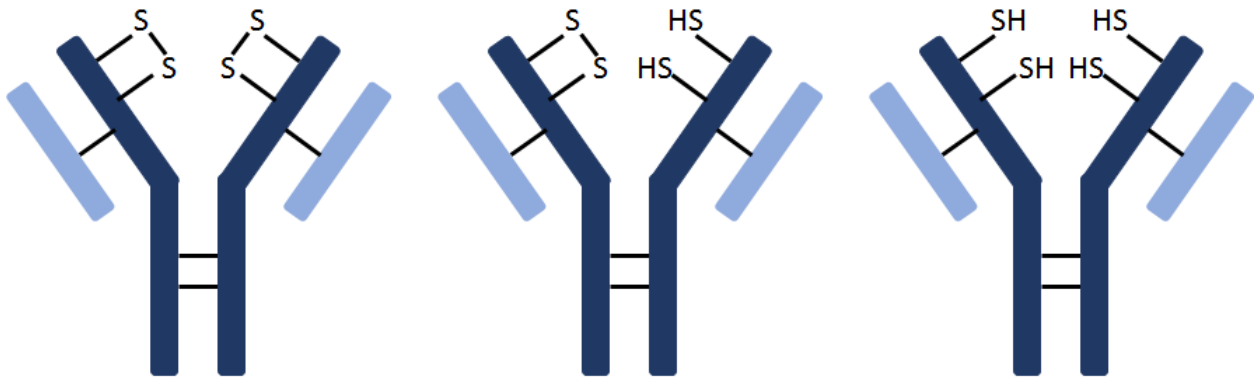


Figure 2.2. Structure for three major forms of the disulfide bond and free thiol variants of the IgG1.

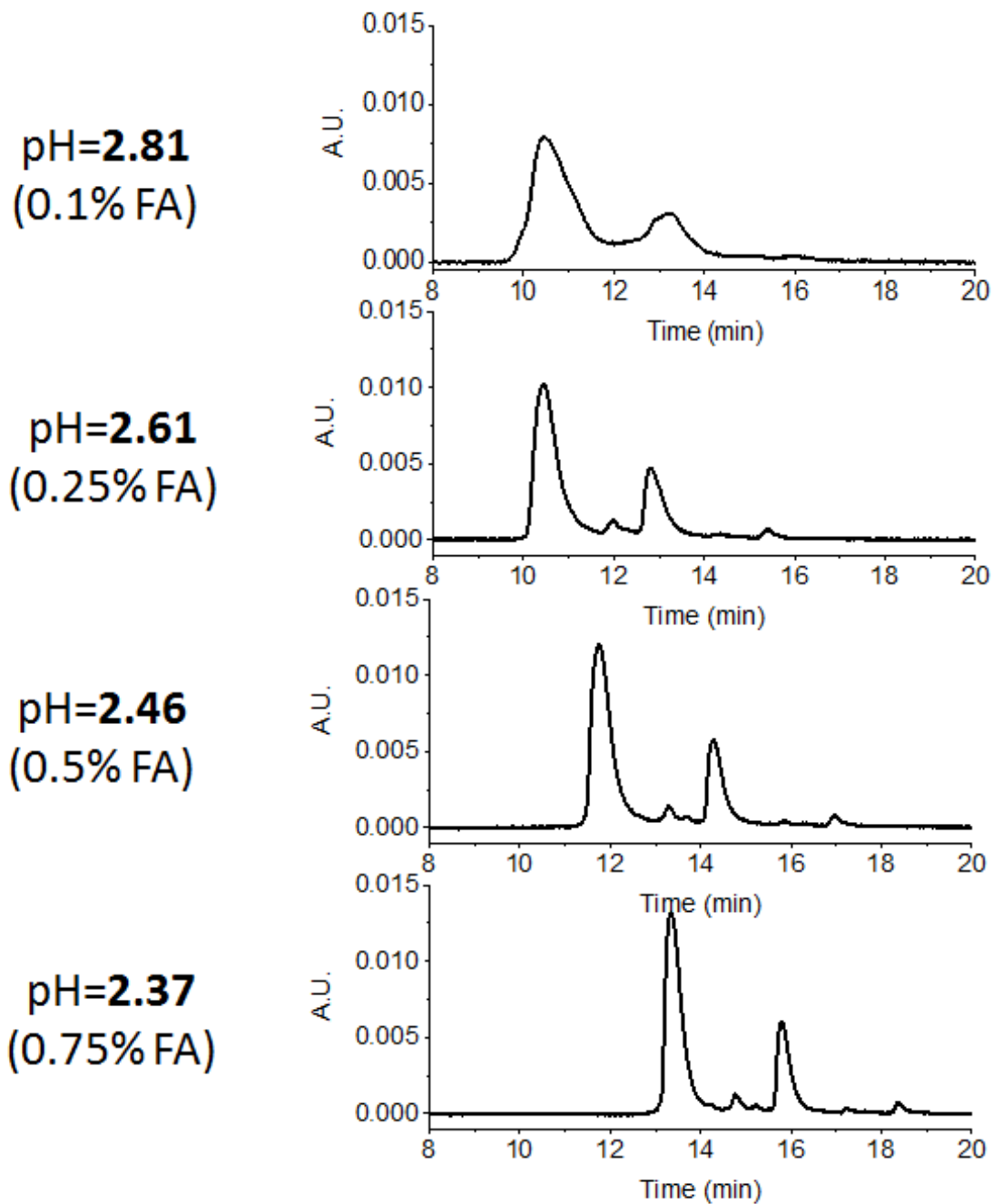


Figure 2.3. Chromatograms of IgG1 separation with different formic acid concentration in the mobile phase. Column: PMMA 60 min column; Gradient: 19-28% ACN in 30 min; Injection amount: 2 μg IgG1; Column temperature: 50 $^{\circ}\text{C}$; Flow rate: 100 $\mu\text{L}/\text{min}$.

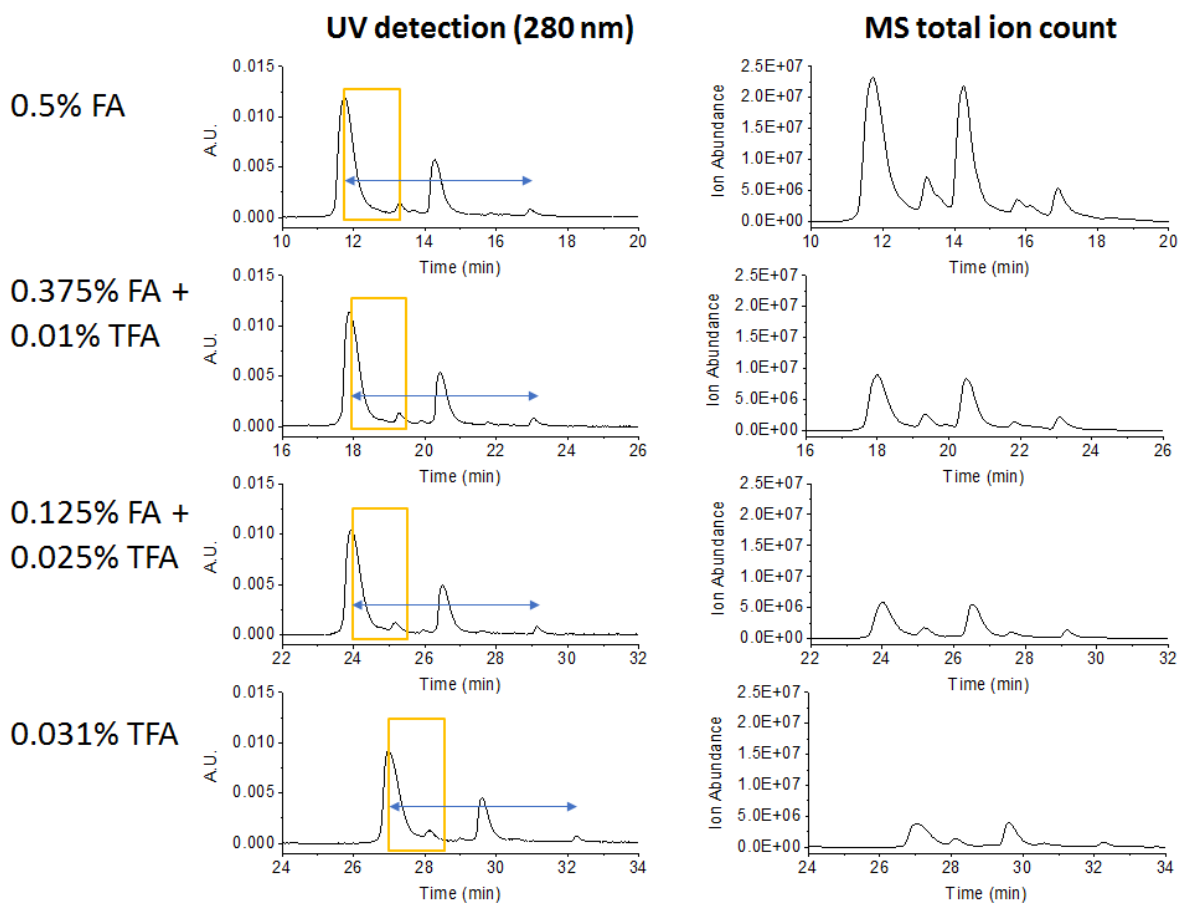


Figure 2.4. Chromatograms of IgG1 separation with different FA and TFA combination in the mobile phase at constant pH. Column: PMMA 60 min column; Gradient: 19-28% ACN in 30 min for the first three chromatograms, 19-34% ACN in 50 min for the last chromatogram; Injection amount: 2 μ g IgG1; Column temperature: 50 $^{\circ}$ C; Flow rate: 100 μ L/min; pH = 2.46.

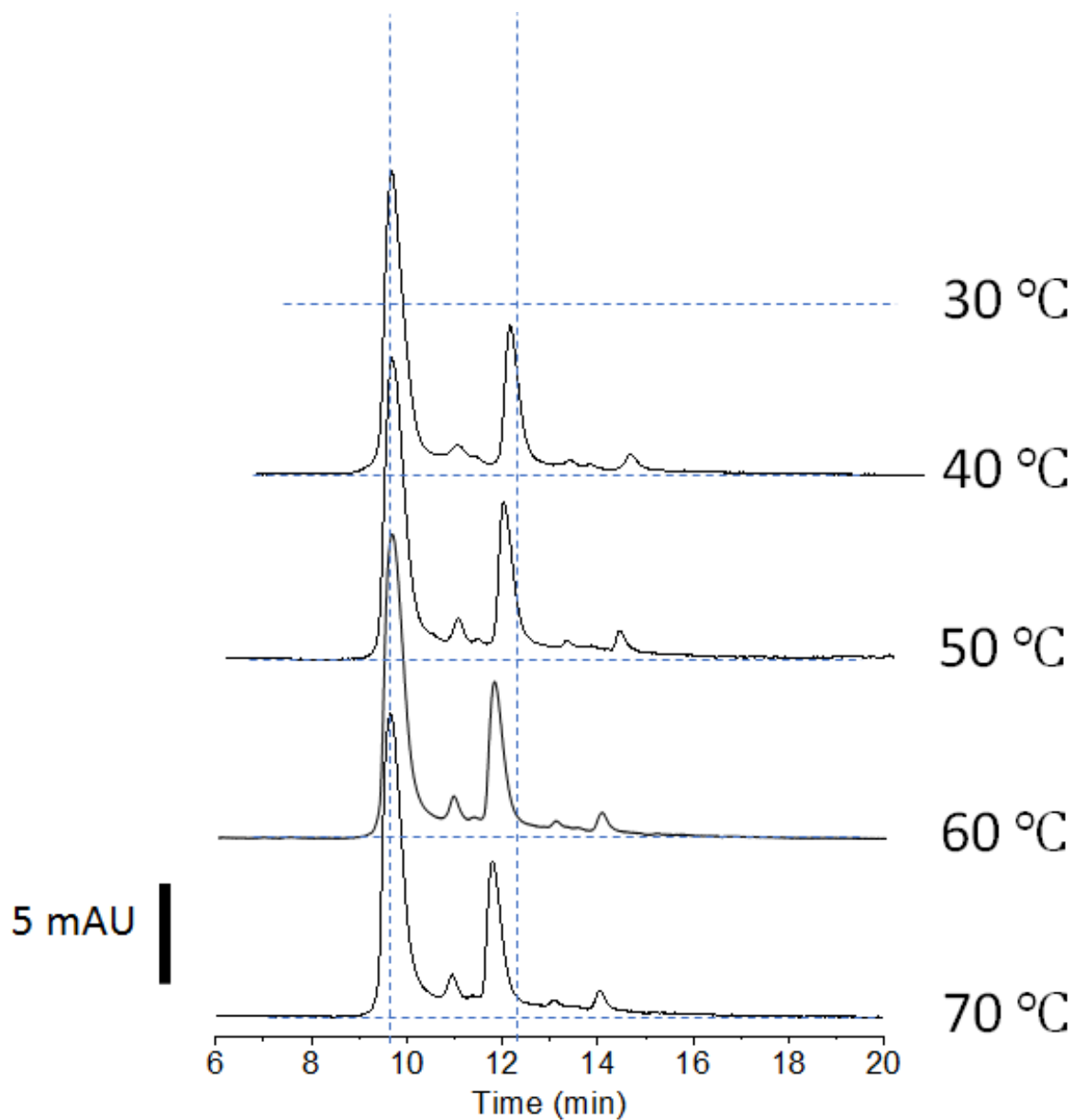


Figure 2.5. Chromatograms of IgG1 separation with different column temperatures. Chromatograms are shifted to align the first peak. The dashed lines indicate the baseline and the distance between the major peaks. Column: PMMA 60 min column; Gradient: 19-28% ACN in 30 min; Injection amount: 2 μg IgG1; Column temperature shown in the figure; Flow rate: 100 $\mu\text{L}/\text{min}$.

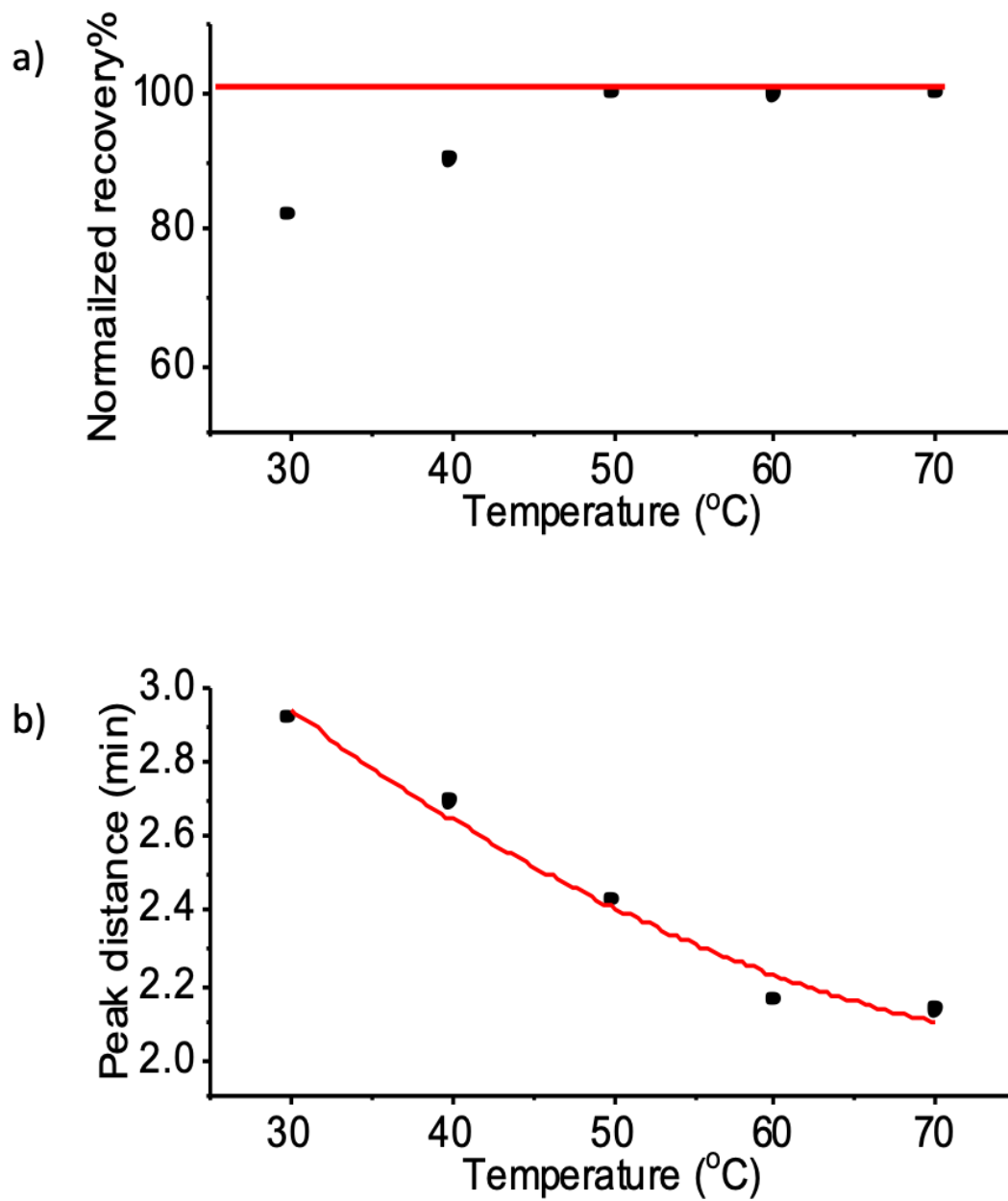


Figure 2.6. a) A plot of the normalized percentage recovery as a function of the column temperature b) Plot of the peak distance between the first two major peaks as a function of the column temperature.

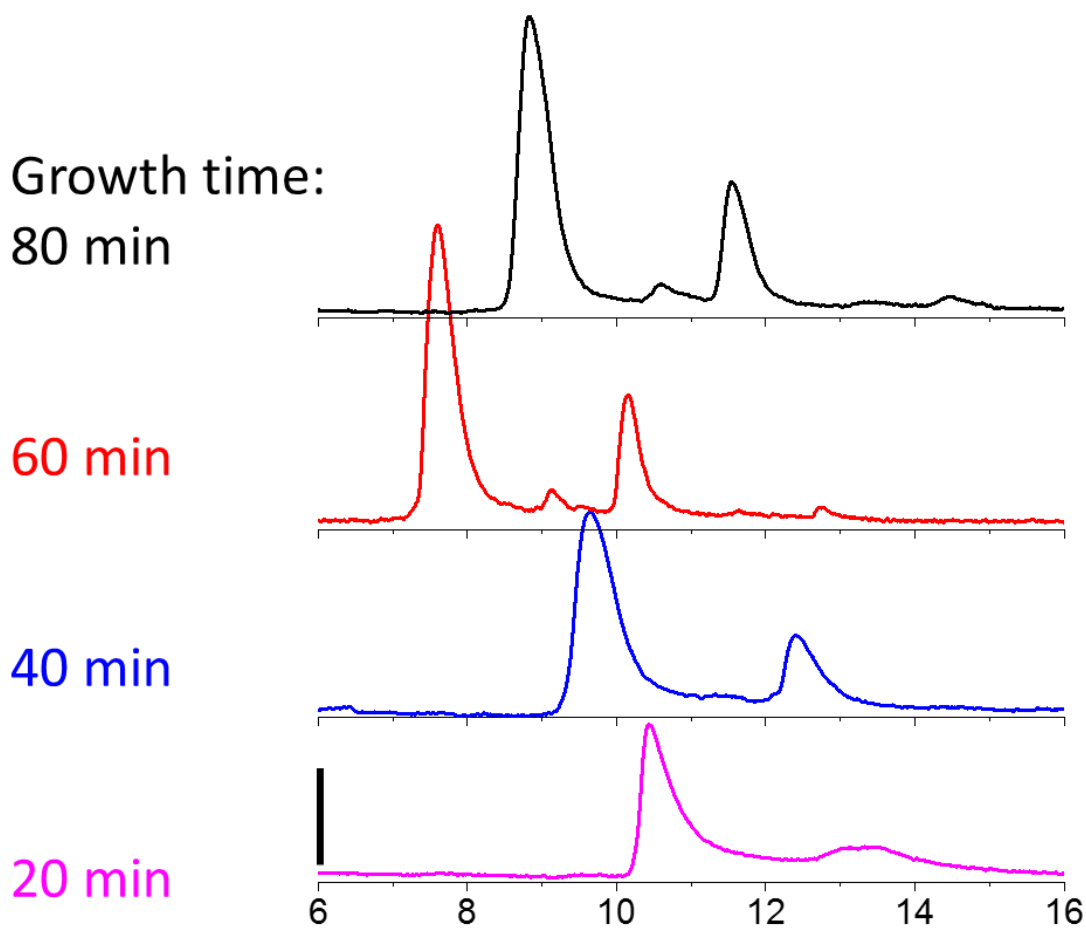


Figure 2.7. RPLC chromatogram for varying PMMA growth time, showing that the 60 min growth time is optimal with respect to resolution. Polymer growth time is labeled in each panel. The gradient for columns of 20, 40, 60, and 80 min PMMA growth time was 20-29% ACN with 0.5% FA in 30 min.

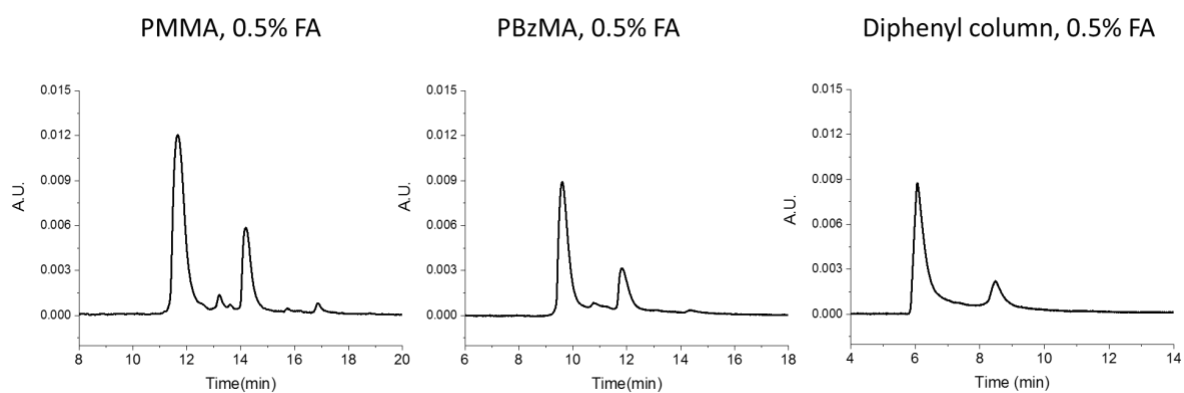


Figure 2.8. Comparison for the RPLC chromatogram of IgG1 using PMMA, PBzMA and Diphenyl column with 0.5% FA in the mobile phase. Gradient: 15% change in 50 min; Flow rate: 100 μ L/min. Column temperature optimized for each of the columns: 50 $^{\circ}$ C for PMMA and PBzMA column, 75 $^{\circ}$ C for the Diphenyl column.

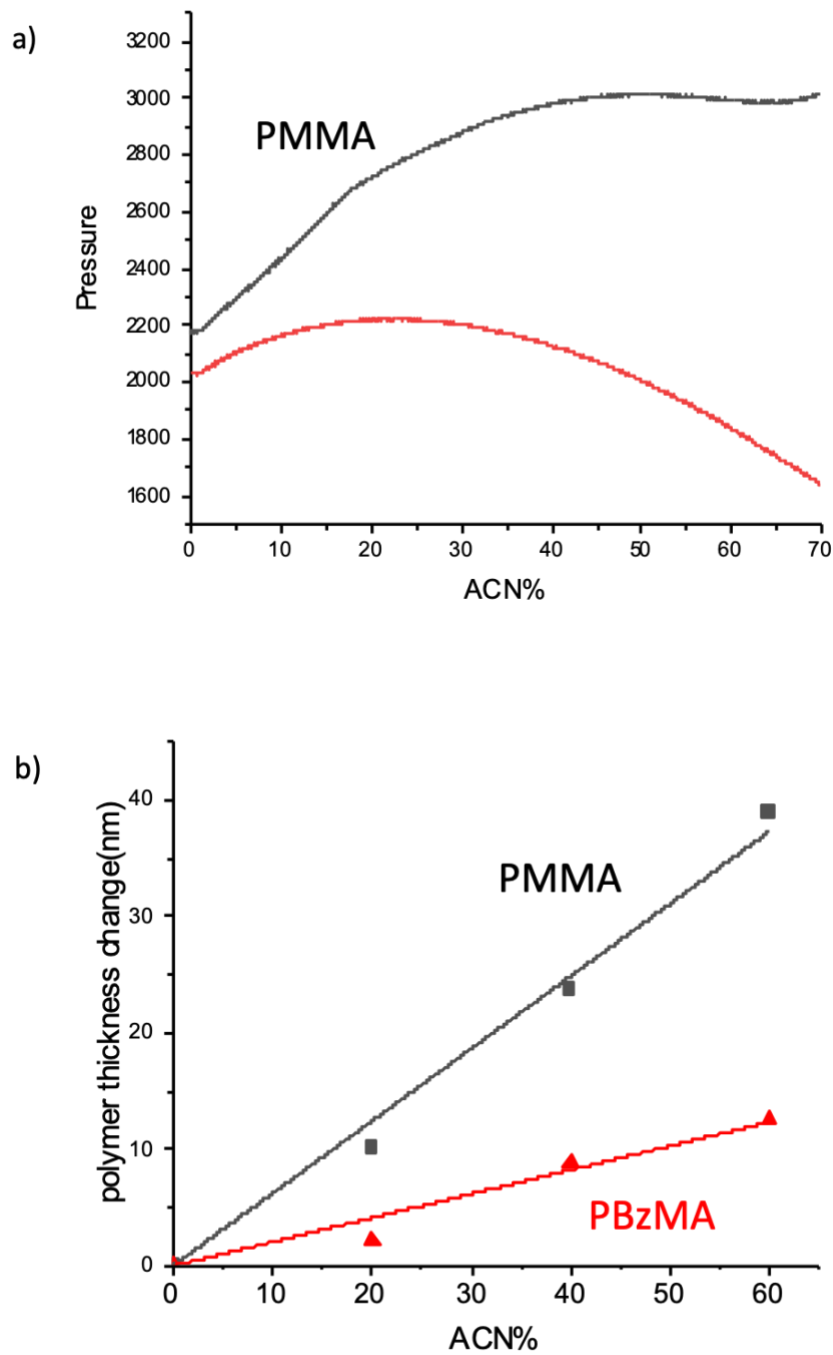


Figure 2.9. a) Overlaid graph of the pressure traces on the PMMA, PBzMA column and the viscosity data. The viscosity value is normalized to the pressure at 0% ACN. b) A plot of polymer thickness change as a function of the ACN percentage in the mobile phase for PMMA and PBzMA.

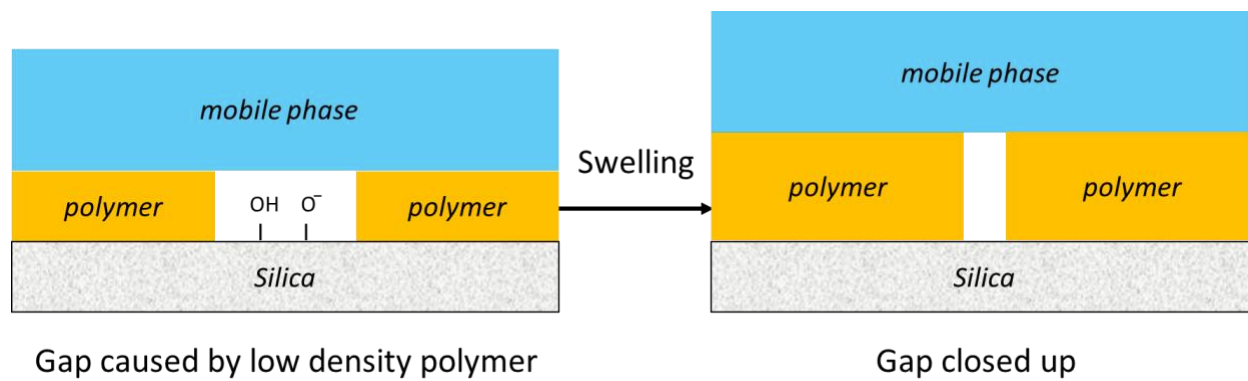


Figure 2.10. Illustration of how swelling behavior could change the polymer structure and block the protein from interacting with the surface silanols.

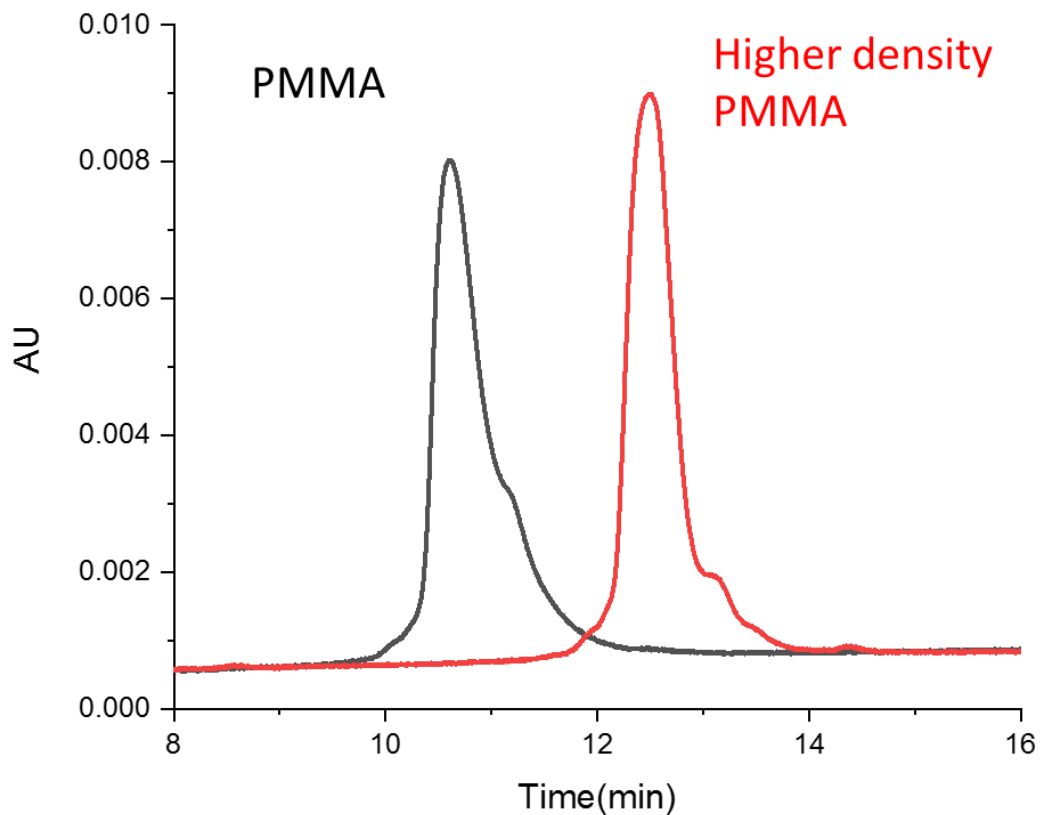


Figure 2.11. Chromatograms for NIST mAb separation using regular PMMA column and high-density PMMA column. Gradient: 25-34% ACN in 30 min with 0.1% TFA in the mobile phase; Injection amount: 0.75 μg NIST mAb; Column temperature: 80 $^{\circ}\text{C}$; Flow rate: 100 $\mu\text{L}/\text{min}$.

CHAPTER 3. NATIVE REVERSED-PHASE LIQUID CHROMATOGRAPHY: A TECHNIQUE FOR LCMS OF INTACT ANTIBODY-DRUG CONJUGATES

A version of this chapter has been published by *Analytical Chemistry*. Reprinted with permission from Tse-Hong Chen, Yun Yang, Zhaorui Zhang, Cexiong Fu, Qunying Zhang, Jon D. Williams and Mary J. Wirth, Native Reversed-Phase Liquid Chromatography: A Technique for LCMS of Intact Antibody-Drug Conjugates. *Analytical Chemistry* **2019**, *91* (4), 2805-2812. DOI: 10.1021/acs.analchem.8b04699. Copyright © 2019 American Chemical Society.

3.1 Introduction

Antibody-drug conjugates (ADCs) are highly selective and potent chemotherapeutics for the treatment of different types of cancer, inspired by Paul Ehrlich¹. An ADC consists of a recombinant monoclonal antibody (mAb) covalently conjugated with a drug via a hydrophilic linker. The mechanism exploits specific binding of tumor-expressed antigens and delivers covalently conjugated cytotoxic payloads to cancer cells selectively over non-malignant cells, resulting in greater efficacy and minimized systemic toxicity. Four ADCs are currently on the market: Adcetris® (brentuximab vedotin) from Seattle Genetics for the treatment of relapsed Hodgkin's lymphoma and systemic anaplastic large-cell lymphoma, Kadcyla® (trastuzumab emtansine), from Genentech for the treatment of metastatic breast cancer²⁻⁴, Mylotarg® (gemtuzumab ozogamicin) from Pfizer for acute myeloid leukemia and Besponsa® (inotuzumab ozogamicin) also from Pfizer for acute lymphoblastic leukemia. More than 60 ADCs have been advanced into clinical trials for cancer treatment,³ and there are currently more than 65 ADCs in clinical evaluation to target different hematologic malignancies and solid tumors^{3, 5}. The vast majority of the cytotoxic warheads of the ADCs currently in clinical trials are conjugated to either lysine or cysteine residues on the antibody,⁶⁻⁸ with most using cysteine residues.⁹ Drug loading in the ADCs is an important design parameter that needs to be characterized.¹⁰

Liquid chromatography separation of cysteine-conjugated ADCs to characterize the drug loading distribution is the topic of this paper. Taking IgG1, for example, a common conjugation approach entails partial reduction of four interchain disulfide bonds to generate up to eight reactive thiol

groups.¹¹⁻¹³ This conjugation scheme yields a mixture of species ranging from 0 to 8 drugs per antibody, which is a broad distribution. The different drug loadings have been reported to affect the pharmacokinetics, stability, and clearance of ADCs.¹⁴⁻¹⁸ Native SEC-MS is a rapid technique for determining the distribution of drug loads, where the SEC serves to de-salt the sample rather than separate the components and relies solely on MS for characterization and quantification.¹⁹ The technique skews the distribution toward lower drug load due to ion suppression and sub-optimal recovery of species with higher drug load.²⁰ Pretreatment by enzymatic cleavage of the hydrophobic drug from the ADC, which leaves the hydrophilic linker attached as a tag, reduces the skewing but does not eliminate it.²¹ Consequently, chromatographic separations are used for quantitative ADC characterization. Reversed-phase liquid chromatography coupled to mass spectrometry (RPLC-MS) is used to determine the average drug-to-antibody ratio (DAR) by separating the denatured subunits of the reduced ADC,²² but this approach loses information about the drug load distribution.²³ Hydrophobic interaction chromatography (HIC) is a non-denaturing separation²⁴⁻²⁶ that is currently the gold standard for resolving the drug distribution of ADCs.²⁷ A gradient of decreasing salt concentration is used for elution,^{28, 29} and the high initial concentration and low volatility of the salts prevent its direct coupling to mass spectrometry for peak identification.³⁰⁻³⁴

The Ge and Alpert groups were the first to show that HIC-MS of intact proteins is possible with volatile salts.^{26, 35} In their papers, MS-compatible ammonium acetate salt was used, with a gradient decreasing from 1 M to 20 mM, concurrent with a gradient of increasing acetonitrile in water from 0 to 50%. Since NH_4OAc has weaker kosmotropic properties than the typical HIC salts of $(\text{NH}_4)_2\text{SO}_4$ and Na_2HPO_4 , they used a bonded phase with increased hydrophobicity, and their results demonstrated that the proteins maintained their native forms. HIC-MS has not yet been reported for intact ADCs.

The considerations for HIC-MS of ADCs are different from that of natural proteins. The conjugated drug of an ADC is far more hydrophobic than the solvent-exposed surface of a native protein, as demonstrated by the elution time increasing with increasing drug load in HIC of ADCs. In light of this, the concept behind our work is that a fixed, low concentration of MS-compatible salt, e.g., 50 mM NH_4OAc , might give retention of ADCs on hydrophobic columns since less

salting-out would be needed. If so, the question then is whether a mild organic additive, isopropanol, can be made to desorb the ADC from the stationary phase without dissociating the noncovalently bound subunits of the antibody. The strategy is to decrease the hydrophobicity of the bonded phase so that less organic component is needed for elution, thereby avoiding the dissociation of the antibody into subunits³⁶. This is the opposite of the strategy used by Chen and co-workers^{26, 35} since ADCs present a different problem than mAbs, which are more hydrophilic than ADCs. The other difference from the prior work is that the salt concentration is fixed at a low level while the organic component is increased, which would make this a reversed-phase separation. Hence the proposed new method is a non-denaturing version of reversed-phase liquid chromatography (RPLC), and we refer to it as native reversed-phase liquid chromatography (nRPLC).

The purpose of this work is to test the idea that a bonded phase with sufficiently low hydrophobicity would enable a new technique, nRPLC-MS, for separating intact ADCs and determining their molecular weights by in-line coupled mass spectrometry. The method is evaluated using both a model ADC and a commercial ADC, where each ADC has a drug mimic or drug coupled to cysteines of the mAb using a hydrophilic linker.

3.2 Materials and methods

3.2.1 Materials

Nonporous silica particles (1500 nm) were purchased from Superior Silica (Tempe, AZ). Empty stainless-steel columns (2.1 mm I.D., 50 mm length), reservoirs (4.6 mm I.D., 150 mm), and frits (0.5 μ m pore diameter) were purchased from Isolation Technologies (Middleboro, MA). Stainless-steel tubing, ferrules, and internal nuts were all purchased from Valco Instruments (Houston, TX). Silanes, i.e., (chloromethyl)phenyldimethylchlorosilane (+99%) and trimethylchlorosilane (+99%), were purchased from Gelest (Morrisville, PA). Methyl methacrylate (MMA, 99%), ethylene glycol dimethacrylate (EGDMA, 98%), sodium ascorbate (\geq 99%), butylamine (99.5%), NH₄OAc (99.99%), ammonium sulfate ((NH₄)₂SO₄, \geq 99%), sodium phosphate (Na₃PO₄, 96%), and ammonium hydroxide were purchased from Sigma–Aldrich (St. Louis, MO). Other chemical used included trifluoroacetic acid (TFA, 99%), difluoroacetic acid (DFA, 98%) and copper(II)

chloride (CuCl_2 , 99%) from Acros Organics (Morris Plains, NJ), tris(2-dimethylaminoethyl)amine (Me_6TREN , +99%) from Alfa Aesar (Haverhill, MA), and formic acid (FA, 99.5%+, LC/MS grade), acetonitrile (ACN), and 2-propanol (IPA) from Fisher Scientific (Hampton, NH). Ultrapure water was obtained from a Milli-Q system (MilliporeSigma, Darmstadt, Germany.)

IgG1 Ab095 was conjugated with drug-linker mimic PZ in-house at AbbVie (North Chicago, IL) as a model ADC. Brentuximab vedotin was obtained from Seattle Genetics. Both ADCs were prepared at 1 mg/mL in NH_4OAc or $(\text{NH}_4)_2\text{SO}_4$ with a final concentration of 0.8–1.0 M.

3.2.2 UHPLC column preparation

The silica particles were modified as described earlier³⁷. Briefly, the silica particles were calcined at 600 °C for 12 h, then annealed at 1050°C for 3 h, and rehydroxylated overnight in 1.0 M HNO_3 . Particles were then rinsed in ultrapure water and dried in a 60 °C vacuum oven. SEM showed that the particles decreased in diameter to 1.2 μm from the heating steps. Freshly rehydroxylated silica particles were suspended in a dry toluene solution containing 2% (v/v) of (chloromethyl)phenyldimethylchlorosilane and 0.1% (v/v) of butylamine. The solution was refluxed for 3 h and then rinsed by dry toluene. The particles were then end-capped by suspending in another dry toluene solution containing 2% (v/v) of trimethylchlorosilane and 0.1% (v/v) of butylamine and refluxed for 3 h. The silylated, end-capped particles were then rinsed with dry toluene and allowed to dry in a 60 °C vacuum oven for 2 h.

For polymer growth, each monomer was dissolved in 40:60 $\text{H}_2\text{O}/\text{IPA}$ (v/v) in a 50 mL round bottom flask for a final concentration of 2.5 M. Two other solutions were made: 1) a solution containing 40 mg of CuCl_2 and 80 μL Me_6TREN , and 2) a solution containing 20 mg sodium ascorbate. These were also prepared in 2.0 mL of 40:60 $\text{H}_2\text{O}/\text{IPA}$. Afterward, the $\text{Cu}/\text{Me}_6\text{TREN}$ solution was added to the round bottom flask, followed by the sodium ascorbate solution. The resulting solution was poured into a plugged reservoir column of 4.6 mm \times 150 mm. A 2.1 mm \times 50 mm column was packed with 0.24 g of silylated, end-capped particles suspended in acetonitrile. The reservoir and column were connected in series. A high-pressure pump, LabAlliance Series 1500 HPLC Pump (Laboratory Alliance of Central New York, LLC, Syracuse, NY) was used for packing and modification. The reaction solution from the reservoir was pumped into the column

starting at 200 $\mu\text{L}/\text{min}$ until the reaction mixture dripped from the end of the column. The flow rate was then lowered to 100 $\mu\text{L}/\text{min}$, and the polymerization reaction was allowed to proceed for a range of reaction times from 40 to 85 min for optimization. After the reaction, the freshly packed column polymethylmethacrylate (PMMA) was rinsed with water for 20 min at 100 $\mu\text{L}/\text{min}$.

For cross-linked PMMA polymer column, methyl methacrylate and ethylene glycol dimethacrylate were mixed at different ratios and added to 50 mL round bottom flask containing 40:60 $\text{H}_2\text{O}/\text{IPA}$ (v/v). Then the same procedures were followed for modifying the particles.

3.2.3 UHPLC

The columns and mobile phases for the various separations are summarized in **Error! Reference source not found.** A Thermo Accela UHPLC system (Thermo-Scientific, Waltham, MA, USA) was used for the development of nRPLC separations at the Purdue lab. Lab-made nRPLC columns (2.1×50 mm, 1.2 μm nonporous silica particles coated with various polyalkylmethacrylates were used as the analytical columns. A commercial column, MabPac HIC-Butyl (4.6×100 mm, 5 μm nonporous), from Thermo Scientific (Waltham, MA) was used under both HIC and nRPLC conditions for comparison since both have polymeric surfaces. UV absorbance wavelength was set to 280 nm. The flow rate was 100 $\mu\text{L}/\text{min}$ for all cases. The column temperature was 30 $^\circ\text{C}$ and the injection volume was 3 μL .

A TSKgel Butyl-NPR column (4.6×35 mm, 2.5 μm , Tosoh, King of Prussia, PA) was used for HIC at the AbbVie site, with an Agilent 1200 HPLC (Agilent, Santa Clara, CA). The system is routinely used for HIC separations of ADCs to calculate DAR. With the mobile phase given in Table 3.1, the gradient started with 90% MPA, decreased to 75% MPA in 2 min followed by a gradient to 0% MPA in 10 min and was held for 2 min before re-equilibrium. The flow rate was 0.8 mL/min and the column temperature was set to 25 $^\circ\text{C}$.

3.2.4 LC-MS

For RPLC-MS of the reduced ADC, this was generated in the Purdue lab by adding 1,4-dithiothreitol (DTT), a Thermo Accela UHPLC was used with a Thermo MabPac RP column (2.1

x 50 mm, 4 μ m, supermacroporous polymer particles) (Thermo-Scientific, Waltham, MA, USA), and the column was coupled to a Thermo LTQ Velos mass spectrometer (Thermo-Scientific, Waltham, MA, USA). With the mobile phase given in Table 3.1, the gradient started with 27% with MPB2, increased to 43% MPB2 in 15 min, and returned to 27% MPB2 for re-equilibrium. The flow rate was 0.2 mL/min and the column temperature was 80 °C. Peak identities were assigned by matching deconvoluted masses with theoretical masses.

For RPLC-MS of the non-reduced ADC (no DTT), a Supelco Bioshell A400 Protein C4 column (2.1 x 100 mm, 3.4 μ m, Sigma-Aldrich, St. Louis, MO) was used in the AbbVie lab. With the mobile phase given in Table 3.1, the gradient started with 90% MPA3, ramped to 69% MPA3 in 1 min followed by a decrease to 52% MPA3 in 13 min, and returned to original condition for re-equilibrium. The flow rate was 0.3 mL/min and the column temperature was 70 °C. The ADC samples were analyzed using an Acquity UPLC H-Class coupled to a Synapt G2 Si mass spectrometer (Waters, Milford, MA). Peak identities were assigned by matching deconvoluted masses with theoretical masses.

For online nRPLC-MS analysis, the polymethylmethacrylate (PMMA) column made in the Purdue lab was used at AbbVie, where the LC-MS system was a Waters Acquity UPLC H-Class coupled to a Xevo G2 qTOF mass spectrometer (Waters, Milford, MA). With the mobile phase given in Table 3.1, the gradient started with 0% MPB4, held for 2 min, ramped to 15% MPB4 in 3 min followed by a gradient to 50% MPB4 in 15 min and held at 50% MPB4 for 6 min before re-equilibrium. The flow rate was reduced to 0.07 mL/min and the column temperature was 30 °C. For MS condition, the capillary voltage was 3.00 kV, Sample cone voltage was 85V, trap collision energy was set to 60 V, source temperature was 140 °C and desolvation temperature was 500 °C. The high sampling cone voltage was used to improve resolution and sensitivity in raw MS spectra, but this more prone to cause in-source fragmentation.

3.3 Results and discussions

3.3.1 ADC structure and DAR characterization

A model ADC was synthesized by AbbVie, with the chemical structure of the linker and drug portions depicted in **Error! Reference source not found.a**. The structure is similar to that of the commercial ADC, Brentuximab, also studied here, with its structure depicted in Figure 3.2b. These are both cysteine-conjugated ADCs using a similar, typical hydrophilic linker with coupling to the mAb cysteines via the maleimide group. The Figure shows that the drug mimic for the AbbVie model ADC and the drug for brentuximab vedotin are quite hydrophobic, each with a log P above 3, where P is the partition coefficient for octanol/water.

ADCs can be characterized with respect to their average DAR by fully reducing the ADCs with DTT and then separating the subunits by RPLC. Sketches to indicate labeling for intact ADCs and the various subunits are given in Figure 3.2a. The RPLC chromatogram for the reduced AbbVie model ADC Ab095-PZ is shown in Figure 3.2b. The mass spectrum of each peak (Figure 3.3) was used to assign each of the six peaks to the subunit, as labeled in the chromatogram. The first two peaks are light chains without (L0) or with (L1) one drug+linker, and the latter four peaks are heavy chains with 0, 1, 2 and 3 drug+linker attachment(s). The average DAR calculated from the relative peak areas is 3.9. The RPLC chromatogram of Ab095-PZ without DTT reduction (i.e., non-reduced RPLC) is shown in Figure 3.2c. The peak assignments from MS show that the model ADC was only partially reduced during the conjugation process, as expected. The results demonstrate that in conventional RPLC, without interchain disulfide bond linkages, the ADC dissociates into subunits. The value of this chromatogram is that it can be later compared to that for native RPLC with DTT absent. The HIC chromatogram of Ab095-PZ, using a commercial HIC-Butyl column and typical HIC salt gradient, is shown in Figure 3.2d. As is common practice, an isopropanol gradient was superimposed on the salt gradient to attain full elution of the ADC constituents. The species with higher drug loading gave multiple peaks, and this is shown later to be due to partial resolution of positional isomers. Mass spectrometry cannot be used to identify the peaks of Figure 3.2d because the conventional HIC salts suppress ionization and cause adduct formation, as discussed earlier. One can make tentative peak assignments based on typical drug loading profile for ADCs with an average DAR of 3.9, as indicated in Figure 3.2d.

3.3.2 nRPLC bonded phase optimization

The proposed strategy described earlier to enable native RPLC-MS is to use no more than 50 mM NH₄OAc. This amount of salt is normally reached at the end of a salt gradient for online HIC-MS;^{25, 26, 38} therefore, there is now little value in even running a salt gradient in RPLC mode. Despite this low level of salt, the same commercial HIC column as used for the HIC of Figure 3.2d (Thermo MabPac HIC-Butyl column) was found to give virtually no elution of the ADC; the retention to the column is too strong for elution. This indicates that the lower kosmotropic power of 50 mM NH₄OAc gives more retention than the higher kosmotropic power of 50 mM sodium phosphate of Figure 3.2d. The strong retention with 50 mM NH₄OAc is attributed to irreversible adsorption of the hydrophobic drug rather than to salting out of the intact ADC. The HIC stationary phase, which is said to be made of butyl groups, is thus too hydrophobic for use with isocratic 50 mM NH₄OAc, i.e., the hydrophobic interactions between ADC and bonded phase surface are stronger than the intramolecular hydrophobic interactions within the ADC. This inspires the proposed strategy to make the bonded phase less hydrophobic so that the free energy barrier for protein desorption is lower than the free energy barrier for protein denaturation.

Native RPLC chromatograms of model ADC Ab095-PZ using isocratic 50 mM NH₄OAc with a gradient of 0-50% isopropanol are shown in Figure 3.4a-d for a series columns with decreasing bonded phase hydrophobicity, including polymethyl-, polyethyl-, polypropyl- and polybutylmethacrylate. The recovery and resolution are progressively higher with lower hydrophobicity, consistent with less denaturation of the ADCs lower mobile phase strength. Polymethylmethacrylate, with the lowest hydrophobicity, gives a chromatogram similar to that of the native HIC chromatogram of Figure 3.2d, suggesting that intact ADCs are indeed eluted under mild organic phase content without dissociation. The chromatogram is quite different from that of the denaturing RPLC case of Figure 3.2c, again arguing that the ADCs are not dissociated.

The downside of the nRPLC separation of the ADCs in Figure 3.4 is that the native antibody, i.e., the species having no conjugated drug, D0, has low retention. This is an inherent outcome of the nRPLC strategy, where the designed retention mechanism is based on the hydrophobic interaction between the exposed/or partially exposed hydrophobic drug with the bonded phase. To increase

the retention of D0 species, some mixed-mode copolymer could potentially be used with minimal effect on the retention of the hydrophobic drug.

3.3.3 Mass spectrometry data

Mass spectrometry is used to test whether the constituents of the ADC peaks are intact vs. dissociated under nRPLC conditions for the column with polymethylmethacrylate grown for 70 min. Figure 3.5a shows the nRPLC chromatogram for the AbbVie model ADC using the polymethylmethacrylate column, now with the gradient adjusted for faster elution. The peaks are labeled in detail based on the mass of the most prevalent protein for each peak. The raw mass spectral data are given in Figure 3.5b. By extracting high mass range (extracted in chromatogram not shown), it was confirmed that the unconjugated species (D0) was barely retained and was nearly co-eluting with the injection peak. The small peak in the chromatogram of Figure 3.5a eluting at 10 min was identified as D1. In Figure 3.5b, the first mass spectrum assigned the peak at 13 min as D2 based on deconvoluted mass, which gives the mass (149,380 Da) corresponding to that expected for D2 (theoretical mass: $147,640 + 2 \times 859$). There are three peaks for D4, labeled as D4(1), D4(2) and D4(3) in the order of elution, and Figure 3.2a showed that there are theoretically four positional isomers for D4. Of note, the positional isomers of D4 that result from conjugation of the upper vs lower cysteine pairs in the hinge region likely co-elute since they are only subtly different in structure. Similarly, D6 gives two peaks when there are expected to be three, but again, as illustrated in Figure 3.2a, two cases differ only by position on the heavy chain (upper hinge cysteine conjugation vs. lower hinge cysteine conjugation). It is novel for a HIC column to resolve different D4 and D6 isoforms from one another, and the separation on this polymethylmethacrylate under nRPLC mode could be advantageous in process understanding and quality control. The mass spectrum of the larger of the two D6 peaks is given in Figure 3.5b. It shows some peak overlap with D4, as indicated by the light blue lines in Figure 3.5b. The mass spectrum of the peak labeled D8 indicates it to be mainly D8 with some overlap from D5, D6 and D7. No peaks due to fragments were observed. It is noteworthy that all ADC mass spectra demonstrated a native-like charge envelope distribution with charge state from 24 to 33, which further supports the conclusion of native RPLC.

Representative mass spectra of model ADC over a wider range of mass-to-charge ratio (m/z) are given in Figure 3.6a. All spectra show strong signals from a heretofore unexpected L1 fragment (light chain plus drug), despite the absence of the corresponding species (ADC minus L1) in the higher mass range for intact ADC. This at first seems to contradict the claim of intact ADC elution during the discussion of Figure 3.5 for the higher mass range. Our conclusion is that this L1 signal in Figure 3.6 arises from two circumstances: 1) in-source fragmentation of the ADC after elution due to the rather high sampling cone voltage and 2) a greater ionization efficiency of the L1 fragment to make its signal appear disproportionately strong compared to that of the intact ADC. If the signal strength were proportional to abundance, there would be a significant amount of ADC-L1 detectable in the higher range of m/z . Therefore, the large peaks for L1 must be due to greater ionization efficiency. In addition, if L1 dissociated from the ADC on the column, the EIC based on L1 would not be correlated with the UV chromatogram. The only reasonable way for the subunits of the ADC to travel together throughout the separation is for the ADC to be intact. An extracted ion chromatogram (EIC) for the L1 fragment is shown in Figure 3.6b, in comparison with the same chromatogram using UV detection. It is clear that the chromatograms closely track one another for the two different modes of detection. Further, the exceptions prove the rule: the blue arrows in Figure 3.6b show a D4 peak that is increased and a D4 peak that is decreased for EIC of L1. These are consistent with the expectation that one D4 should have two L1 species and one should have none. The inset images in Figure 3.6b depict the structures of the positional isomers. D4(2) has twice as many light chains with a drug compared to D4(1), which would make its signal increase for EIC of L1. Likewise, D4(3) has no light chain with drug, hence signal would decrease for EIC of L1. The EIC supports the conclusion that L1 dissociated post-column and all ADCs remained intact throughout the nRPLC separation. It is remarkable that D8, with fully reduced interchain disulfide bonds between subunits, eluted intact.

The native RPLC-MS strategy was also tested for a commercial ADC, brentuximab vedotin, which is a well-characterized commercial ADC, with an average DAR of 4.0, comparable to that of the AbbVie model ADC.³⁹ HIC was performed to compare DAR profiles of the two ADCs. The results are provided in Figure 3.7, confirming that the DAR profiles of these two ADCs are qualitatively similar. The chromatograms show that the D0 peak elutes later for brentuximab vedotin, indicating that the brentuximab (mAb of brentuximab vedotin) sequence is more hydrophobic than that of

the AbbVie model ADC. This is offset by the drug of brentuximab vedotin being less hydrophobic than the drug-linker of the AbbVie model ADC, with its lower octanol/water partition coefficient, $\log P = 3.01$, for MC-VC-MMAE compared to that of the AbbVie model drug, $\log P = 3.35$. The elution times of peaks with higher drug load in HIC are similar in both chromatograms: 10 min.

The nRPLC chromatogram for brentuximab vedotin, using the same polymethylmethacrylate column and separation conditions as for the AbbVie model ADC, is given in Figure 3.8a. The chromatogram is similar to that for the AbbVie model ADC, with differences in relative peak heights and a small extra peak before D6. The D0 species is now slightly retained in nRPLC, owing to the greater hydrophobicity of the mAb that was noted using HIC. All ADC peaks elute somewhat earlier in nRPLC for brentuximab vedotin, consistent with the lower hydrophobicity of the drug. The mass spectra, detailed in Figure 3.8b, show that the D2 peak and the first D4 peak, D4(1), are intact, with no loss of L1. The other two D4 peaks, D4(2) and D4(3) show some loss of one or two light chains with one drug (D4-L1 and D4-2xL1), in addition to the intact forms being observed. Overall, the results show that it is much easier to lose L1 from brentuximab vedotin than it is from the AbbVie model ADC.

As was done with the AbbVie model ADC to distinguish on-column vs. in-source dissociation, Figure 3.9a shows representative mass spectra over a wider range of m/z for brentuximab vedotin. The relative signals from the L1 fragment are much stronger than those of the AbbVie model ADC, again illustrating the greater ease of loss of L1 for brentuximab vedotin. To determine whether L1 dissociated on-column or in-source, the EIC for the L1 fragment is shown in Figure 3.9b, in comparison with the same chromatogram using UV detection. As with the case for the AbbVie model ADC, the UV and extracted ion chromatograms closely track one another. The lack of an L1 background across the chromatogram confirms that all of the ADCs remain intact throughout the course of the nRPLC separation. As with the AbbVie model ADC, the L1 fragment signal is more pronounced in the D4(2) position than the latter peak D4(3), indicated by the blue arrows. As with the case for the AbbVie model ADC, the relative abundances of the L1 fragment peaks are likely associated with same two factors: a) the L1 molar ratio in the positional isomer: 1, 2, 0, for D4(1), D4(2) and D4(3), respectively; and b) strength of the noncovalent interaction between L1 and heavy chains in the MS source. These two factors reflect on the L1 fragment peak

abundance in the order of D4(2)>D4(1)>>D4(3). The Comparison of EIC and UV chromatograms again supports the conclusion that nRPLC elutes intact brentuximab vedotin species. The greater loss of L1 in the source for brentuximab vedotin relative to the AbbVie model ADC indicates that the noncovalent interactions between light and heavy chains are weaker for brentuximab vedotin than that of the AbbVie model ADC Ab095-PZ.

3.4 Conclusion

A novel protein chromatography technique intersecting HIC and RPLC modes was developed, termed native reverse-phase liquid chromatography, nRPLC. nRPLC employs the solvent elution model and MS compatibility of RPLC, while preserving the native form of protein and ADC as in HIC. This new nRPLC technique is an alternative to HIC for ADCs when in-line coupling of MS is desired by virtue of using only 50 mM NH₄OAc. The nRPLC method eluted intact ADCs for both a model ADC from AbbVie and a commercial ADC from Seattle Genetics. The key to this chromatographic advance was lower hydrophobicity of the bonded phase to make drug-surface hydrophobic interactions weaker than the intramolecular hydrophobic interactions that maintain the noncovalent complexes. Inherent to this strategy of designing retention only for interactions between the attached drug and chromatographic surface is that the D0 species has little retention at this stage in column development. The column gives partial resolution of positional isomers, thereby providing additional characterization beyond what is typically obtained using HIC. The lesser number of peaks in HIC permits full resolution of the ADC based on drug loading, which enables precise calculation of DAR. With its greater resolution of positional isomers that currently overlap, nRPLC will be a companion rather than a replacement for HIC until the resolution is improved. Longer nRPLC columns, refinement of polymer growth conditions and optimization of separation conditions could lead to sufficient resolution to determine DAR while also characterizing positional isomers. To our knowledge, this is the first time that intact ADCs made from reduced cysteines have been separated based on DAR using an MS-compatible mobile phase.

3.5 Future work

The same bonded phase, PMMA, was used for the IgG1 disulfide bond and free thiol variants characterization using RPLC-MS. The difference between RPLC separation and nRPLC

separation is that nRPLC separation is running at neutral pH, hence the surface charge density is higher on the silica surface as shown in Figure 3.10. Therefore, a thicker layer of polymer is required for shielding the electrostatic interaction between the analyte and the surface in nRPLC. Chromatograms of the AbbVie model ADC using PMMA with different growth times show a good agreement with the idea in Figure 3.11. In IgG1 RPLC separation, best resolution and recovery are observed with PMMA 60 min column, while in nRPLC, 70 min is the optimized polymer growth time.

Chemical crosslinking could produce polymer new polymer derivatives that have improved performance or even distinctive new chemical and physical properties. Compared with free polymer, crosslinked polymer typically shows improved thermal stability, mechanical stability and, increased solvent resistance and chemical resistance^{40, 41}. Different crosslinking strategies including free radical polymerization⁴², condensation reactions⁴³, and small molecule crosslinker⁴⁴. Here a crosslinked PMMA polymer is synthesized using the one-pot ATRP method by mixing the methyl methacrylate and ethylene glycol dimethacrylate together in the reaction mixture. Ethylene glycol dimethacrylate has the same functional group and similar backbone structure as methyl methacrylate, therefore, it should functionalize as the bridging group with changing the hydrophobicity of the bonded phase. In the application as the chromatographic surface, crosslinked PMMA could reduce the tangling between polymer chains and prevent protein from trapping in the polymer chains. Besides, more crosslinking could sterically prevent protein from directly contacting the silica surface and provide a better screening effect for the surface charge. The nRPLC chromatograms of the AbbVie model ADC using PMMA and crosslinked PMMA column are shown in Figure 3.12. For the comparison, 25 mM NH₄OAc is used to increase the charge interactions. Less peak tailing for D2 peak and better resolution for the higher DAR peaks are observed when the same gradient condition applied. The preliminary data show improved chromatographic performance of the crosslinked polymer.

3.6 Reference

1. Hughes, B., Antibody-drug conjugates for cancer: poised to deliver? *Nature reviews. Drug discovery* **2010**, 9 (9), 665-7.

2. Thomas, A.; Teicher, B. A.; Hassan, R., Antibody–drug conjugates for cancer therapy. *Lancet Oncol.* **2016**, *17* (6), e254-e262.
3. Beck, A.; Goetsch, L.; Dumontet, C.; Corvaia, N., Strategies and challenges for the next generation of antibody-drug conjugates. *Nature reviews. Drug discovery* **2017**, *16* (5), 315-337.
4. Polakis, P., Antibody Drug Conjugates for Cancer Therapy. *Pharmacological reviews* **2016**, *68* (1), 3-19.
5. Lambert, J. M.; Berkenblit, A., Antibody-Drug Conjugates for Cancer Treatment. *Annu. Rev. Med.* **2018**, *69*, 191-207.
6. Tsuchikama, K.; An, Z., Antibody-drug conjugates: recent advances in conjugation and linker chemistries. *Protein & cell* **2018**, *9* (1), 33-46.
7. Flygare, J. A.; Pillow, T. H.; Aristoff, P., Antibody-drug conjugates for the treatment of cancer. *Chemical biology & drug design* **2013**, *81* (1), 113-21.
8. Peters, C.; Brown, S., Antibody-drug conjugates as novel anti-cancer chemotherapeutics. *Bioscience reports* **2015**, *35* (4).
9. Jain, N.; Smith, S. W.; Ghone, S.; Tomczuk, B., Current ADC Linker Chemistry. *Pharmaceutical Research* **2015**, *32* (11), 3526-3540.
10. Hamblett, K. J.; Senter, P. D.; Chace, D. F.; Sun, M. M. C.; Lenox, J.; Cervený, C. G.; Kissler, K. M.; Bernhardt, S. X.; Kopcha, A. K.; Zabinski, R. F.; Meyer, D. L.; Francisco, J. A., Effects of drug loading on the antitumor activity of a monoclonal antibody drug conjugate. *Clinical Cancer Research* **2004**, *10* (20), 7063-7070.
11. Behrens, C. R.; Ha, E. H.; Chinn, L. L.; Bowers, S.; Probst, G.; Fitch-Bruhns, M.; Monteon, J.; Valdiosera, A.; Bermudez, A.; Liao-Chan, S.; Wong, T.; Melnick, J.; Theunissen, J. W.; Flory, M. R.; Houser, D.; Venstrom, K.; Levashova, Z.; Sauer, P.; Migone, T. S.; van der Horst, E. H.; Halcomb, R. L.; Jackson, D. Y., Antibody-Drug Conjugates (ADCs) Derived from Interchain Cysteine Cross-Linking Demonstrate Improved Homogeneity and Other Pharmacological Properties over Conventional Heterogeneous ADCs. *Molecular pharmaceutics* **2015**, *12* (11), 3986-98.
12. Sanderson, R. J.; Hering, M. A.; James, S. F.; Sun, M. M. C.; Doronina, S. O.; Siadak, A. W.; Senter, P. D.; Wahl, A. F., In vivo Drug-Linker Stability of an Anti-CD30 Dipeptide-Linked Auristatin Immunoconjugate. *Clin. Cancer Res.* **2005**, *11*, 843-852.
13. Sun, M. M. C.; Beam, K. S.; Cervený, C. G.; Hamblett, K. J.; Blackmore, R. S.; Torgov, M. Y.; Handley, F. G. M.; Ihle, N. C.; Senter, P. D.; Alley, S. C., Reduction-Alkylation Strategies for the Modification of Specific Monoclonal Antibody Disulfides. *Bioconjug. Chem.* **2005**, *16*, 1282-1290.

14. Ducry, L., *Antibody-Drug Conjugates*. Humana Press: New York City, NY, 2013; Vol. 1045.
15. Shen, B. Q.; Xu, K.; Liu, L.; Raab, H.; Bhakta, S.; Kenrick, M.; Parsons-Reponte, K. L.; Tien, J.; Yu, S. F.; Mai, E.; Li, D.; Tibbitts, J.; Baudys, J.; Saad, O. M.; Scales, S. J.; McDonald, P. J.; Hass, P. E.; Eigenbrot, C.; Nguyen, T.; Solis, W. A.; Fuji, R. N.; Flagella, K. M.; Patel, D.; Spencer, S. D.; Khawli, L. A.; Ebens, A.; Wong, W. L.; Vandlen, R.; Kaur, S.; Sliwkowski, M. X.; Scheller, R. H.; Polakis, P.; Junutula, J. R., Conjugation site modulates the in vivo stability and therapeutic activity of antibody-drug conjugates. *Nat. Biotechnol.* **2012**, *30* (2), 184-9.
16. Adem, Y. T.; Schwarz, K. A.; Duenas, E.; Patapoff, T. W.; Galush, W. J.; Esue, O., Auristatin antibody drug conjugate physical instability and the role of drug payload. *Bioconjug. Chem.* **2014**, *25* (4), 656-64.
17. Boswell, C. A.; Mundo, E. E.; Zhang, C.; Bumbaca, D.; Valle, N. R.; Kozak, K. R.; Fourie, A.; Chuh, J.; Koppada, N.; Saad, O.; Gill, H.; Shen, B. Q.; Rubinfeld, B.; Tibbitts, J.; Kaur, S.; Theil, F. P.; Fielder, P. J.; Khawli, L. A.; Lin, K., Impact of drug conjugation on pharmacokinetics and tissue distribution of anti-STEAP1 antibody-drug conjugates in rats. *Bioconjug. Chem.* **2011**, *22* (10), 1994-2004.
18. Lyon, R. P.; Bovee, T. D.; Doronina, S. O.; Burke, P. J.; Hunter, J. H.; Neff-LaFord, H. D.; Jonas, M.; Anderson, M. E.; Setter, J. R.; Senter, P. D., Reducing hydrophobicity of homogeneous antibody-drug conjugates improves pharmacokinetics and therapeutic index. *Nat. Biotechnol.* **2015**, *33* (7), 733-5.
19. Valliere-Douglass, J. F.; McFee, W. A.; Salas-Solano, O., Native Intact Mass Determination of Antibodies Conjugated with Monomethyl Auristatin E and F at Interchain Cysteine Residues. *Analytical Chemistry* **2012**, *84* (6), 2843-2849.
20. Firth, D.; Bell, L.; Squires, M.; Estdale, S.; McKee, C., A rapid approach for characterization of thiol-conjugated antibody-drug conjugates and calculation of drug-antibody ratio by liquid chromatography mass spectrometry. *Analytical biochemistry* **2015**, *485*, 34-42.
21. Chen, J.; Yin, S.; Wu, Y. J.; Ouyang, J., Development of a Native Nanoelectrospray Mass Spectrometry Method for Determination of the Drug-to-Antibody Ratio of Antibody-Drug Conjugates. *Analytical Chemistry* **2013**, *85* (3), 1699-1704.
22. Wiggins, B.; Liu-Shin, L.; Yamaguchi, H.; Ratnaswamy, G., Characterization of cysteine-linked conjugation profiles of immunoglobulin G1 and immunoglobulin G2 antibody-drug conjugates. *J. Pharm. Sci.* **2015**, *104* (4), 1362-72.
23. Fekete, S.; Veuthey, J. L.; Beck, A.; Guillaume, D., Hydrophobic interaction chromatography for the characterization of monoclonal antibodies and related products. *Journal of pharmaceutical and biomedical analysis* **2016**, *130*, 3-18.

24. J. Alpert, A., High-performance hydrophobic-interaction chromatography of proteins on a series of poly(alkyl aspart-amide)-silicas. *J. Chromatogr. A* **1986**, 359, 85-97.
25. Xiu, L.; Valeja, S. G.; Alpert, A. J.; Jin, S.; Ge, Y., Effective protein separation by coupling hydrophobic interaction and reverse phase chromatography for top-down proteomics. *Anal. Chem.* **2014**, 86 (15), 7899-906.
26. Chen, B.; Peng, Y.; Valeja, S. G.; Xiu, L.; Alpert, A. J.; Ge, Y., Online Hydrophobic Interaction Chromatography-Mass Spectrometry for Top-Down Proteomics. *Anal. Chem.* **2016**, 88 (3), 1885-91.
27. Wiggins, B.; Liu-Shin, L.; Yamaguchi, H.; Ratnaswamy, G., Characterization of Cysteine-Linked Conjugation Profiles of Immunoglobulin G1 and Immunoglobulin G2 Antibody-Drug Conjugates. *Journal of Pharmaceutical Sciences* **2015**, 104 (4), 1362-1372.
28. McCue, J. T., Theory and Use of Hydrophobic Interaction Chromatography in Protein Purification Applications. *Methods Enzymol.* **2009**, 463, 405-414.
29. J.A. Queiroz, C. T. T., J.M.S. Cabral, Hydrophobic interaction chromatography of proteins. *J. Biotechnol.* **2001**, 87 (143-159).
30. Géza Rippel, L. S., Hydrophobic interaction chromatography of proteins on an Alkyl-Superose column. *J. Chromatogr. A* **1994**, 664, 27-32.
31. Christine Machold, K. D., Rainer Hahn, Alois Jungbauer, Hydrophobic interaction chromatography of proteins I. Comparison of selectivity. *J. Chromatogr. A* **2002**, 972, 3-19.
32. Xia, F.; Nagrath, D.; Garde, S.; Cramer, S. M., Evaluation of selectivity changes in HIC systems using a preferential interaction based analysis. *Biotechnology and bioengineering* **2004**, 87 (3), 354-63.
33. To, B. C.; Lenhoff, A. M., Hydrophobic interaction chromatography of proteins. II. Solution thermodynamic properties as a determinant of retention. *J. Chromatogr. A* **2007**, 1141 (2), 235-43.
34. Baca, M.; De Vos, J.; Bruylants, G.; Bartik, K.; Liu, X.; Cook, K.; Eeltink, S., A comprehensive study to protein retention in hydrophobic interaction chromatography. *J Chromatogr. B.* **2016**, 1032, 182-188.
35. Chen, B. F.; Lin, Z. Q.; Alpert, A. J.; Fu, C. X.; Zhang, Q. Y.; Pritts, W. A.; Ge, Y., Online Hydrophobic Interaction Chromatography-Mass Spectrometry for the Analysis of Intact Monoclonal Antibodies. *Anal. Chem.* **2018**, 90 (12), 7135-7138.
36. Bobaly, B.; Beck, A.; Veuthey, J. L.; Guillarme, D.; Fekete, S., Impact of organic modifier and temperature on protein denaturation in hydrophobic interaction chromatography. *Journal of pharmaceutical and biomedical analysis* **2016**, 131, 124-132.

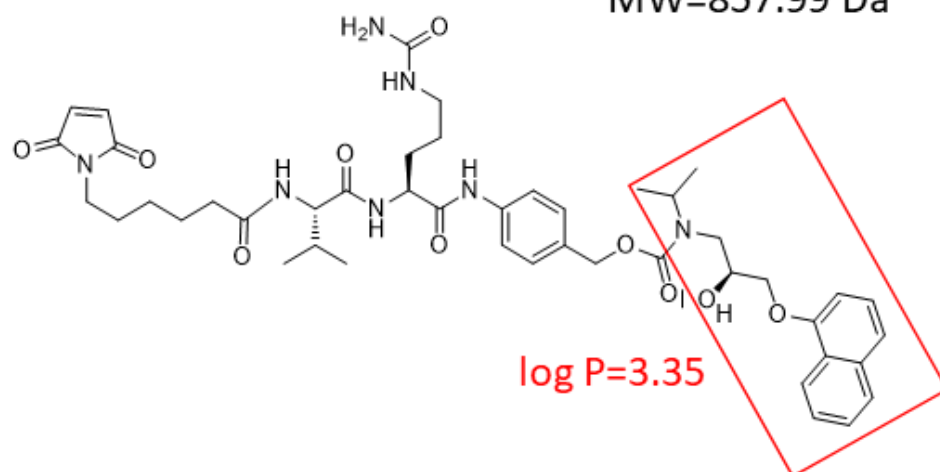
37. Huang, X.; Wirth, M. J., Surface-Initiated Radical Polymerization on Porous Silica. *Anal. Chem.* **1997**, *69* (22), 4577-4580.
38. Valeja, S. G.; Xiu, L.; Gregorich, Z. R.; Guner, H.; Jin, S.; Ge, Y., Three dimensional liquid chromatography coupling ion exchange chromatography/hydrophobic interaction chromatography/reverse phase chromatography for effective protein separation in top-down proteomics. *Anal Chem* **2015**, *87* (10), 5363-5371.
39. Janin-Bussat, M. C.; Dillenbourg, M.; Corvaia, N.; Beck, A.; Klinguer-Hamour, C., Characterization of antibody drug conjugate positional isomers at cysteine residues by peptide mapping LC-MS analysis. *J. Chromatogr. B* **2015**, *981*, 9-13.
40. Min, K.; Silberstein, M.; Aluru, N. R., Crosslinking PMMA: Molecular dynamics investigation of the shear response. *Journal of Polymer Science Part B: Polymer Physics* **2014**, *52* (6), 444-449.
41. Albeladi, H.; Al-Romaizan, A.; Hussein, M., Role of cross-linking process on the performance of PMMA. *Int. J. Biosens. Bioelectron* **2017**, *3*, 279-284.
42. Roice, M.; Subhashchandran, K.; Gean, A.; Franklin, J.; Pillai, V. R., Synthesis and characterization of glycerol dimethacrylate cross-linked polymethyl methacrylate: a resin for solid phase peptide synthesis. *Polymer* **2003**, *44* (4), 911-922.
43. Hussein, M. A.; El-Shishtawy, R. M.; Abu-Zied, B. M.; Asiri, A. M., The impact of cross-linking degree on the thermal and texture behavior of poly (methyl methacrylate). *Journal of Thermal Analysis and Calorimetry* **2016**, *124* (2), 709-717.
44. Hopwood, D., A comparison of the crosslinking abilities of glutaraldehyde, formaldehyde and α -hydroxyadipaldehyde with bovine serum albumin and casein. *Histochemie* **1969**, *17* (2), 151-161.

Table 3.1. Summary of HPLC columns and their applications

Column	Application	Mobile Phase A; B
Thermo MabPac RP	RPLC, reduced ADC	H ₂ O+0.1% DFA; ACN + 0.1% DFA
Supelco Bioshell A400	RPLC, non-reduced ADC	H ₂ O+0.1% FA+0.015% TFA; ACN + 0.1% FA +0.015% TFA
Thermo-HIC butyl	HIC, ADC (Purdue)	50 mM Na ₃ PO ₄ +1 M (NH ₄) ₂ SO ₄ , pH 7; 50 mM Na ₃ PO ₄ +30% IPA, pH 7
Tosoh TSKgel Butyl	HIC, ADC (AbbVie)	25 mM Na ₃ PO ₄ +1.5 M (NH ₄) ₂ SO ₄ , pH 7; 25 mM Na ₃ PO ₄ +25% IPA, pH 7
PMMA, nonporous	nRPLC, ADC	50 mM NH ₄ OAc, pH 7; 50 mM NH ₄ OAc+50% IPA, pH7

a) linker+drug in AbbVie model ADC, Ab095-PZ

MW=857.99 Da



b) linker+drug in brentuximab vedotin

MW=1316.63 Da

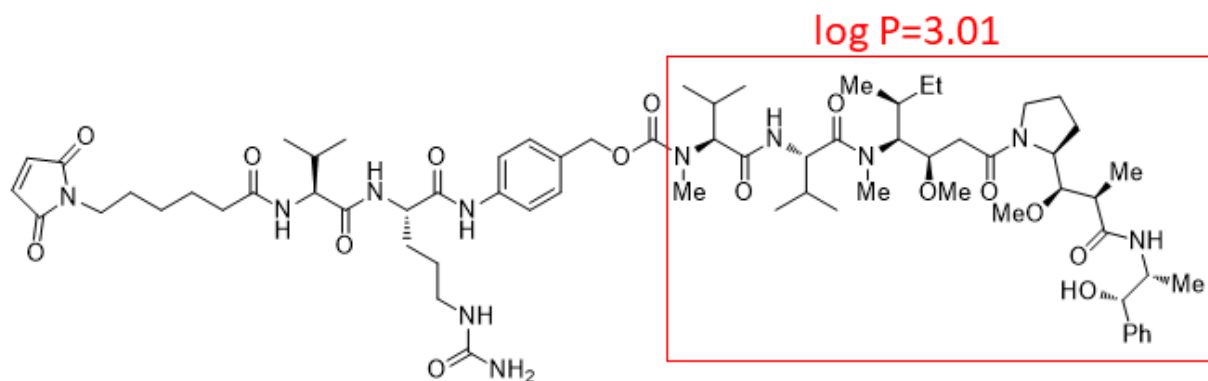


Figure 3.1. Chemical structures of linker-drug combination for a) the AbbVie model ADC, Ab095-PZ and b) brentuximab vedotin. Each drug or drug mimic part is in the red square, and its hydrophobicity is expressed by log P, where P represents the octanol/water partition coefficient.

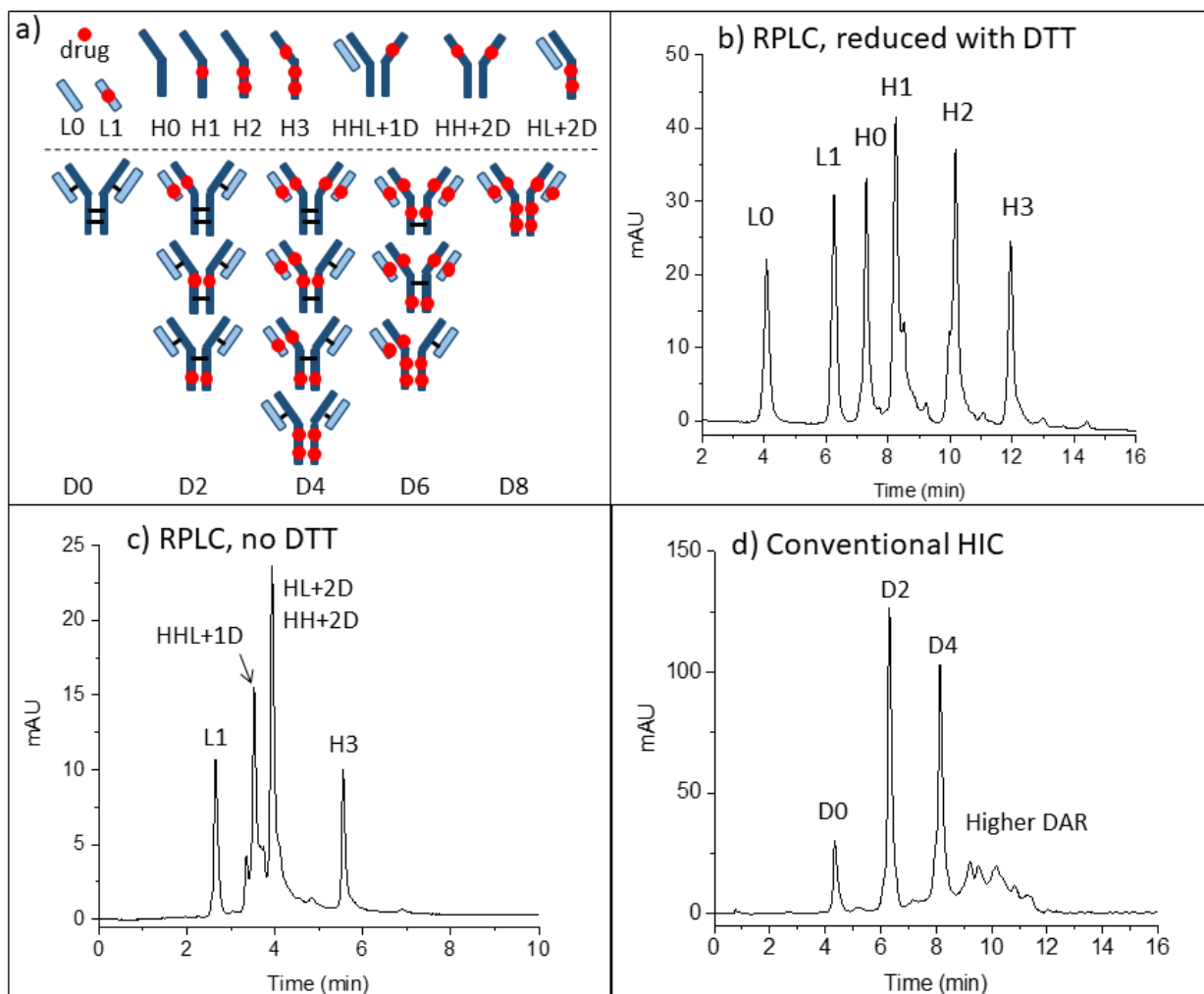


Figure 3.2. a) Sketches explain abbreviations for peak assignments. b) RPLC of the model ADC after reduction with DTT. c) RPLC of the model ADC without DTT. d) HIC of the intact ADC with tentative peak assignments.

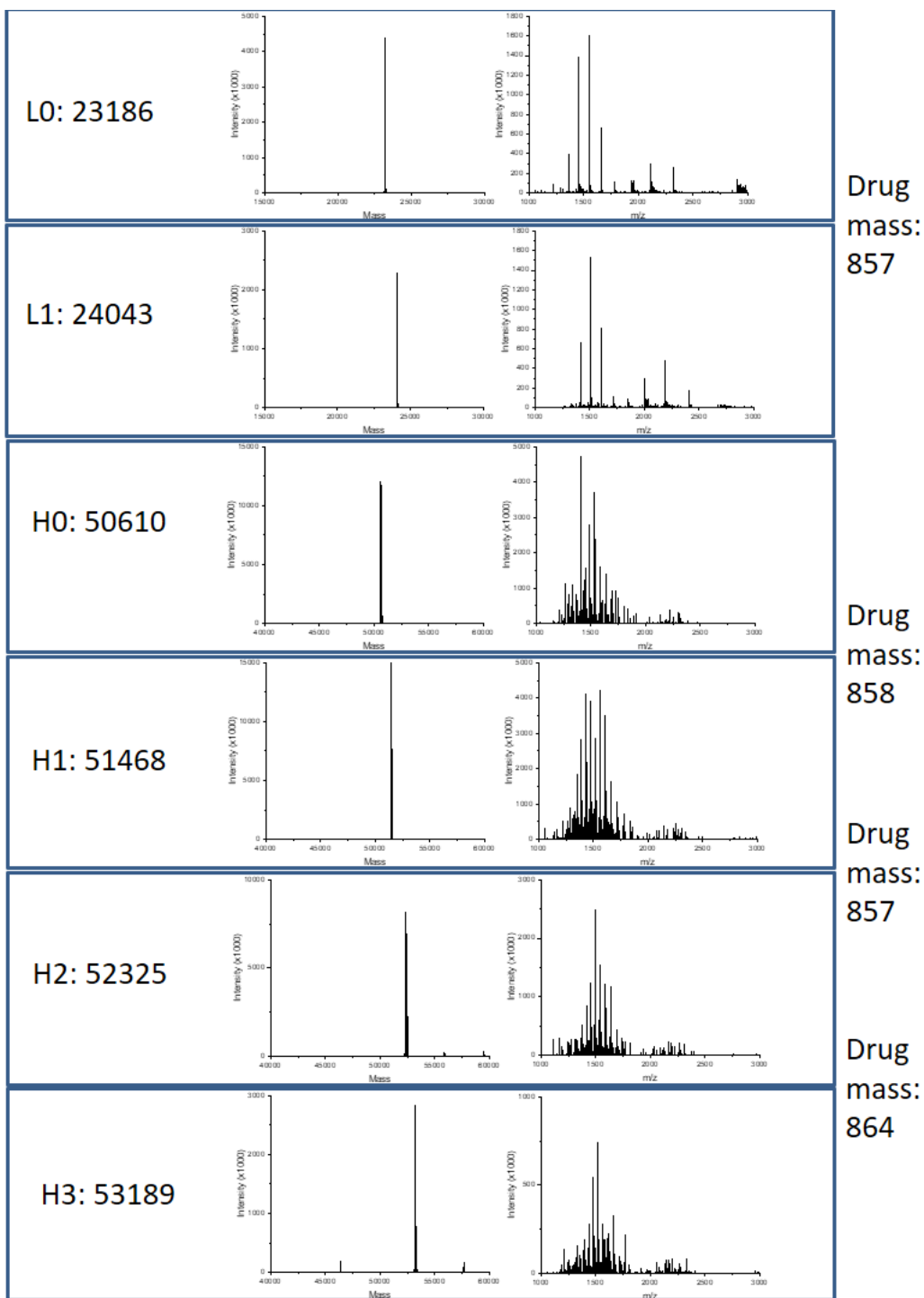


Figure 3.3. Raw mass spectra (right) and deconvoluted mass spectra (left) for each peak in the chromatograms of Figure 3.2b.

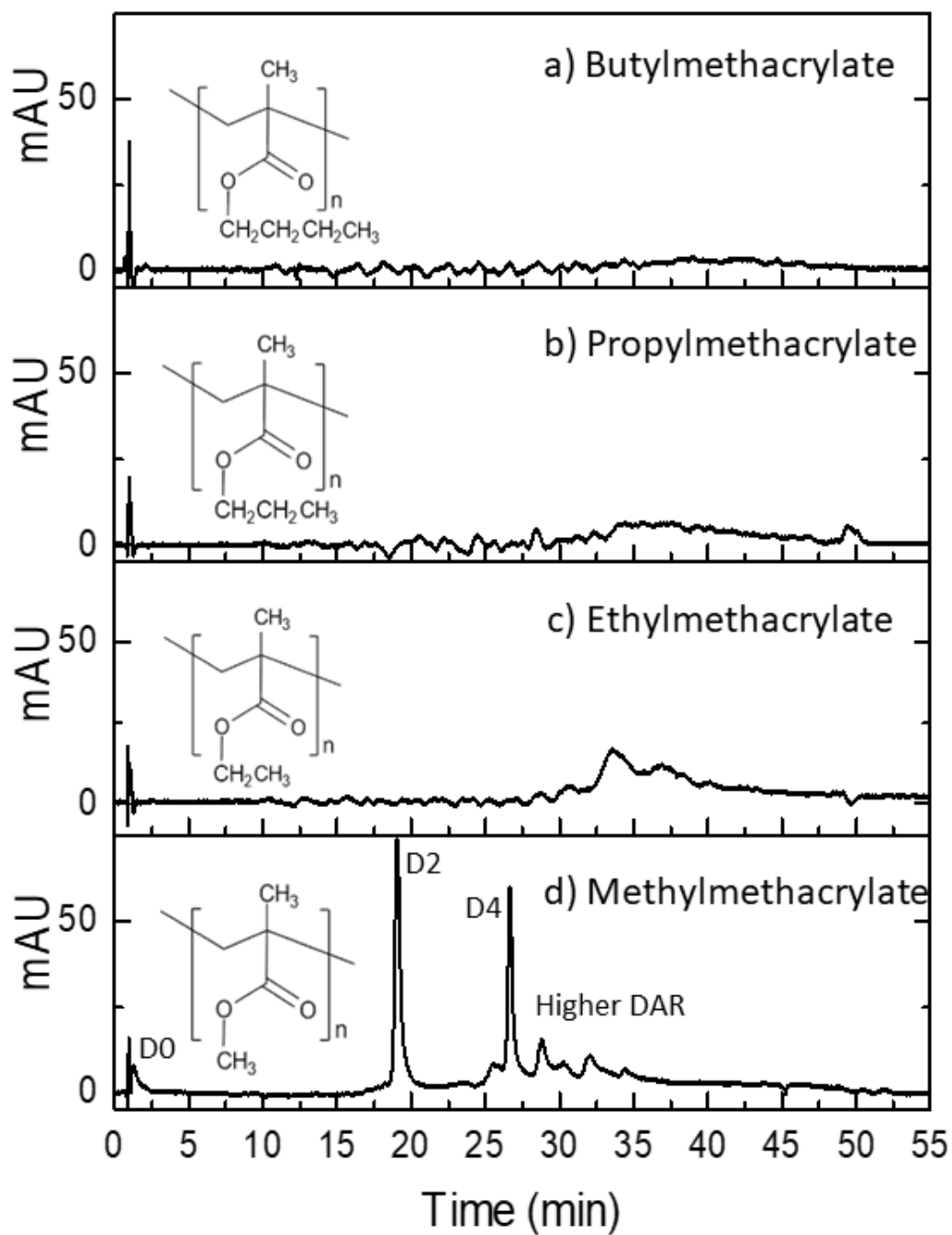


Figure 3.4. nRPLC of AbbVie model ADC with varying hydrophobicity of bonded phase, as denoted by the structures. Gradient conditions are A: 50 mM NH₄OAc, pH 7, B: 50 mM NH₄OAc, 50% IPA, pH 7, 0-100 %B /40 min, 100 %B /5 min, 100 μ L/min, 30 $^{\circ}$ C. The same tentative labels as for the HIC chromatogram of Figure 3.2d are made due to the similarity.

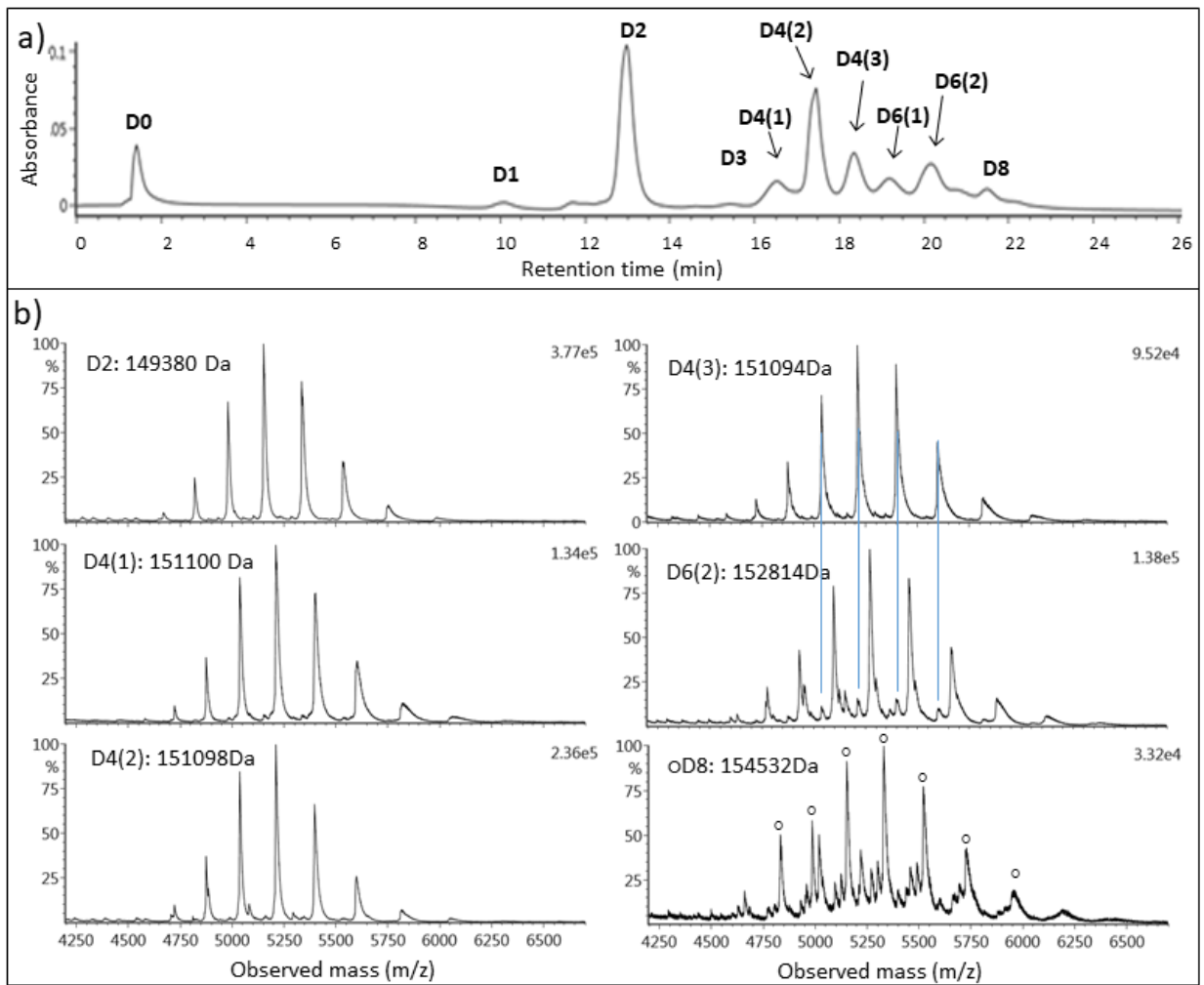


Figure 3.5. a) nRPLC of the AbbVie model ADC Ab095-PZ, with peaks labeled based on the mass spectra. Gradient: 0 to 4.5% IPA/water over 3 min., then 4.5 to 50% IPA/water over 20 min. Detection at 280 nm. b) Raw mass spectra for peaks as labeled, with the molecular weight based on deconvoluted mass spectra for peak ID. The blue lines show that extra peaks are from the overlap.

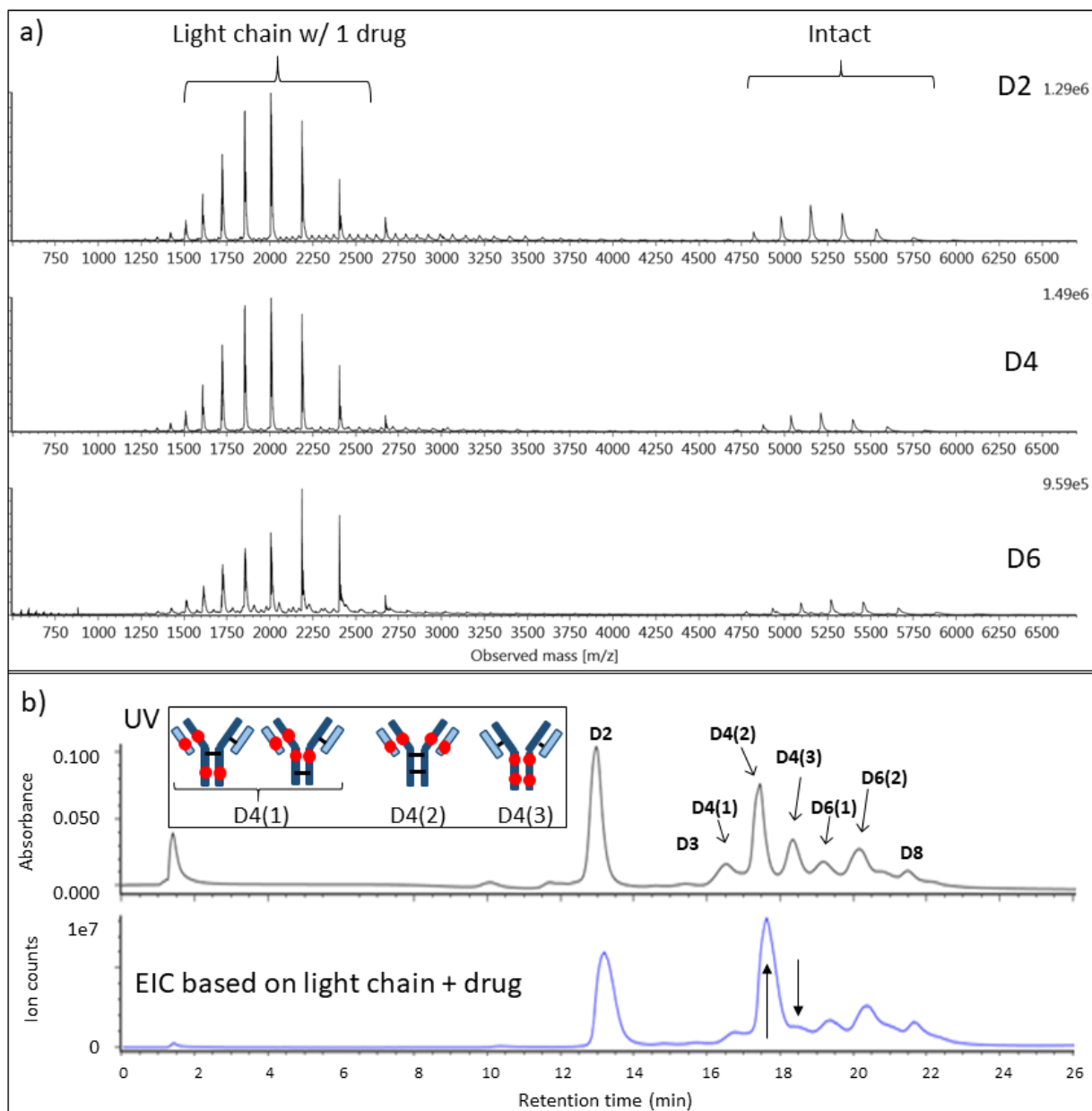


Figure 3.6. Evidence that light chain dissociates in MS source for AbbVie model ADC. a) Full-range raw mass spectra show large signals for light chain+drug, but no significant signals for ADC minus light chain+drug. b) Chromatogram with UV detection (top) and EIC based on light chain+drug (bottom). The blue arrows point to two peaks that changed intensities, and the inset depicts the structures for the isomers consistent with these intensity changes.

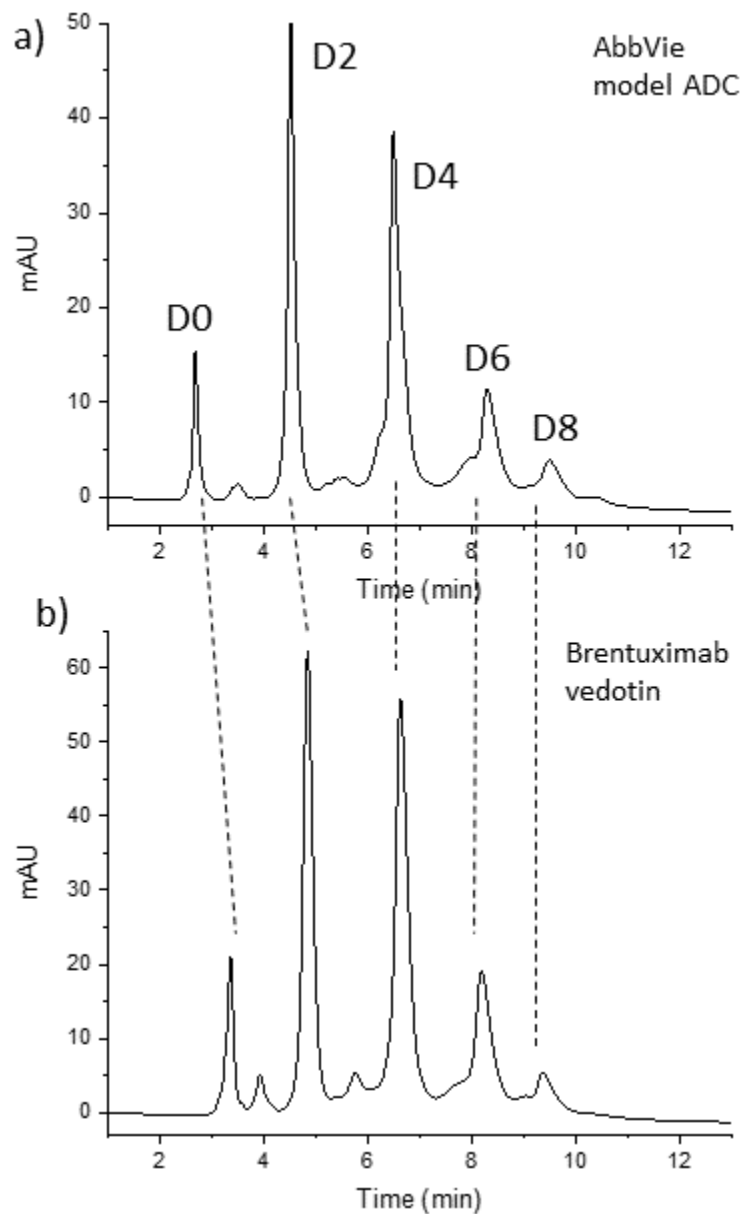


Figure 3.7. HIC separation of a) model ADC and b) commercial ADC Brentuximab vedotin. The dashed lines illustrate the greater hydrophobicity of the mAb itself for Brentuximab vedotin. Tosoh TSKgel Butyl-NPR, 4.6x35mm, 2.5 μ m. MPA: 1.5M ammonium sulfate, 25 mM sodium phosphate pH 7.0; MPB: 25 mM sodium phosphate pH 7.0 with 25% IPA; Flow rate: 0.8 mL/min; Column temp: 25 $^{\circ}$ C

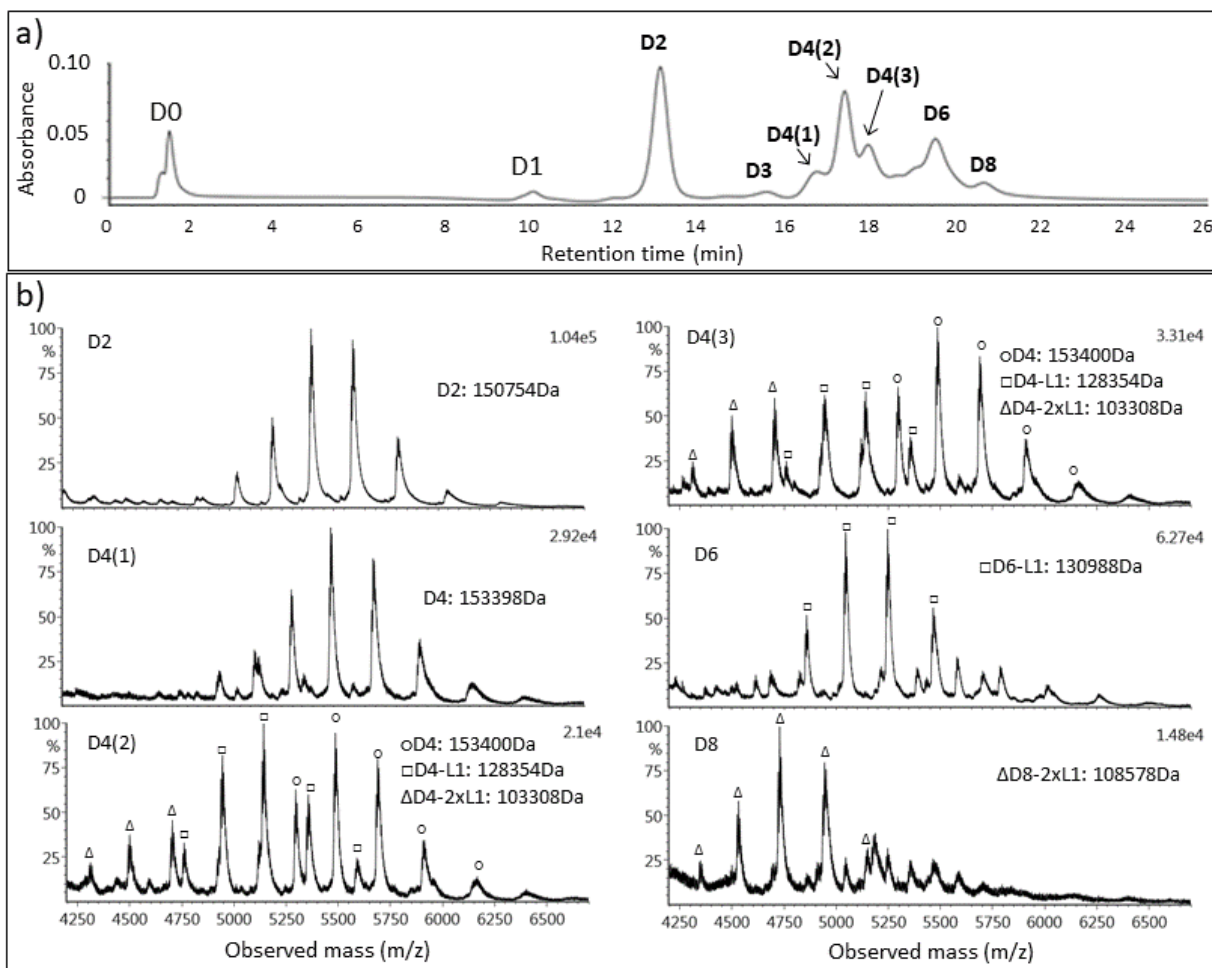


Figure 3.8. nRPLC and mass spectra for commercial ADC: brentuximab vedotin. a) nRPLC with detection at 280 nm. Conditions are the same as for Figure 2.6. b) Raw mass spectra for D2, D4(1,2,3), D6, D8, with the molecular weight based on deconvoluted mass spectra.

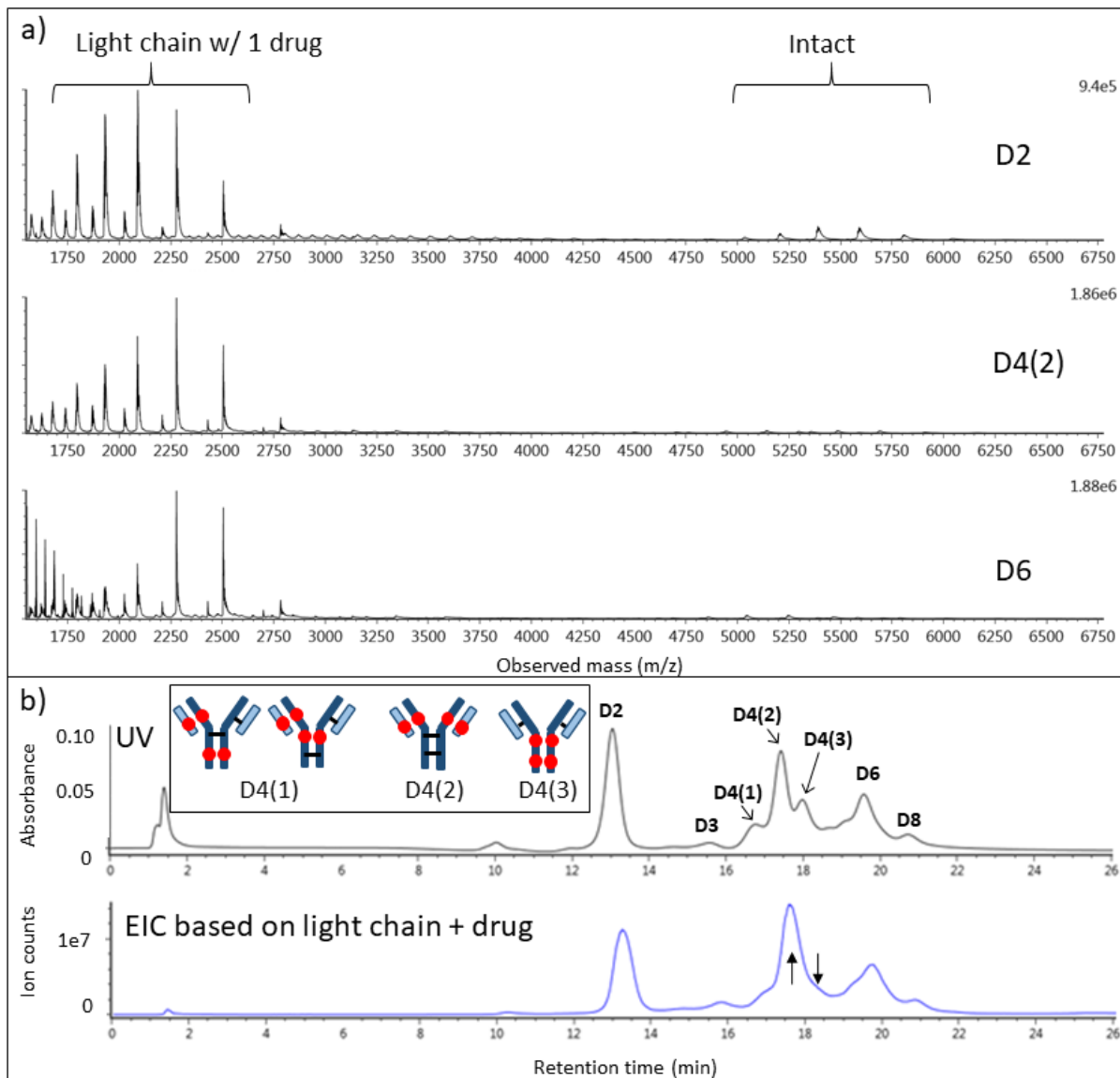
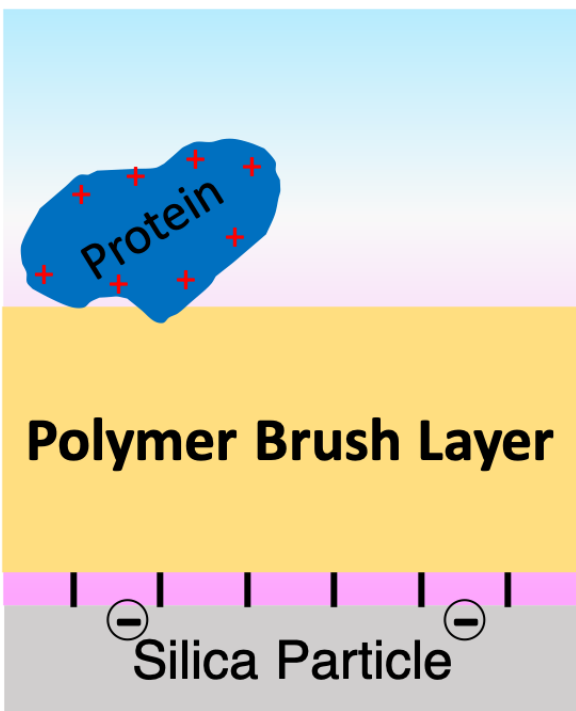


Figure 3.9. a) LCMS data for brentuximab vedotin, analogous to Figure 5. a) Full-range raw mass spectra show even stronger signals for light chain+drug than observed for the AbbVie model ADC. b) Chromatogram for UV detection (top) approximately tracks that of EIC for the signal of light chain+drug, again indicating light chain+drug dissociated after separation. Again, the blue arrows show two peaks that changed intensities, and the inset depicts the structures for the D4 isomers that are consistent with these changes.

RPLC, pH = 2.5



HIC, pH = 7

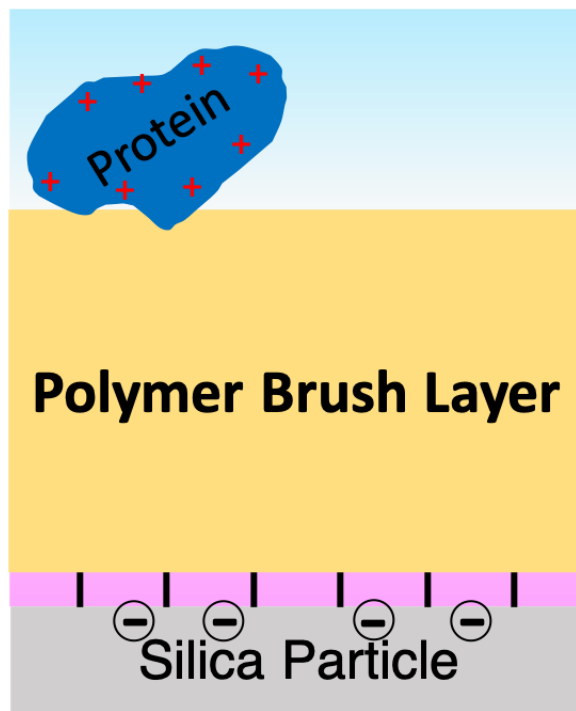


Figure 3.10. Illustration of the surface charge density in RPLC and HIC.

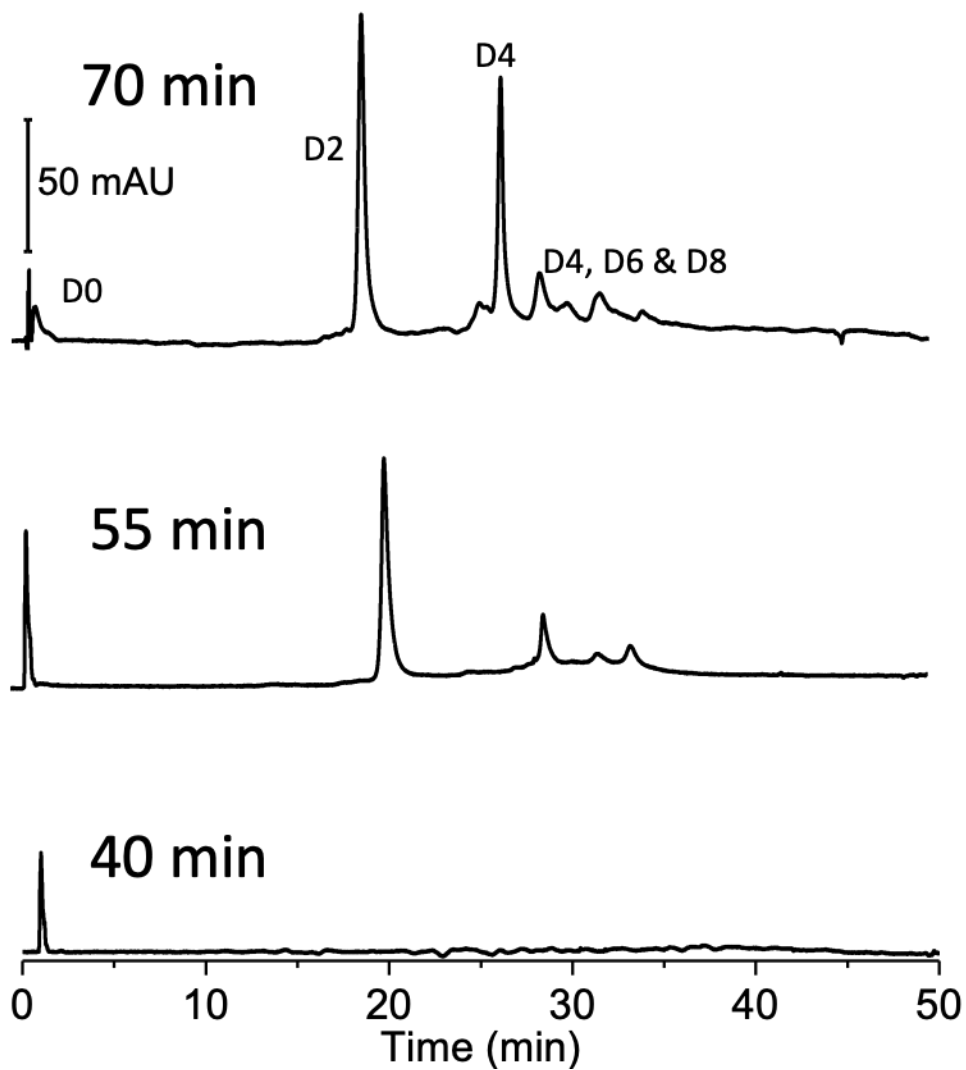


Figure 3.11. nRPLC chromatogram for varying PMMA growth time using the same non-denaturing conditions as in, showing that the 70 min growth time is optimal with respect to resolution and recovery. Polymer growth time is labeled in each panel.

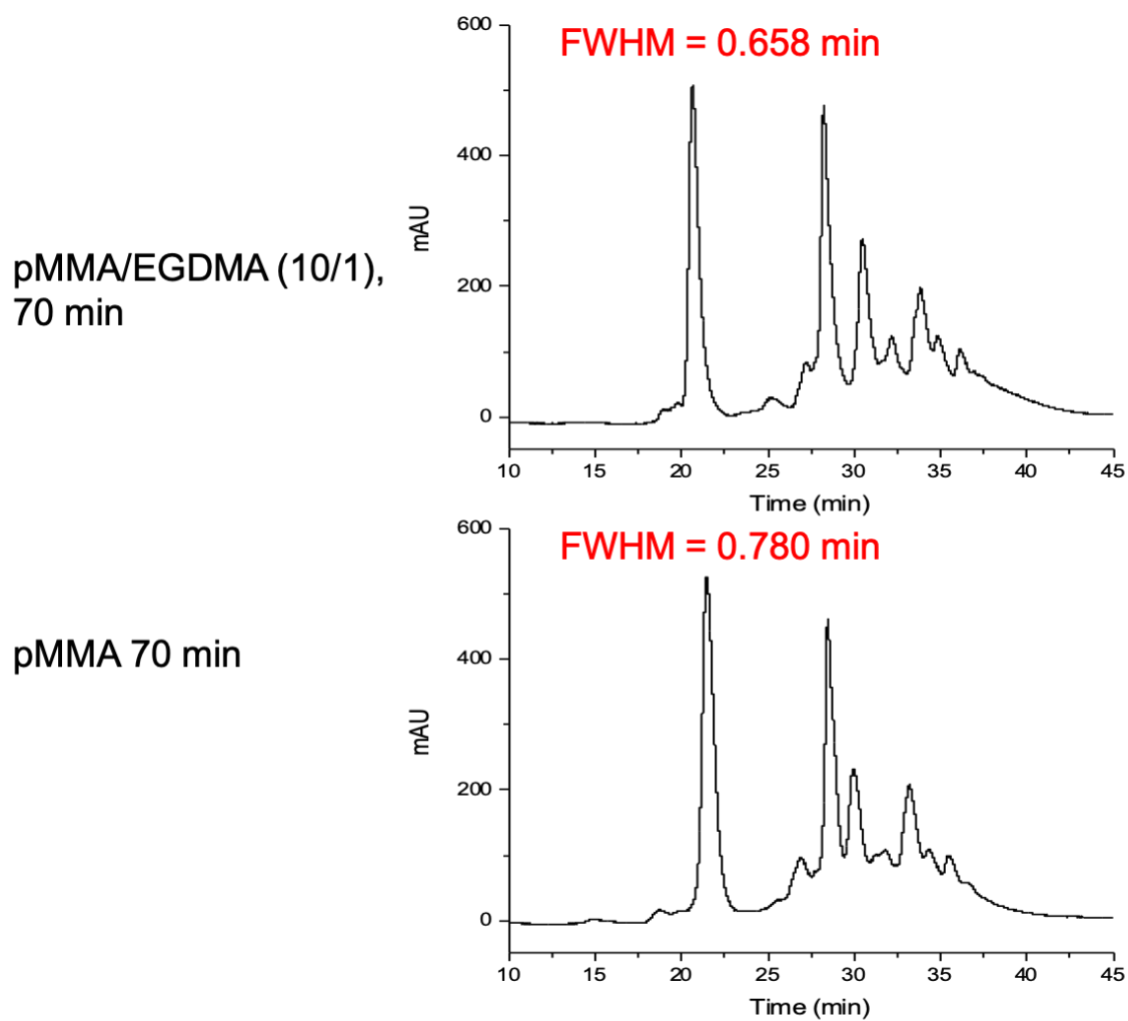


Figure 3.12. nRPLC chromatograms of the AbbVie model ADC using PMMA and crosslinked PMMA column. Gradient conditions are A: 25 mM NH₄OAc, pH 7, B: 25 mM NH₄OAc, 50% IPA, pH 7, 0-100 %B /40 min, 100 %B /5 min, 100 μ L/min, 30 $^{\circ}$ C.

CHAPTER 4. MEASUREMENT AND SIMULATION OF TAILING ZONES OF PROTEIN IN REVERSED-PHASE LIQUID CHROMATOGRAPHY

4.1 Introduction

Liquid chromatography coupled to mass spectrometry provides a robust method for the identification, characterization, and quantification of biomolecules, including peptides and proteins¹⁻³. However, peak tailing is still a widespread problem for the separation of peptides and proteins in reversed-phase liquid chromatography (RPLC)⁴. The physical origin of the peak tailing on silica-based materials in reversed-phase liquid chromatography of small molecules has been investigated previously. The ‘mixed-mode’ interaction with the combined effect of both the hydrophobic monolayer and the active silanols contributes to the analyte retention^{5,6}. Results show that the interaction with the rare, active silanol group on the silica surface causes overloading at low concentrations to give tailing⁷.

Chromatographic simulation are used here to understand the tailing behavior by revealing the adsorption isotherm and kinetics for separation in RPLC. The simplest models is the Langmuir adsorption isotherm, which has been studied extensively in gradient elution RPLC both for small molecules^{8,9} and large molecules like peptides¹⁰. More complicated models including bi-Langmuir isotherm¹¹, tri-Langmuir isotherm¹², quadri-Langmuir¹² isotherm, and S-shaped isotherm¹³ have been investigated as well. Physical constants of the bonded phase including the equilibrium constant, the surface coverage, and the desorption rate can be generated from the best-fit value of the simulation. The free energy distribution from interacting with different sites can be calculated to study the influence of the silanols¹⁴. Typically the model is based on the single-component system, while a more practical competitive adsorption model was built for the separation of multiple components¹⁵ and/or at the presence of an adsorbing additive¹⁶ as well. The fundamental work of chromatographic simulation provides a quantitative understanding of the tailing behavior in both isocratic elution and gradient elution of RPLC. The simulation work offers an accurate and rapid procedure for predicting the individual band profiles in preparative scale chromatography which can reduce the number of experiments needed and save a considerable amount of chemicals¹⁷. It has also been applied to optimize the workflow for Simulated Moving Bed (SMB)

technology, which has been extremely successful in chiral separations in the fine chemical and pharmaceutical industries¹⁸. The knowledge of the interaction with the silanols also provides valuable insights for making better bonded phase materials. The silanol activity is measured for several RPLC columns to compare the peak tailing behaviors¹⁹. The invention of Type B silica greatly improves the performance of chromatographic separation by increasing the density of surface silanols to better form a hydrogen bond network and decrease the isolated silanols⁷.

It is not known, a priori, whether the retention of proteins can be described by a simple bi-Langmuir adsorption isotherm. This chapter shows that a protein, ribonuclease A, does indeed behave in accord with the two site model. This enables its use in studying differences in two common types of particle morphologies used in RPLC columns.

Different stationary phase morphologies have been developed to improve the performance of protein characterization with liquid chromatography²⁰. Among all the advancements, the application for superficially porous particles (SPP) has a serious impact on liquid chromatography separations. The improved packed bed homogeneity and mass transfer property of superficially porous particles account for the superior performance compared with the traditional fully porous particles (FPP). In this report, the chromatographic simulation is used to study the retention model and peak tailing behavior of a model protein in RPLC separation using both the SPP C4 column and the FPP C4 column. The acidic modifier and the mobile phase composition are varied to investigate the effect on the adsorption parameters. The chromatographic performance and the simulated parameters of the SPP C4 column and the FPP C4 column are compared in the same condition as well.

4.2 Materials and methods

4.2.1 Materials

Difluoroacetic acid (DFA, 98%), trifluoroacetic acid (TFA, 99%), benzene (analytical standard), toluene (analytical standard), ethylbenzene (analytical standard), propylbenzene (analytical standard), butylbenzene (analytical standard), ribonuclease A from bovine pancreas (RNase A, 13.7 kDa), Microparticle size standard based on polystyrene monodisperse (0.1 μm) were

purchased from Sigma–Aldrich (St. Louis, MO). NativeMark™ (720, 1048 and 1236 kDa) unlabeled protein standards were purchased from Thermo Fisher Scientific (Waltham, MA). A sample of pharmaceutical-grade monoclonal antibody IgG4 was provided by Eli Lilly (Indianapolis, IN). Acetonitrile (ACN) from Fisher Scientific (Hampton, NH) was used as well. Ultrapure water was obtained from a Milli-Q system (MilliporeSigma, Darmstadt, Germany.)

4.2.2 Chromatographic conditions

The RPLC separation was performed on a Waters Acquity UPLC I-Class (Waters, Milford, MA). A commercial superficially porous particle (SPP) C4 column, HALO protein (2.1 × 100 mm. 2.7 μm, 1000 Å, Advanced Materials Technology, Wilmington, DE) and a commercial fully porous particle (FPP) C4 column, ACQUITY UPLC Protein BEH C4 (2.1 × 100 mm. 1.7 μm, 300 Å, Waters Corporation, Milford, MA) were used as the analytical columns for separation. Mobile phase A (MPA) and B (MPB) were water and acetonitrile, with different percentages of TFA, DFA as acidic modifiers. The gradient is detailed in the result and discussion section. UV absorbance wavelength was set to 280 nm. The column temperature was set at 30 °C.

For studying the concentration dependence, RNase A protein was prepared in water/ACN solution that matched the separation running condition. The injection volume was 5 μL with a full loop injection mode and the flow rate was 0.2 mL/min. The injected concentration of RNase A was 0.025, 0.05, 0.1, 0.25 and 0.5 mg/mL. For studying the flow rate dependence, the injection concentration was 0.025 mg/mL. The flow rate was set at 0.1, 0.15, 0.2, 0.25, 0.3 and 0.4 mL/min to generate the chromatograms. For measuring the phase ratio, benzene, toluene, ethylbenzene, propylbenzene and butylbenzene were diluted 100 X with water/ACN solution that matched the separation running condition. The injection volume was 5 μL and the flow rate was 0.2 mL/min. The retention time for each of the analytical standard was used for the calculation of phase ratio. For studying the pore accessibility of the SPP C4 and FPP C4 column, the protein and polystyrene microparticles are prepared in water/ACN (1:1) solution. The mobile phase is acetonitrile/water (v/v) with 0.1% TFA to ensure that the analyte was not retained on the stationary phase.

4.2.3 Simulation

Fortran software for the simulations was kindly donated by Professor Georges Guiochon of the University of Tennessee. A bi-Langmuir adsorption isotherm with two sites of interaction was used to model the analyte retention on the stationary phase. The equilibrium-dispersive model was used to account for the zone broadening from all sources under the assumption that analyte absorption and desorption is a fast process^{21, 22}. We translated the code for the operation with the computer program MATLAB R2018b. There are five independent parameters in the chromatographic simulation program, the equilibrium constant for the strong site, the saturated surface coverage of the strong site in relation to the total saturated surface coverage of all sites, the equilibrium constant for the weak site, the number of the theoretical plates, the desorption rate, and the phase ratio²³. To determine the best-fit parameters, a previously published procedure was followed while some adjustments were made to the original code¹¹. The equilibrium constant for the strong sites was systematically varied from 10000 to 150000 and the corresponding fraction of the strong sites were then optimized to fit the experimental data. The summation of the fraction of the strong sites and weak sites was 100%. The equilibrium constant for the weak sites can be calculated from the retention time. The desorption rate for the strong sites and the weak sites were set to be the same, giving a net desorption rate. and was determined from the slopes of the Van Deemter plots using RNase A solutions with the lowest concentration. The intrinsic column efficiency, which is the A term in the van Deemter equation, was calculated from the same Van Deemter plots.

4.3 Results and discussions

Figure 4.1 shows the chromatograms of RNases A at five different injected concentrations, 0.025, 0.05, 0.1, 0.25 and 0.5 mg/mL with the fully porous C4 column with 0.1% TFA present in the mobile phase. The retention time becomes smaller with higher injection concentration, which is a known phenomenon that indicates nonlinear tailing is occurring. The chromatogram with the lowest concentration, 0.025 mg/mL, in Figure 4.2 demonstrates that the peak becomes symmetric at sufficiently low concentration. Two peaks are observed in the chromatogram; yet baseline separation of the peaks is achieved within the concentration range used in this study, hence the earlier peak does not interfere. The second peak is then used for the chromatographic simulation.

Figure 4.3 shows the chromatograms of the same set of RNases A samples with the superficially porous C4 column under the same mobile phase condition. Chromatographic simulations will be done on both of the columns to study the peak tailing behavior and compare with separation with different column and under different conditions. Details of calculating and optimizing the simulation parameters are discussed next.

4.3.1 Phase ratio measurement

The separation process in RPLC is considered to occur by partitioning^{24, 25}. The observed retention factor k_j for a compound j can be related to the equilibrium constant K_j that governing the partition equilibrium of j between the mobile phase and stationary phase²⁶.

$$k_j = K_j \phi$$

ϕ is the phase ratio that defined as the ratio between the volume of the stationary phase and the volume of the mobile phase, which is the void volume of the column as well, for common HPLC columns.

$$\phi = \frac{V_{st}}{V_0}$$

Here a previously reported method is used to determine the phase ratio of the column. It is based on the measurements of retention factors k for several hydrocarbons in a homologous series, along with the values for octanol/water partition coefficients K_{ow} for the same compounds^{27, 28}. The following equation is used to calculate the phase ratio.

$$\log k_j = a \log K_{ow} + \log \phi$$

The octanol/water partition coefficients and the measure retention factor for both the SPP C4 column and the FPP C4 column are summarized in Table 4.1. The phase ratio for the SPP C4 calculated from the table is 0.06902 while the phase ratio for the FPP column is 0.171. The calculated phase ratio shows a good agreement with the BET surface area for the 2.7 μm superficially porous particle and 1.7 μm fully porous particles that fully porous particles typically have larger surface area²⁹. The measurement for the phase ratio based on the retention factor for these small molecules is overestimated for proteins due to size exclusion. RNase A protein, the model protein used in this study, is 13.6 kDa in size and much larger than the traditional small molecule. Larger analytes have less access to the free volume inside pores, leading to the loss of

accessible surface area. To remedy this, pore accessibility is calculated based on the injection time for analyte with different sizes assuming the smallest analyte can access all the pore volume while the largest one has no pore access. The calculated pore accessibility for RNase A on the SPP C4 column and FPP C4 column are 74.6% and 49.1%, respectively, in agreement with the wider average pore size reported for the SPP column. While the average pore sizes for both columns are larger than the diameter of the protein, the pore-size distribution of the superficially porous particle as reported is skewed toward larger pores³⁰. From these measurements, the actual phase ratio for RNase A is then calculated to be 0.05147 for the SPP C4 column and 0.0840 for the FPP C4 column. These are used as input parameters for the simulations.

4.3.2 Van Deemter plot

Van Deemter equation summarizes the flow and kinetic parameters that contribute to the theoretical plate height H , which is proportional to peak variance.

$$H = A + \frac{B}{v} + Cv$$

The term v is the flow velocity. A term represents the contribution to the broadening that are independent of the flow rate. B term is from the diffusion along the separation axis. C term is from the slow mass transfer. Figure 4.4 shows the Van Deemter plot for the SPP C4 column and the FPP C4 column based on the flow rate study. The plate height H has a linear dependence on the mobile phase flow velocity, which indicates negligible contribution of the B term in the equation. The diffusion coefficient of the protein in the mobile phase is small, thus the calculated contribution from B/v is below the noise on a van Deemter plot. Then C term for both the SPP C4 column and FPP C4 column can be calculated from the van Deemter plot. For the flow velocity of the simulated chromatograms, which is 100 cm/min, the C term dominates the zone broadening. The maximum column efficiency is calculated from extrapolating the van Deemter plot to zero velocity.

4.3.3 Optimization of the simulation parameters

As shown in Figure 4.1, the peak retention time begins to shorten noticeably between 0.025 and 0.1 mg/mL indicates that the equilibrium constant for the site being saturated is between $1/(32.5 \mu\text{M})$ and $1/(7.9 \mu\text{M})$, i.e., between 30,000 and 130,000. Based on the relationship between the retention factor and the equilibrium constant, for $K \geq 30000$, the retention time is estimated to be

1600 min for the SPP C4 column and 2600 min for the FPP C4 column if there were only one type of adsorption site. The actual retention time observed is 6.7 min for the SPP C4 column and 6.5 min column. This demonstrates that there must be at least two sites, and the strong site with a high equilibrium constant that causes the non-linear tailing must be very rare to enable such early retention. The low equilibrium constant of the abundant weak site corresponds to a short retention time.

For the chromatographic simulations for the protein require a model describing the retention of the protein on the column, the simplest model is preferred. As discussed previously, the one-site Langmuir adsorption isotherm is not a suitable model. Bi-Langmuir adsorption isotherm is the next simplest model with the expression as following.

$$\Gamma = \Gamma_{strong,sat} \frac{K_{strong}c}{1 + K_{strong}c} + \Gamma_{weak,sat} \frac{K_{weak}c}{1 + K_{weak}c}$$

K is the equilibrium constant and c is the analyte concentration and $\Gamma_{strong,sat}$ and $\Gamma_{weak,sat}$ are the saturated surface coverage for the strong site and weak site. Physically, this means that there is a narrow distribution of equilibrium constants for the desired reversed-phase retention mechanism, e.g, a preferred orientation of the adsorbed protein, and a narrow distribution of equilibrium constants for the strong site, e.g., a preferred moiety of the protein interacting with active silanol sites. While the two-site model describes nearly perfectly the tailing zones of a small cationic dye in RPLC₁₁, It is not obvious that it would work for a protein.

The chromatogram of the lowest concentration sample where the peak is symmetric can also be used to estimate the desorption rate of the strong and weak site. Without non-linear tailing caused by the overloading, the slow desorption is the major contributor to the peak broadening. Figure 4.5 shows the simulated chromatogram overlaid with the experimental data. The desorption rate to generate the simulated chromatogram is labeled on the graph, while the rest of the simulation parameters are the same. We can see that fast desorption from the stationary phase makes the peak sharper. Then the desorption rates for the strong site and the weak site are optimized to be 450 min^{-1} for the FP C4 column. Another observation is that the effect of the desorption rate for the strong site and weak site on peak broadening are not linearly independent, therefore, for the chromatographic simulation, the desorption rate is kept the same for the two sites.

The best-fit parameters were first determined for the FPP C4 column with 0.1% TFA by systematically increasing the value of K_{strong} starting at 15,000. The simulated chromatograms are shown to fit well, although not perfectly, to the experimental chromatograms as shown in Figure 4.6. This means that the two site model is a good approximation for describing retention of this protein in RPLC. The lack of perfect agreement is most likely due to there being a multiple ways the protein can interact with hydrophobic and or charged silanol sites. Nonetheless, the agreement is remarkable and is sufficient to provide insight. The raw data show that the SPP column exhibits more overloading, and the fitting parameters indicates, as expected, that this owes to either more strong sites or a higher equilibrium constant for the strong sites. Due to the imprecise fit, there is a range of best-fit parameters shown in Table 4.2. Since both columns are silica based, with attached hydrophobic groups, we make the reasonable assumption that the ratio K_{strong}/K_{weak} is the same for both columns. There is only one set of parameters for the two types of columns that gives the same ratio, and that set has $K_{strong} = 80000$ and $K_{weak} = 50$, with a ratio of 1700. With this interpretation, the SPP column has about four times as many strong adsorption sites, explaining the greater amount of overloading.

Simulations under varying conditions can provide further insight into RPLC of the protein. First, the overloading behavior of protein under different mobile acidic modifiers is studied. TFA and DFA are added to the mobile phase while the pH is kept constant to be 1.95. In order to get the same retention factor for the two conditions, less organic solvent (B%) is needed for DFA. This demonstrates the ion-pairing effect of TFA could increase the hydrophobicity of the protein, thus more ACN is required for elution. We can no longer make the assumption that the ratio K_{strong}/K_{weak} is constant, of course. To obtain a unique set of parameters, we can make the assumption that the number of active silanols is unchanged. Active silanols are sites of topographical asperities that prevent silanols from hydrogen bonding with neighbors, hence they are available to hydrogen bond to the protein. Their abundance would not be changed by the mobile phase composition. While it is not known if they are acidic, maintaining the same pH ensures that their charge state is not changed. Shown in Figure 4.7 are the chromatograms of RNase A obtained with TFA and DFA while the simulated chromatograms are overlaid. The fraction of the strong sites is kept constant for comparing the best-fit parameters summarized in Table 4.3 because the

pH of the mobile phase is the same. The equilibrium constant for the weak site decreases with DFA agrees with the weak ion-pairing effect of DFA. However, the equilibrium constant for the strong site increases with DFA, which indicates the strong ion pairing effect does not only increase the hydrophobicity of the analyte but also masks the positive charge on the analyte and shields the electrostatic interactions^{31, 32}. The negatively charged counter ion TFA^- will neutralize the positive charge on the protein arising from the basic side chains including arginine (Arg), lysine (Lys), and histidine (His). The weak ion pairing effect of the DFA which results in a large equilibrium constant for the strong sites causes more peak tailing in the separation using DFA.

Second, the overloading behavior of protein under different organic composition is studied to determine the change in the retention behavior. The mobile phase composition is varied from 24.8%, 24.6%, 24.4%, 24.2% to 24.0% ACN while 0.1% TFA is used for all the chromatograms. As the organic percentage decreases in the mobile phase, the retention time of the peak increases, and more overloading is observed. The results for chromatographic simulation are presented in Figure 4.8 with the best-fit parameters summarized in Table 4.4. The fraction of the strong sites is kept constant since the pH of the mobile phase is the same. The equilibrium constants for the strong sites and weak sites are both increasing with less ACN. The interpretation is that adsorption to the strong site also involves hydrophobic interactions between the protein and the hydrocarbon moiety, as originally shown by Bidlingmeier.

Information about the strength for the interaction between protein and strong site can be inferred. The linear solvent strength model was developed to describe the change in the retention of an analyte with the concentration of organic modifier, φ , typically expressed as the volumetric fraction of the strong solvent^{33, 34}.

$$\ln k = \ln k_0 - S\varphi$$

k_0 is the retention factor of analyte in water, which is the weak solvent in RPLC, and S describes the elution strength for the strong solvent, which is known as the solvent strength parameter for the LSS model. The equilibrium constants of the strong sites and weak sites are plotted against the concentration of the organic modifier in Figure 4.9. The organic solvent dependence for both of the equilibrium constant described by an exponential equation. This reveals that free energy of interaction between the protein and the strong adsorption site will contain a contribution from the

interaction of the protein with the nearby hydrocarbon group, i.e. C4 group for the column in this project. However, the slope of K_{strong} and K_{weak} vs φ is different by 6% which is larger than the error caused by the linear fitting. Assuming the interaction with the active silanol shouldn't change with the concentration of the organic modifier, the contribution of K_{weak} when protein is adsorbed onto the strong site is corrected. The free energy of interaction of the protein with the isolated silanol can be calculated by subtraction.

$$\Delta G_{SiOH} = \Delta G_{strong} - a\Delta G_{weak} = RT\ln K_{strong} - aRT\ln K_{weak}$$

The calculated ΔG_{SiOH} is 19kJ/mol which is the free energy of the electrostatic interaction with the isolated silanols.

Other insights can be obtained from the van Deemter plots and the simulations. Chromatographic simulations are performed to study the surface chemistry and the overloading behavior on the SPP C4 column for comparison as well. Comparing the van Deemter plot for the SPP C4 column and FPP C4 column, the A term which is the Eddy diffusion term is smaller with the SPP C4 column. The underlying improved packing homogeneity could be attributed to the narrower particle size distribution^{35, 36}, and higher surface roughness³⁷ for the superficially porous particles. The C term which is the mass transfer term represented by the slope of the curve is smaller on the FPP C4 column. Although the diffusion distance is reduced due to the presence of the solid core in the superficially porous particle, the magnitude of this contribution to the total plate height is proved to be rather small³⁸. The rate constant for protein diffusion into the shell is much larger than that of its diffusion into the stagnant mobile phase impregnating the particle pores from the mobile phase outside the pores. The rate of transferring protein into the pores is related to the average and pore size distribution. The pore sizes for both the SPP C4 column, 1000 \AA , and the FPP C4 column, 300 \AA are considerably larger than the size of RNase A₃₀, therefore, the rate constant should be similar for the two columns. This leaves the slow desorption from the stationary phase to be the major contributor to the plate height. Chromatographic simulations are used to compare the overloading of RNases A on the SPP C4 and FPP C4 column under the same mobile phase condition with experimental chromatograms shown in Figure 4.1 and Figure 4.3. Figure 4.10 shows the overlaid graph. More overloading is observed with the SPP C4 column as the change in the retention time is larger and peaks become more asymmetric. The best-fit parameters are summarized in Table 4.5. The results show that the desorption rate is higher on the FPP C4 column

which agrees with the smaller C_4 term calculated from the van Deemter plot. Besides, the fraction of the strong site on both columns is really small, less than 1%. The fraction of the strong site is almost four times higher on the SPP C4 column and the presence of more strong sites leads to more peak tailing in the SPP C4 column.

4.4 Conclusion

Simulations of the chromatograms of the RNases have been performed to study the retention mode and the tailing behaviors of proteins in reversed-phase liquid chromatography separation. A bi-Langmuir adsorption isotherm describes the retention of protein in RPLC with the presence of strong sites and weak sites in the stationary phase. Compared with the fully porous C4 column, more overloading is observed for the chromatogram with the superficially porous C4 column. The fewer number of the strong sites on the FPP C4 column leads to less tailing behavior for protein peaks in reversed-phase liquid chromatography. When the percentage of acetonitrile in the mobile phase is varied, the ratio $K_{\text{Strong}}/K_{\text{Weak}}$ remains approximately constant, supporting the interpretation that the electrostatic contribution is constant at a give pH and the hydrophobic contribution is variable with percent acetonitrile. The ion-pairing effect of TFA reduce peak tailing by masking the positive charge group on protein to decrease the equilibrium constant for the interaction with the strong site. The equilibrium constant for the weak site is relatively unchanged between TFA and DFA. Chromatographic simulation is used to compare the performance of two commercial C4 columns.

4.5 Future work

For this project, RNases A is used as the model protein because there are only a few variants in RNases A. Baseline separation for the major peak can be achieved in RPLC within the concentration range. For the two columns used as a comparison in this project, the pore size is considered to be much larger than the size of the protein. Therefore, the actual pore size doesn't matter. The superficially porous particles with 1000 Å pores are shown to have better performance for larger molecule separation including monoclonal antibodies, DNA fragments and polymers^{30, 39}. Therefore, the chromatographic simulation can be applied to study the overloading behavior of large molecules with the wide pore superficially porous particle as well.

As has been discussed in Chapter 2 and Chapter 3, a novel stationary phase based on the polymer brush layer bonded silica is developed by our group to improve the separation performance for large protein including antibody and antibody-drug conjugates. Chromatographic simulation can be applied to study the retention model and the peak tailing behavior on the polymer shell bonded phase as well. Preliminary data reveal that the resolution of the polymer shell bonded phase shows a strong dependence on the thickness of the polymer brush layers shown in Figure 4.11. When the polymer thickness increases from 9 nm to 34 nm, the peak width becomes narrower and less tailing is observed. In addition, peak retention time decreases. This could be explained by the decreased equilibrium constant of the strong site. Since the distance-dependent electrostatic interaction with the active silanol contributes to the adsorption of the strong site, the equilibrium constant will decrease with a thicker polymer. While the difference with the 46 nm polymer layer can be attributed to the increased interaction with the polymer brush layer due to the tangling between the polymer and protein molecules. Overloading experiments are needed for polymer shell bonded columns with different polymer thickness to get a better understanding of the adsorption isotherm on the column.

4.6 Reference

1. Ali, I.; Aboul-Enein, H. Y.; Singh, P.; Singh, R.; Sharma, B., Separation of biological proteins by liquid chromatography. *Saudi Pharmaceutical Journal* 2010, 18 (2), 59-73.
2. Rauh, M., LC-MS/MS for protein and peptide quantification in clinical chemistry. *Journal of Chromatography B* 2012, 883, 59-67.
3. Delahunty, C.; Yates Iii, J. R., Protein identification using 2d-lc-ms/ms. *Methods* 2005, 35 (3), 248-255.
4. Hancock, W. S., *Handbook of HPLC for the separation of amino acids, peptides, and proteins*. 1984.
5. Cox, G. B., The influence of silica structure on reversed-phase retention. *Journal of Chromatography A* 1993, 656 (1-2), 353-367.
6. Bij, K. E.; Horváth, C.; Melander, W. R.; Nahum, A., Surface silanols in silica-bonded hydrocarbonaceous stationary phases: II. Irregular retention behavior and effect of silanol masking. *Journal of Chromatography A* 1981, 203, 65-84.

7. Köhler, J.; Kirkland, J., Improved silica-based column packings for high-performance liquid chromatography. *Journal of Chromatography A* 1987, 385, 125-150.
8. El Fallah, M. Z.; Guiochon, G., Comparison of experimental and calculated results in overloaded gradient elution chromatography for a single-component band. *Analytical Chemistry* 1991, 63 (9), 859-867.
9. Stanley, B. J.; Krance, J.; Roy, A., Determination of the thermodynamic contribution to peak asymmetry of basic solutes in reversed-phase liquid chromatography. *Journal of Chromatography A* 1999, 865 (1-2), 97-109.
10. Marchetti, N.; Dondi, F.; Felinger, A.; Guerrini, R.; Salvadori, S.; Cavazzini, A., Modeling of overloaded gradient elution of nociceptin/orphanin FQ in reversed-phase liquid chromatography. *Journal of Chromatography A* 2005, 1079 (1-2), 162-172.
11. Wirth, M. J.; Smith, E. A.; Anthony, S. R., Measurement and simulation of tailing zones of a cationic dye in analytical-scale reversed phase chromatography. *Journal of Chromatography A* 2004, 1034 (1-2), 69-75.
12. Gritti, F.; Guiochon, G., Physical origin of peak tailing on C18-bonded silica in reversed-phase liquid chromatography. *Journal of Chromatography A* 2004, 1028 (1), 75-88.
13. Guiochon, G.; Golshan-Shirazi, S.; Jaulmes, A., Computer simulation of the propagation of a large-concentration band in liquid chromatography. *Analytical Chemistry* 1988, 60 (18), 1856-1866.
14. Neue, U. D.; Tran, K.; Méndez, A.; Carr, P. W., The combined effect of silanols and the reversed-phase ligand on the retention of positively charged analytes. *Journal of chromatography A* 2005, 1063 (1-2), 35-45.
15. Åsberg, D.; Leško, M.; Enmark, M.; Samuelsson, J.; Kaczmarek, K.; Fornstedt, T., Fast estimation of adsorption isotherm parameters in gradient elution preparative liquid chromatography. I: The single component case. *Journal of Chromatography A* 2013, 1299, 64-70.
16. Åsberg, D.; Leško, M.; Leek, T.; Samuelsson, J.; Kaczmarek, K.; Fornstedt, T., Estimation of nonlinear adsorption isotherms in gradient elution RP-LC of peptides in the presence of an adsorbing additive. *Chromatographia* 2017, 80 (6), 961-966.
17. Golshan-Shirazi, S.; Guiochon, G., Modeling of preparative liquid chromatography. *Journal of Chromatography A* 1994, 658 (2), 149-171.
18. Abel, S.; Mazzotti, M.; Morbidelli, M., Solvent gradient operation of simulated moving beds: 2. Langmuir isotherms. *Journal of chromatography A* 2004, 1026 (1-2), 47-55.
19. Mendez, A.; Bosch, E.; Roses, M.; Neue, U. D., Comparison of the acidity of residual silanol groups in several liquid chromatography columns. *Journal of Chromatography A* 2003, 986 (1), 33-44.

20. Astefanei, A.; Dapic, I.; Camenzuli, M., Different stationary phase selectivities and morphologies for intact protein separations. *Chromatographia* 2017, 80 (5), 665-687.
21. Dondi, F.; Guiochon, G., Theoretical advancement in chromatography and related separation techniques. Springer Science & Business Media: 2012; Vol. 383.
22. Wang, H.; Harris, J. M., Surface diffusion of organosiloxane ligands covalently bound to silica. *Journal of the American Chemical Society* 1994, 116 (13), 5754-5761.
23. Smith, E. A.; Wirth, M. J., pH dependence of tailing in reversed-phase chromatography of a cationic dye: measurement of the strong adsorption site surface density. *Journal of Chromatography A* 2004, 1060 (1-2), 127-134.
24. Dill, K. A., The mechanism of solute retention in reversed-phase liquid chromatography. *Journal of physical chemistry* 1987, 91 (7), 1980-1988.
25. Vailaya, A.; Horváth, C., Retention in reversed-phase chromatography: partition or adsorption? *Journal of Chromatography A* 1998, 829 (1-2), 1-27.
26. Moldoveanu, S. C.; David, V., Essentials in modern HPLC separations. Newnes: 2012.
27. Moldoveanu, S.; David, V., Estimation of the phase ratio in reversed-phase high-performance liquid chromatography. *Journal of Chromatography A* 2015, 1381, 194-201.
28. Caiali, E.; David, V.; Aboul-Enein, H. Y.; Moldoveanu, S. C., Evaluation of the phase ratio for three C18 high performance liquid chromatographic columns. *Journal of Chromatography A* 2016, 1435, 85-91.
29. DeStefano, J. J.; Schuster, S. A.; Lawhorn, J. M.; Kirkland, J. J., Performance characteristics of new superficially porous particles. *Journal of Chromatography A* 2012, 1258, 76-83.
30. Wagner, B. M.; Schuster, S. A.; Boyes, B. E.; Shields, T. J.; Miles, W. L.; Haynes, M. J.; Moran, R. E.; Kirkland, J. J.; Schure, M. R., Superficially porous particles with 1000 Å pores for large biomolecule high performance liquid chromatography and polymer size exclusion chromatography. *Journal of Chromatography A* 2017, 1489, 75-85.
31. Shibue, M.; Mant, C.; Hodges, R., Effect of anionic ion-pairing reagent hydrophobicity on selectivity of peptide separations by reversed-phase liquid chromatography. *Journal of chromatography A* 2005, 1080 (1), 68-75.
32. Shibue, M.; Mant, C.; Hodges, R., Effect of anionic ion-pairing reagent concentration (1–60 mM) on reversed-phase liquid chromatography elution behaviour of peptides. *Journal of Chromatography A* 2005, 1080 (1), 58-67.
33. Valkó, K.; Snyder, L. R.; Glajch, J. L., Retention in reversed-phase liquid chromatography as a function of mobile-phase composition. *Journal of Chromatography A* 1993, 656 (1-2), 501-520.

34. Snyder, L. R.; Kirkland, J. J.; Dolan, J. W., Introduction to modern liquid chromatography. John Wiley & Sons: 2011.
35. Fanigliulo, A.; Cabooter, D.; Bellazzi, G.; Tramarin, D.; Allieri, B.; Rottigni, A.; Desmet, G., Comparison of performance of high-performance liquid chromatography columns packed with superficially and fully porous 2.5 μm particles using kinetic plots. *Journal of separation science* 2010, 33 (23-24), 3655-3665.
36. Cabooter, D.; Fanigliulo, A.; Bellazzi, G.; Allieri, B.; Rottigni, A.; Desmet, G., Relationship between the particle size distribution of commercial fully porous and superficially porous high-performance liquid chromatography column packings and their chromatographic performance. *Journal of Chromatography A* 2010, 1217 (45), 7074-7081.
37. Gritti, F.; Leonardis, I.; Abia, J.; Guiochon, G., Physical properties and structure of fine core-shell particles used as packing materials for chromatography: Relationships between particle characteristics and column performance. *Journal of Chromatography A* 2010, 1217 (24), 3819-3843.
38. Gritti, F.; Guiochon, G., Mass transfer mechanism in liquid chromatography columns packed with shell particles: Would there be an optimum shell structure? *Journal of Chromatography A* 2010, 1217 (52), 8167-8180.
39. McCalley, D. V.; Guillarme, D., Evaluation of additives on reversed-phase chromatography of monoclonal antibodies using a 1000 Å stationary phase. *Journal of Chromatography A* 2020, 1610, 460562.

Table 4.1. Summary of the partition coefficient and the retention factor measured with the SPP C4 and FPP C4 columns

	Log $K_{ow,j}$	k_j on SPP C4 column	k_j on FPP C4 column
Benzene	2.13	0.95	1.94
Toluene	2.73	1.79	3.51
Ethylbenzene	3.15	3.42	6.39
Propylbenzene	3.69	6.91	12.21
Butylbenzene	4.38	14.00	23.51

Table 4.2. Summary of the best-fit parameters for the simulation of the FPP C4 and SPP C4 columns

FPP C4	K_{strong}	40000	50000	60000	80000	100000	120000
	$\Gamma_{strong,sat}$	0.00077	0.0005	0.00036	0.000215	0.000145	0.000105
	K_{weak}	37.2	43	46.4	50.75	53.5	54.8
	$\Gamma_{weak,sat}$	0.99923	0.9995	0.99964	0.999785	0.999855	0.999895
	Desorption rate	450	450	450	450	450	450
	K_{strong}/K_{weak}	1075	1163	1293	1576	1869	2190
SPP C4	K_{strong}	40000	50000	60000	80000	100000	120000
	$\Gamma_{strong,sat}$	0.0031	0.002	0.0014	0.00083	0.00055	0.00039
	K_{weak}	-12	12.1	28.1	45.7	57.1	65.3
	$\Gamma_{weak,sat}$	0.9969	0.998	0.9986	0.99917	0.99945	0.99961
	Desorption rate	430	430	430	430	430	430
	K_{strong}/K_{weak}	-3333	4132	2135	1751	1751	1838

Table 4.3. Summary of best-fit parameters under different acidic modifier conditions

	TFA 0.1%	DFA 0.1%
pH	1.96	1.96
K_{strong}	80000	105000
$\Gamma_{strong,sat}$	0.000215	0.000215
K_{weak}	50.75	43.7
$\Gamma_{weak,sat}$	0.999785	0.999785
Desorption rate	450	420

Table 4.4. Summary of the best-fit parameters under different organic solvent compositions

	24.8% ACN	24.6% ACN	24.4% ACN	24.2% ACN	24.0% ACN
K_{strong}	78000	95000	115000	140000	175000
$\Gamma_{strong,sat}$	0.000215	0.000215	0.000215	0.000215	0.000215
K_{weak}	46.8	57.1	70	87.5	109.8
$\Gamma_{weak,sat}$	0.999785	0.999785	0.999785	0.999785	0.999785
Desorption rate	450	450	450	450	450

Table 4.5. Summary of HPLC columns and their applications

	SPP C4 column	FPP C4 column
K_{strong}	80000	80000
$\Gamma_{strong,sat}$	0.00083	0.000215
K_{weak}	45.7	50.75
$\Gamma_{weak,sat}$	0.99917	0.999785
Desorption rate	430	450

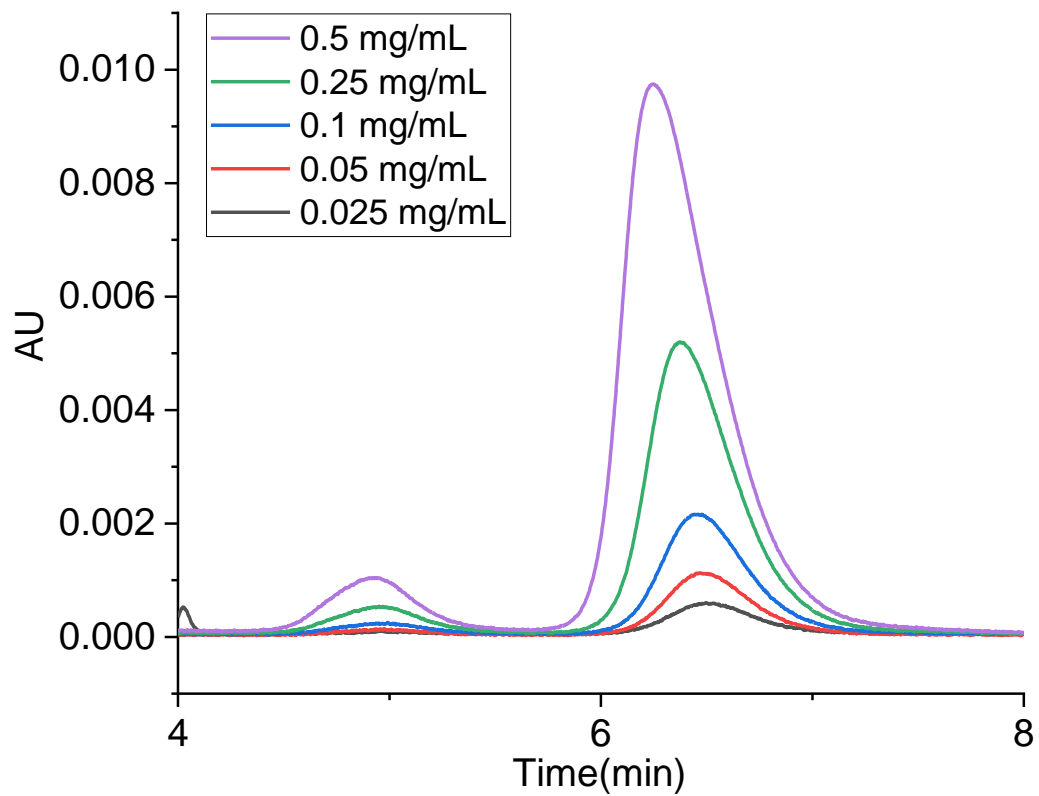


Figure 4.1. Chromatograms of RNases A at five different concentration, 0.025, 0.05, 0.1, 0.25, 0.5 mg/mL. Column: Fully porous C4 column; Mobile phase: 24.8% ACN with 0.1% TFA; Flow rate: 0.2 mL/min; Column temperature: 30 °C.

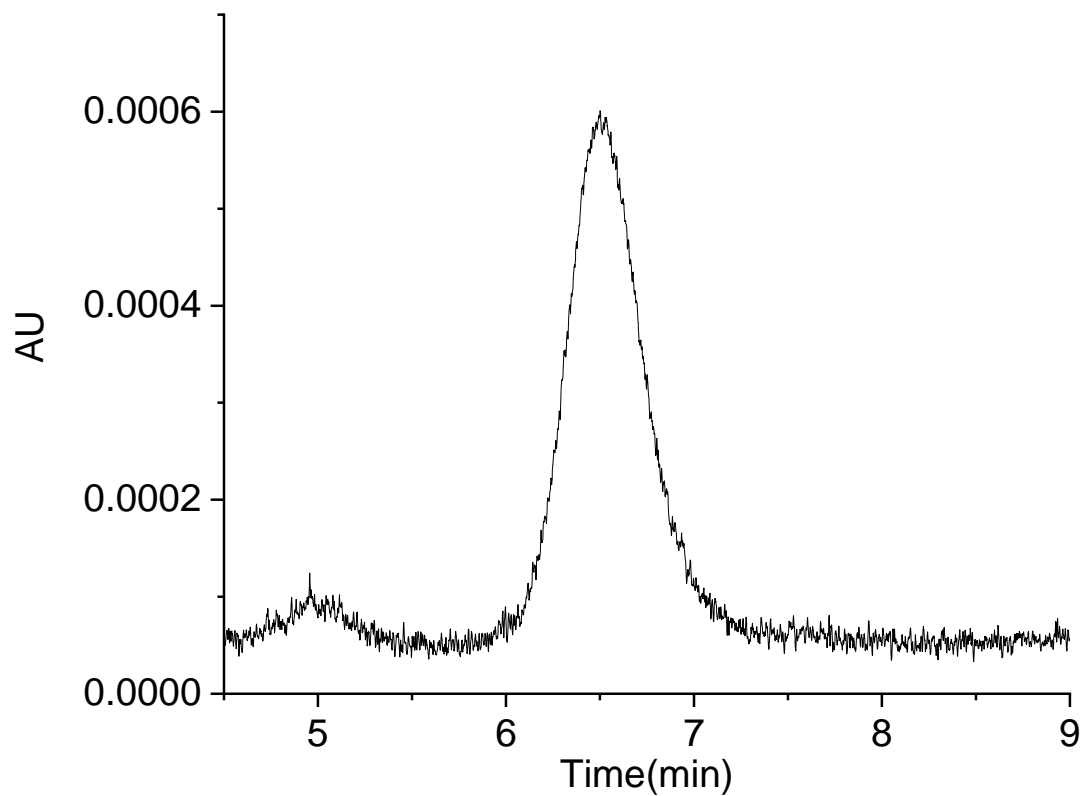


Figure 4.2. Chromatograms of RNases A at the concentration of 0.025 mg/mL. Column: Fully porous C4 column; Mobile phase: 24.8% ACN with 0.1% TFA; Flow rate: 0.2 mL/min; Column temperature: 30 °C.

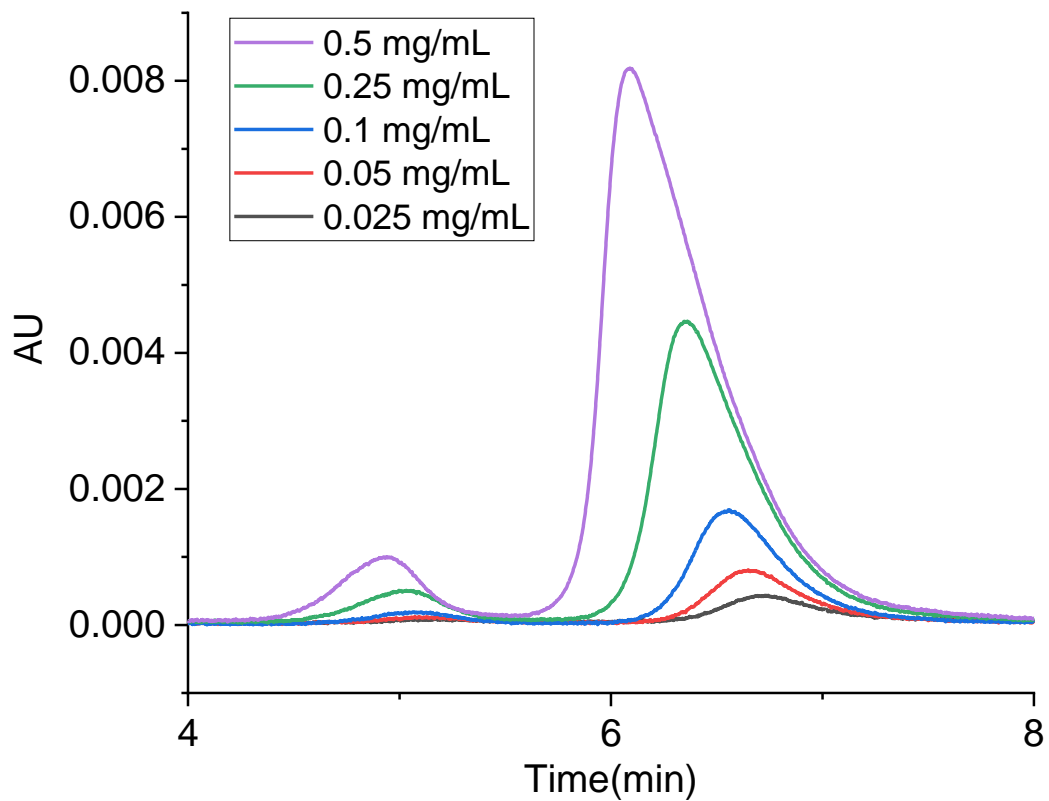


Figure 4.3. Chromatograms of RNases A at five different concentration, 0.025, 0.05, 0.1, 0.25, 0.5 mg/mL. Column: Superficially porous C4 column; Mobile phase: 24.8% ACN with 0.1% TFA; Flow rate: 0.2 mL/min; Column temperature: 30 °C.

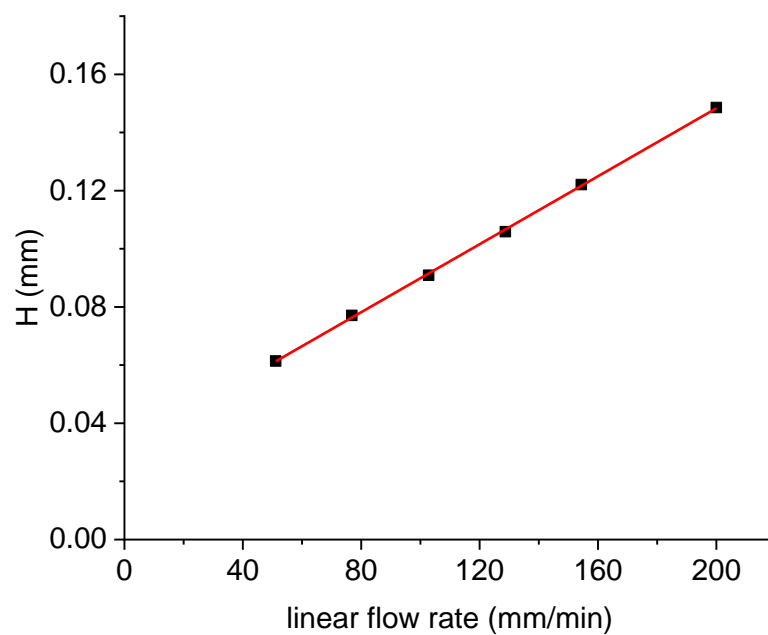
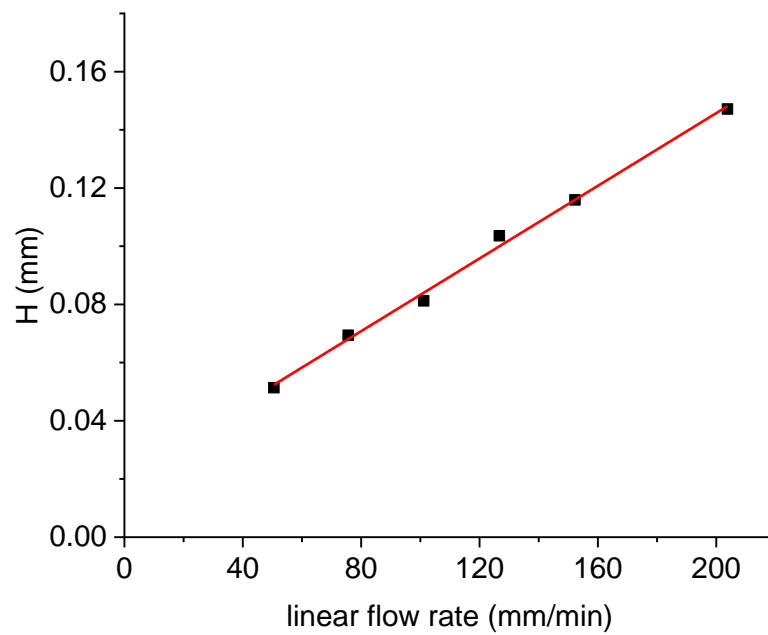


Figure 4.4. Van Deemter plot for RNase A on the SPP C4 column (top) and FPP C4 column (bottom). Mobile phase condition: 24.8% ACN with 0.1% TFA; Flow rate as shown in the plot; Column temperature: 30 °C.

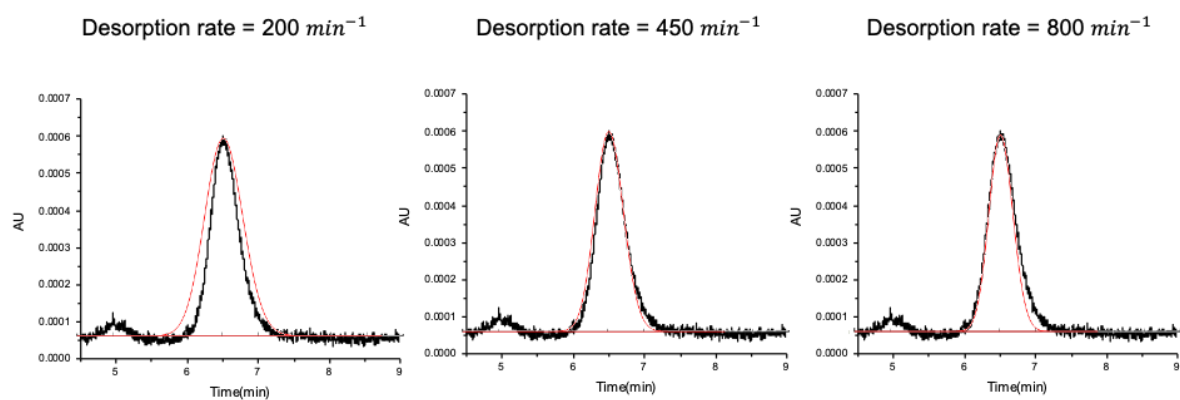


Figure 4.5. Overlaid graph of the simulated chromatograms (blue trace) with the experimental data (black trace) of the lowest concentration to show the effect of desorption rate on the peak retention. Column: Fully porous C4 column; Mobile phase: 24.8% ACN with 0.1% TFA; Flow rate: 0.2 mL/min; Column temperature: 30 °C.

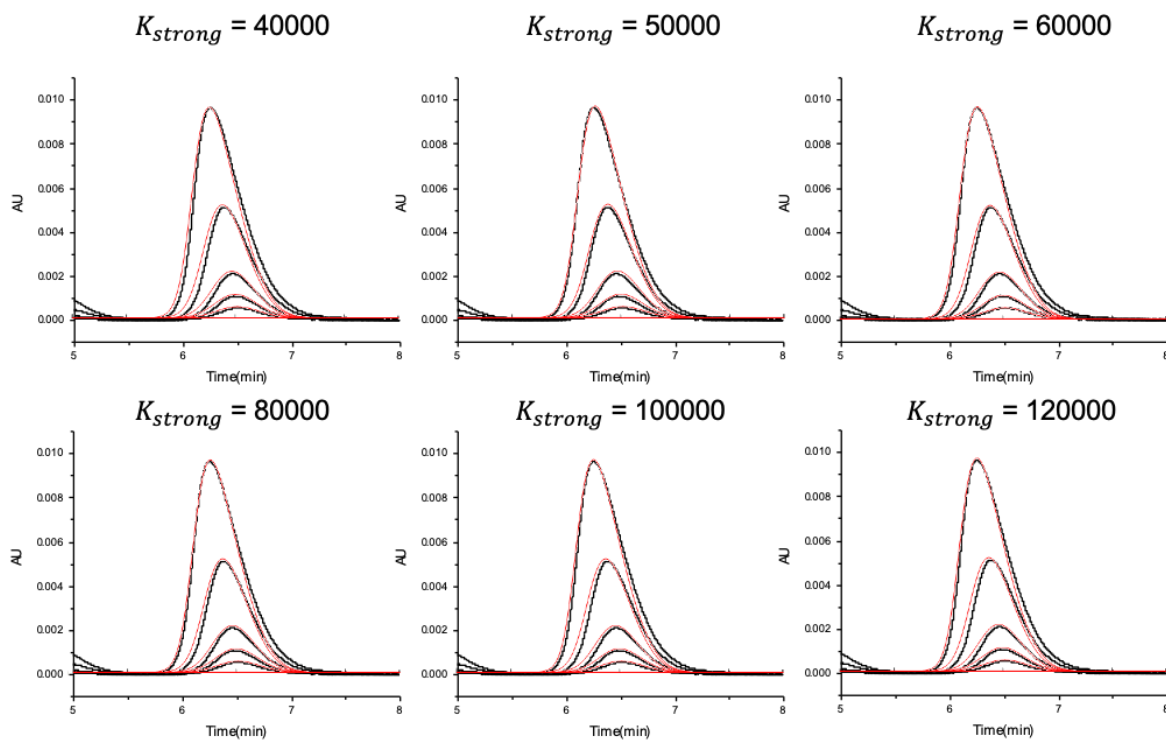


Figure 4.6. Overlaid graph of the simulated chromatograms with the experimental data of the overloading study to show the sets of the solutions for the best-fit parameters. The corresponding K_{strong} value are labeled on the graph. The set of best-fit parameters are summarized in Table 4.2. Column: Fully porous C4 column; Mobile phase: 24.8% ACN with 0.1% TFA; Flow rate: 0.2 mL/min; Column temperature: 30 °C.

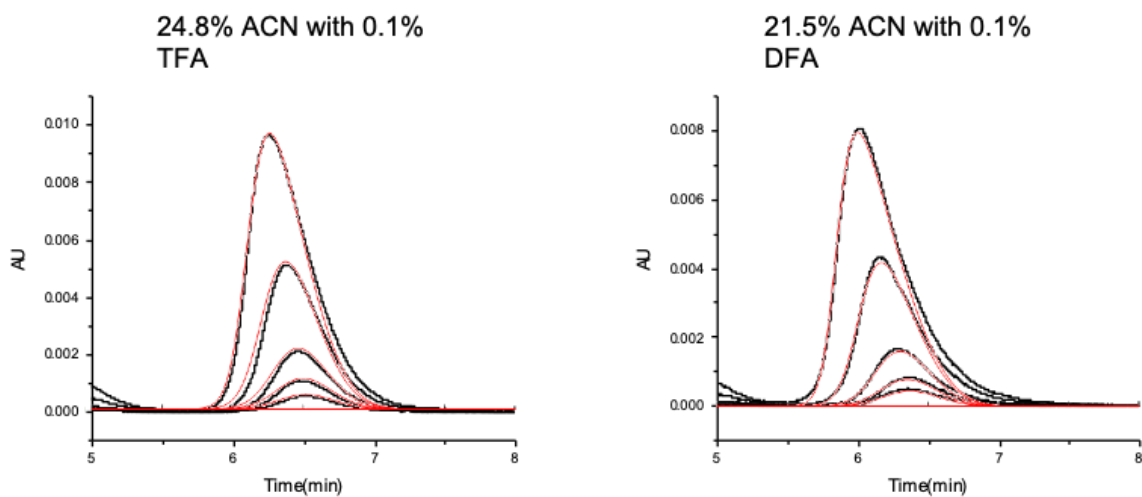


Figure 4.7. Overlaid graph of the simulated chromatograms with the experimental data of the overloading study to show the effect of the acidic modifier on the peak retention. Column: Fully porous C4 column; Mobile phase as labeled in the figure; Flow rate: 0.2 mL/min; Column temperature: 30 °C.

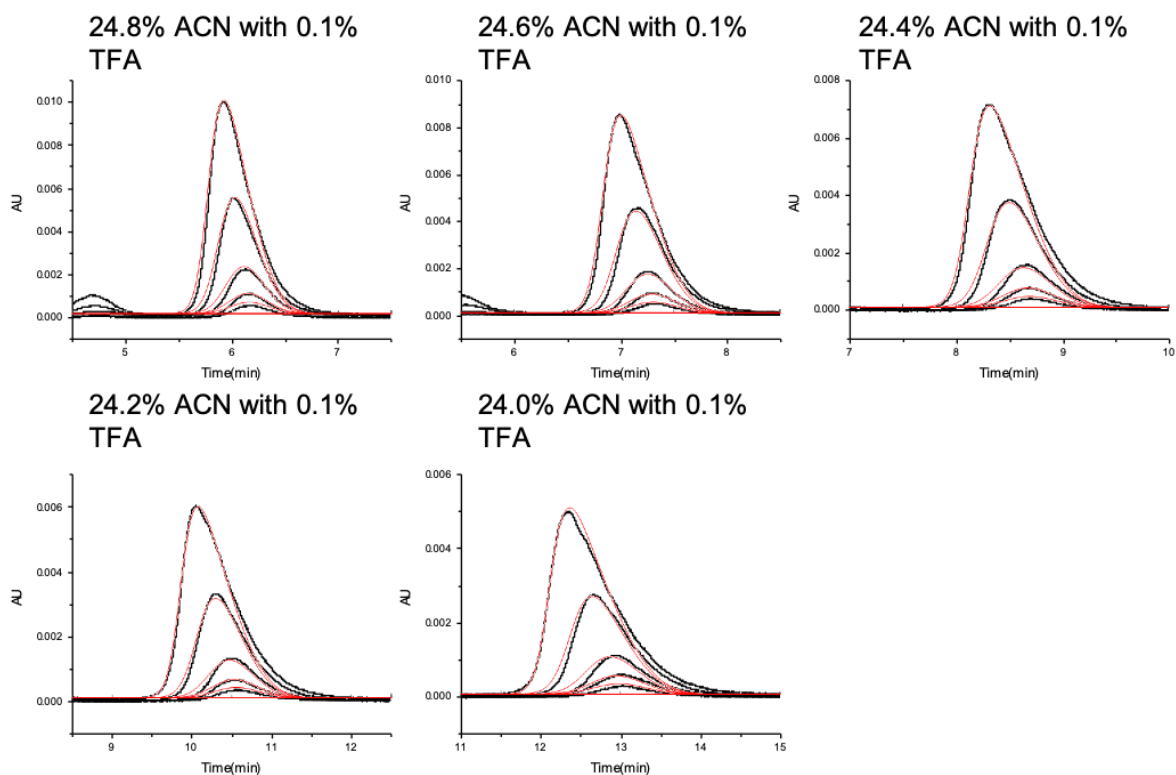


Figure 4.8. Overlaid graph of the simulated chromatograms with the experimental data of the overloading study to show the effect of the organic solvent composition on the peak retention. Column: Fully porous C4 column; Mobile phase as labeled in the figure; Flow rate: 0.2 mL/min; Column temperature: 30 °C.

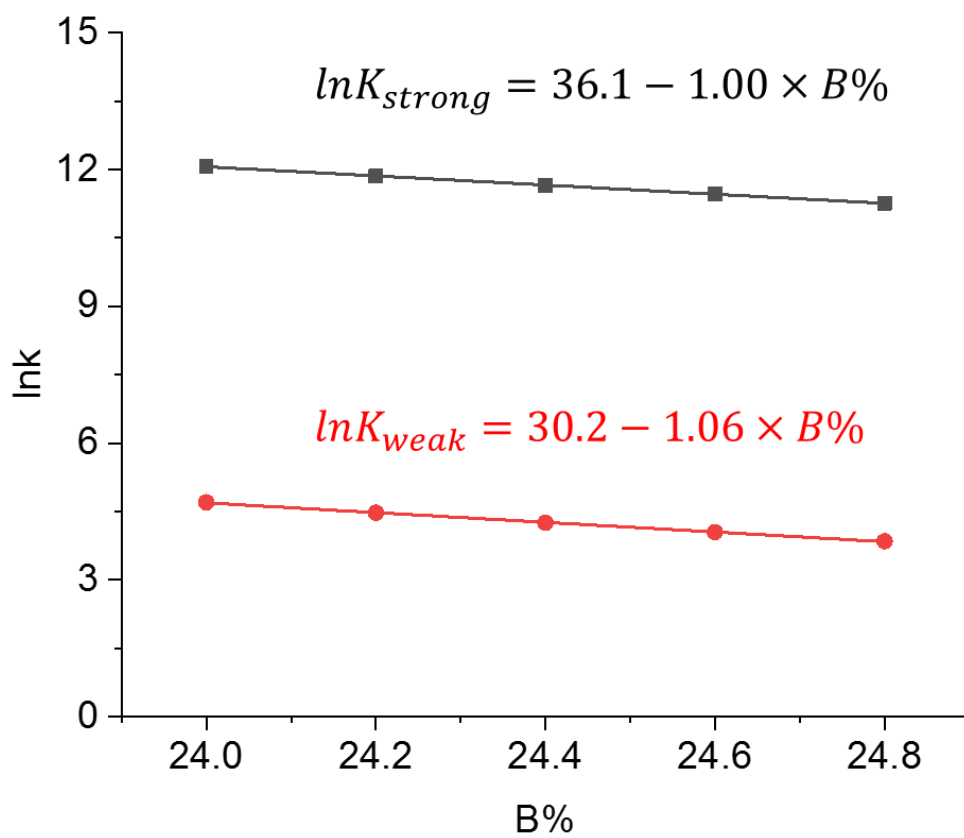


Figure 4.9. A plot of the equilibrium constant of the strong sites and weak sites as a function of the organic solvent composition in the mobile phase. Fitted linear equations are labeled on the figure.

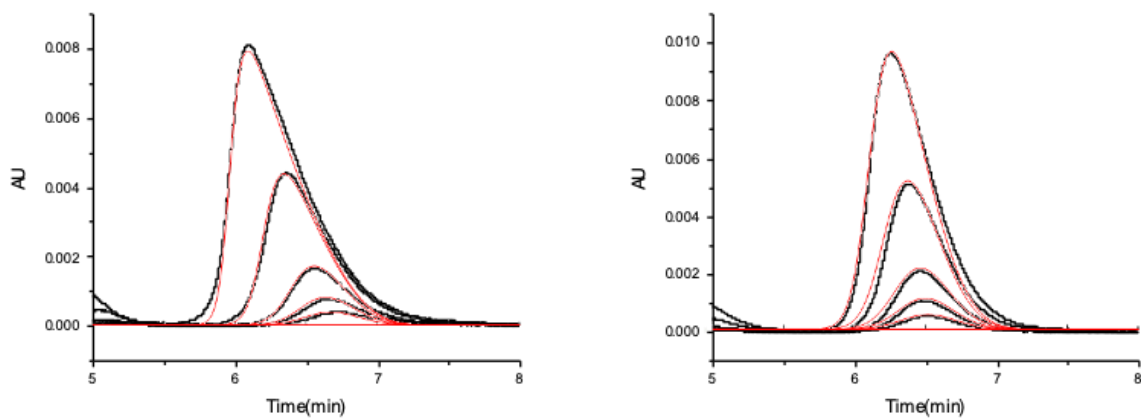


Figure 4.10. Overlaid graph of the simulated chromatograms with the experimental data for SPP C4 column (left) and FPP C4 column (right). Mobile phase condition: 24.8% ACN with 0.1% TFA; Flow rate: 0.2 mL/min; Column temperature: 30 °C.

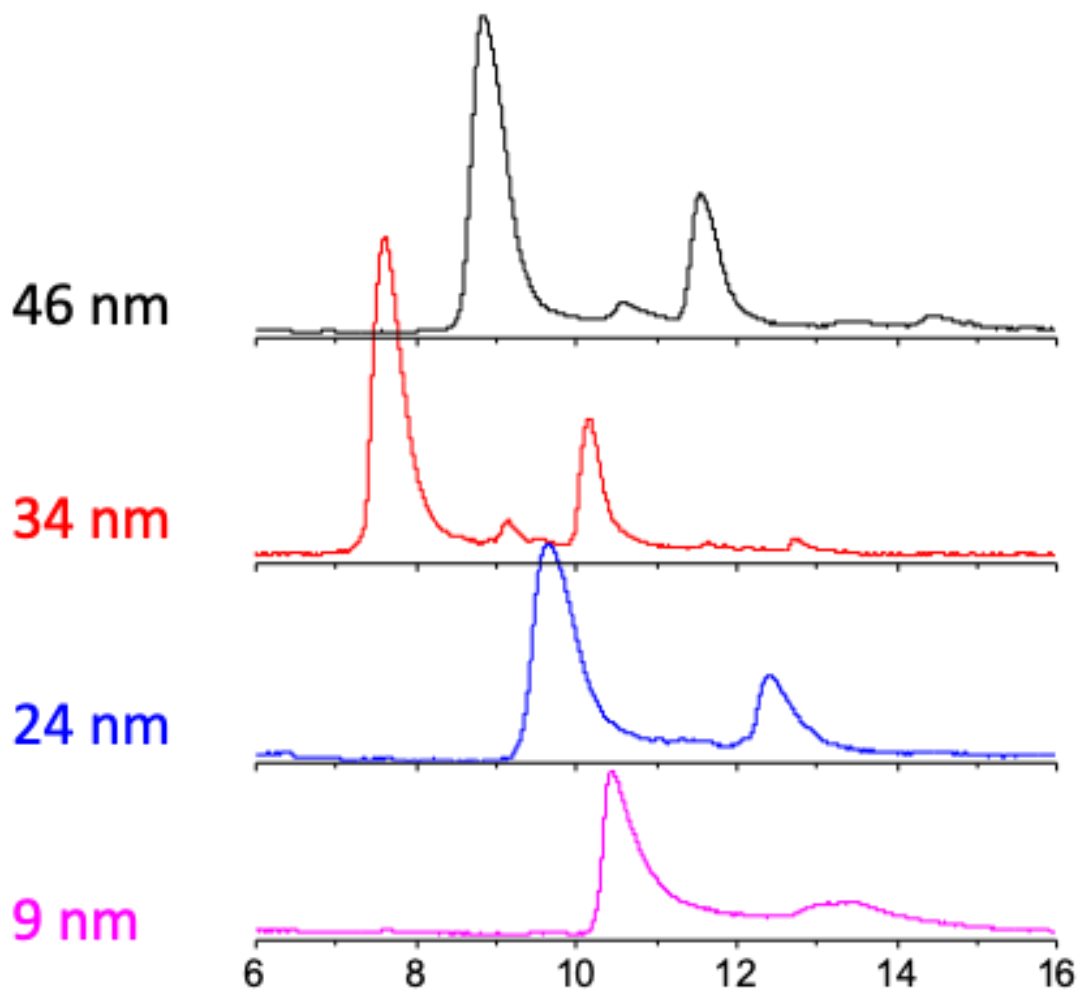


Figure 4.11. RPLC chromatogram for varying PMMA thickness, showing that the retention and peak tailing depends on the polymer thickness. Polymer thickness is labeled in each panel.

Gradient: 20-29% ACN with 0.5% FA in 30 min.

CHAPTER 5. CONCLUSIONS AND FUTURE DIRECTIONS

5.1 Conclusions

This dissertation discusses the development of novel bonded phases to improve the separation performance for proteins, monoclonal antibodies, and antibody-drug conjugates. Peak tailing is a widespread problem for protein separations in reversed-phase liquid chromatography. The active silanols present on the silica surface interact with the basic side chain of protein to cause peak broadening in reversed-phase liquid chromatography and other separation modes. Polymer brush layer bonded to the silica surface is designed to address the problem.

Calcination, annealing, and rehydroxylation of the particle is intended to smooth the silica surface and promote the formation of hydrogen bonds network within the surface silanol groups. End-capping with less sterically hindered silane could decrease the density of the active silanols. Coating the silica surface with a thicker polymer layer could further reduce the electrostatic interaction between the positively charged analyte and the negatively charged silanol by pushing the analyte further away from the surface. The availability of monomers with a broad variety of functional groups allows the fine-tuning of the selectivity for different separation modes. In this work, the polymer-bonded silica has been applied for the characterization of the structural heterogeneities of the monoclonal antibody. High LC resolution and MS sensitivity can be achieved at the same time without the presence of TFA in the mobile phase. An innovative method for characterizing the drug loading profile of ADCs via online LC-MS detection is developed based on the polymer-bonded silica surface. Other than the RPLC separation presented in this work, the applications for polymer shell bonded column on hydrophilic interaction chromatography for glycoprotein separation, ion-exchange chromatography for protein charge variant separation, capillary electrophoresis for protein size separation have been explored by our group as well. Improved performance for LC-MS analysis is achieved with the polymer shell bonded column for various applications.

Chromatographic simulations are used as a tool to get a fundamental understanding of the retention mechanism and peak tailing behavior in RPLC separation for protein. The mixed-mode interaction

with both the hydrophobic ligand and the active silanols on the surface can be described by a bi-Langmuir adsorption isotherm. The knowledge of the retention model and the physical constants for the interaction of the different sites could provide a better understanding of peak tailing.

5.2 Future directions

In Chapter 2, the polymer shell bonded silica column is applied for the characterization for a subclass of monoclonal antibodies, IgG1. Structural heterogeneities also appear in other classes of the antibodies. The requirement for the bonded phase with selectivity suitable for separating those structural variants might be different. For example, hinge cysteines can form intrachain disulfide as well as interchain linkages in IgG2. Therefore, we have been putting effort in optimizing the reaction condition for more complex polymer brush architectures to fine-tune the surface selectivity. Block polymer, random copolymers, and crosslinked polymers and binary brushes can be developed to improve the separation performance for different applications.

In Chapter 3, an online LC-MS method is developed to characterize the drug-loading profile for ADCs. The key for online LC-MS detection is to use a low concentration of volatile salt with the polymer shell bonded column. Similar conditions have been used in the size-exclusion chromatography as well. Polymer shell bonded column with a polymer layer that doesn't interact with the protein analyte can be designed to separate the monomers, aggregates, and fragments of the protein and coupled with online MS detection. The thickness of the polymer needs to be optimized for the fully porous particle and the superficially porous particles.

In Chapter 4, the chromatographic simulations are performed on two commercial C4 columns to study the retention mechanism and the surface chemistry of the columns. The same methodology can be applied to the polymer shell bonded column to investigate the retention model of the polymer shell as well. However, since there are multiple functional groups on the polymer shell, a more complicated adsorption isotherm might be needed for the simulation program. The superior performance of the polymer shell bonded phase can be explained with the knowledge of the physical parameters got from the simulation.

VITA

In 2012, Yun was admitted to Hong Kong University of Science and Technology as an undergraduate student majoring in Chemistry. Yun later joined Prof. Shihe Yang's group and worked on synthesis and characterization for perovskite materials for solar cells. After one year of research, Yun decided to pursue a higher degree in chemistry and applied for graduate school.

In 2016, Yun joined the Ph.D. program in the Department of Chemistry at Purdue University with a major of division in Analytical Chemistry. In Prof. Mary Wirth's lab, Yun worked on developing analytical methods for biomolecule characterization using liquid chromatography and mass spectrometry. Yun developed two novel bonded phases materials for the monoclonal antibody and antibody-drug conjugates separation and improved the LC-MS resolution and studied the mechanism for protein separation in reversed-phase liquid chromatography.

Native Reversed-Phase Liquid Chromatography: A Technique for LCMS of Intact Antibody–Drug Conjugates

Tse-Hong Chen,[†] Yun Yang,[†] Zhaorui Zhang,[‡] Cexiong Fu,^{‡,1} Qunying Zhang,[‡] Jon D. Williams,[§] and Mary J. Wirth^{*†}

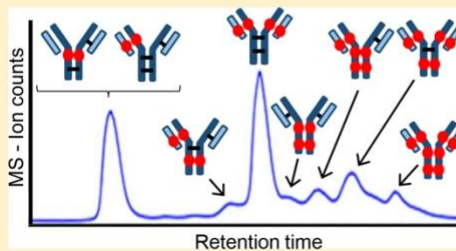
[†]Department of Chemistry, Purdue University, 560 Oval Drive, West Lafayette, Indiana 47907, United States

[‡]Process Analytical Chemistry, AbbVie, Inc. 1 N. Waukegan Road, North Chicago, Illinois 60064, United States

[§]Discovery Structural Chemistry, AbbVie, Inc. 1 N. Waukegan Road, North Chicago, Illinois 60064, United States

Supporting Information

ABSTRACT: The synthesis of antibody–drug conjugates (ADCs) using the interchain cysteines of the antibody inherently gives a mixture of proteins with varying drug-to-antibody ratio. The drug distribution profiles of ADCs are routinely characterized by hydrophobic interaction chromatography (HIC). Because HIC is not in-line compatible with mass spectrometry (MS) due to the high salt levels, it is laborious to identify the constituents of HIC peaks. An MS-compatible alternative to HIC is reported here: native reversed phase liquid chromatography (nRPLC). This novel technique employs a mobile phase 50 mM ammonium acetate for high sensitivity in MS and elution with a gradient of water/isopropanol. The key to the enhancement is a bonded phase giving weaker drug–surface interactions compared to the noncovalent interactions holding the antibody–drug conjugates together. The hydrophobicity of the bonded phase is varied, and the least hydrophobic bonded phase in the series, poly(methyl methacrylate), is found to resolve the intact constituents of a model ADC (Ab095-PZ) and a commercial ADC (brentuximab vedotin) under the MS-compatible conditions. The nRPLC-MS data show that all species, ranging from drug-to-antibody ratios of 1 to 8, remained intact in the column. Another desired advantage of the nRPLC is the ability of resolving multiple positional isomers of ADC that are not well-resolved in other chromatographic modes. This supports the premise that lower hydrophobicity of the bonded phase is the key to enabling online nRPLC-MS analysis of antibody–drug conjugates.



Antibody–drug conjugates (ADCs) are highly selective and potent chemotherapeutics for the treatment of different types of cancer, inspired by Paul Ehrlich.¹ An ADC consists of a recombinant monoclonal antibody (mAb) covalently conjugated with a drug via a hydrophilic linker. The mechanism exploits specific binding of tumor-expressed antigens and delivers covalently conjugated cytotoxic payloads to cancer cells selectively over nonmalignant cells, resulting in greater efficacy and minimized systemic toxicity. Four ADCs are currently on the market: Adcetris (brentuximab vedotin) from Seattle Genetics for the treatment of relapsed Hodgkin's lymphoma and systemic anaplastic large-cell lymphoma, Kadcyla (trastuzumab emtansine) from Genentech for the treatment of metastatic breast cancer,^{2–4} Mylotarg (gemtuzumab ozogamicin) from Pfizer for acute myeloid leukemia, and Besponsa (inotuzumab ozogamicin) also from Pfizer for acute lymphoblastic leukemia. More than 60 ADCs have been advanced into clinical trials for cancer treatment,³ and there are currently more than 65 ADCs in clinical evaluation to target different hematologic malignancies and solid tumors.^{3,5} The vast majority of the cytotoxic warheads of the ADCs currently in clinical trials are conjugated to either lysine or cysteine

residues on the antibody,^{6–8} with most using cysteine residues.⁹ Drug loading in the ADCs is an important design parameter that needs to be characterized.¹⁰

Liquid chromatography separation of cysteine-conjugated ADCs to characterize the drug loading distribution is the topic of this paper. Taking IgG1, for example, a common conjugation approach entails partial reduction of four interchain disulfide bonds to generate up to eight reactive thiol groups.^{11–13} This conjugation scheme yields a mixture of species ranging from 0 to 8 drugs per antibody, which is a broad distribution. The different drug loadings have been reported to affect the pharmacokinetics, stability, and clearance of ADCs.^{14–18} Native SEC-MS is a rapid technique for determining the distribution of drug loads, where the SEC serves to desalt the sample rather than separate the components and relies solely on MS for characterization and quantitation.¹⁹ The technique skews the distribution toward

Received: October 12, 2018

Accepted: January 20, 2019

Published: January 21, 2019

lower drug load due to ion suppression and suboptimal recovery of species with higher drug load.²⁰ Pretreatment by enzymatic cleavage of the hydrophobic drug from the ADC, which leaves the hydrophilic linker attached as a tag, reduces the skewing but does not eliminate it.²¹ Consequently, chromatographic separations are used for quantitative ADC characterization. Reversed-phase liquid chromatography coupled to mass spectrometry (RPLC-MS) is used to determine the average drug-to-antibody ratio (DAR) by separating the denatured subunits of the reduced ADC,²² but this approach loses information about the drug load distribution.²³ Hydrophobic interaction chromatography (HIC) is a nondenaturing separation^{24–26} that is currently the gold standard for resolving the drug distribution of ADCs.²⁷ A gradient of decreasing salt concentration is used for elution,^{28,29} and the high initial concentration and low volatility of the salts prevent its direct coupling to mass spectrometry for peak identification.^{30–34}

The Ge and Alpert groups were the first to show that HIC-MS of intact proteins is possible with volatile salts.^{26,35} In their papers, MS-compatible ammonium acetate salt was used, with a gradient decreasing from 1 M to 20 mM, concurrent with a gradient of increasing acetonitrile in water from 0 to 50%. Because NH_4OAc has kosmotropic properties weaker than those of the typical HIC salts of $(\text{NH}_4)_2\text{SO}_4$ and Na_2HPO_4 , they used a bonded phase with increased hydrophobicity, and their results demonstrated that the proteins maintained their native forms. HIC-MS has not yet been reported for intact ADCs.

The considerations for HIC-MS of ADCs are different from those of natural proteins. The conjugated drug of an ADC is far more hydrophobic than the solvent-exposed surface of a native protein, as demonstrated by the elution time increasing with increasing drug load in HIC of ADCs. In light of this, the concept behind our work is that a fixed, low concentration of MS-compatible salt, e.g., 50 mM NH_4OAc , might give retention of ADCs on hydrophobic columns because less salting-out would be needed. If so, the question then is whether a mild organic additive, isopropanol, can be made to desorb the ADC from the stationary phase without dissociating the noncovalently bound subunits of the antibody. The strategy is to decrease the hydrophobicity of the bonded phase so that less organic component is needed for elution, thereby avoiding the dissociation of the antibody into subunits.³⁶ This is the opposite of the strategy used by Chen and coworkers^{26,35} because ADCs present a different problem than mAbs, which are more hydrophilic than ADCs. The other difference from the prior work is that the salt concentration is fixed at low level while the organic component is increased, which would make this a reversed-phase separation. Hence, the proposed new method is a nondenaturing version of reversed-phase liquid chromatography (RPLC), and we refer to it as native reversed-phase liquid chromatography (nRPLC).

The purpose of this work is to test the idea that a bonded phase with sufficiently low hydrophobicity would enable a new technique, nRPLC-MS, for separating intact ADCs and determining their molecular weights by in-line coupled mass spectrometry. The method is evaluated using both a model ADC and a commercial ADC, where each ADC has a drug mimic or drug coupled to cysteines of the mAb using a hydrophilic linker.

MATERIALS AND METHODS

Materials. Nonporous silica particles (1500 nm) were purchased from Superior Silica (Tempe, AZ). Empty stainless-steel columns (2.1 mm ID, 50 mm length), reservoirs (4.6 mm ID, 150 mm), and frits (0.5 μm pore diameter) were purchased from Isolation Technologies (Middleboro, MA). Stainless-steel tubing, ferrules, and internal nuts were all purchased from Valco Instruments (Houston, TX). Silanes, i.e., (chloromethyl)phenyldimethylchlorosilane (+99%) and trimethylchlorosilane (+99%), were purchased from Gelest (Morrisville, PA). Methyl methacrylate (MMA, 99%), sodium ascorbate ($\geq 99\%$), butylamine (99.5%), NH_4OAc (99.99%), ammonium sulfate ($(\text{NH}_4)_2\text{SO}_4$, $\geq 99\%$), sodium phosphate (Na_3PO_4 , 96%), and ammonium hydroxide were purchased from Sigma-Aldrich (St. Louis, MO). Other chemicals used included trifluoroacetic acid (TFA, 99%), difluoroacetic acid (DFA, 98%), and copper(II) chloride (CuCl_2 , 99%) from Acros Organics (Morris Plains, NJ), tris(2-dimethylaminoethyl)amine (Me_6TREN , +99%) from Alfa Aesar (Haverhill, MA), and formic acid (FA, 99.5%+, LC/MS grade), acetonitrile (ACN), and 2-propanol (IPA) from Fisher Scientific (Hampton, NH). Ultrapure water was obtained from a Milli-Q system (MilliporeSigma, Darmstadt, Germany).

IgG1 Ab095 was conjugated with drug-linker mimic PZ in-house at AbbVie (North Chicago, IL) as a model ADC. Brentuximab vedotin was obtained from Seattle Genetics. Both ADCs were prepared at 1 mg/mL in NH_4OAc or $(\text{NH}_4)_2\text{SO}_4$ with final concentration 0.8–1.0 M.

UHPLC Column Preparation. The silica particles were modified as described earlier.³⁷ Briefly, the silica particles were calcined at 600 °C for 12 h, then annealed at 1050 °C for 3 h, and rehydroxylated overnight in 1.0 M HNO_3 . Particles were then rinsed in ultrapure water and dried in a 60 °C vacuum oven. SEM showed that the particles decreased in diameter to 1.2 μm from the heating steps. Freshly rehydroxylated silica particles were suspended in a dry toluene solution containing 2% (v/v) of (chloromethyl)phenyldimethylchlorosilane and 0.1% (v/v) of butylamine. The solution was refluxed for 3 h and then rinsed with dry toluene. The particles were then end-capped by suspending in another dry toluene solution containing 2% (v/v) of trimethylchlorosilane and 0.1% (v/v) of butylamine and refluxed for 3 h. The silylated, end-capped particles were then rinsed with dry toluene and allowed to dry in a 60 °C vacuum oven for 2 h.

For polymer growth, each monomer was dissolved in 50:50 $\text{H}_2\text{O}/\text{IPA}$ (v/v) in a 50 mL round-bottom flask for a final concentration of 2.5 M. Two other solutions were made: (1) a solution containing 40 mg of CuCl_2 and 80 μL of Me_6TREN and (2) a solution containing 20 mg of sodium ascorbate. These were also prepared in 2.0 mL of 50:50 $\text{H}_2\text{O}/\text{IPA}$. Afterward, the $\text{Cu}/\text{Me}_6\text{TREN}$ solution was added to the round-bottom flask, followed by the sodium ascorbate solution. The resulting solution was poured into a plugged reservoir column of 4.6 \times 150 mm. A 2.1 \times 50 mm column was packed with 0.24 g of silylated, end-capped particles suspended in acetonitrile. The reservoir and column were connected in series. A high-pressure pump, LabAlliance Series 1500 HPLC Pump (Laboratory Alliance of Central New York, LLC, Syracuse, NY) was used for packing and modification. The reaction solution from the reservoir was pumped into the column starting at 200 $\mu\text{L}/\text{min}$ until the reaction mixture dripped from the end of the column. The flow rate was then

lowered to 100 $\mu\text{L}/\text{min}$, and the polymerization reaction was allowed to proceed for a range of reaction times from 40 to 85 min for optimization. After reaction, the freshly packed column poly(methyl methacrylate) (PMMA) was rinsed with water for 20 min at 100 $\mu\text{L}/\text{min}$.

UHPLC. The columns and mobile phases for the various separations are summarized in Table 1.

Table 1. Summary of HPLC Columns and Their Applications Herein

column	application	mobile phase A; B
Thermo MabPac RP	RPLC, reduced ADC	$\text{H}_2\text{O} + 0.1\% \text{ DFA}; \text{ACN} + 0.1\% \text{ DFA}$
Supelco Bioshell A400	RPLC, nonreduced ADC	$\text{H}_2\text{O} + 0.1\% \text{ FA} + 0.015\% \text{ TFA}; \text{ACN} + 0.1\% \text{ FA} + 0.015\% \text{ TFA}$
Thermo-HIC butyl	HIC, ADC (Purdue)	50 mM $\text{Na}_3\text{PO}_4 + 1 \text{ M } (\text{NH}_4)_2\text{SO}_4$, pH 7; 50 mM $\text{Na}_3\text{PO}_4 + 30\% \text{ IPA}$, pH 7
Tosoh TSKgel Butyl	HIC, ADC (AbbVie)	25 mM $\text{Na}_3\text{PO}_4 + 1.5 \text{ M } (\text{NH}_4)_2\text{SO}_4$, pH 7; 25 mM $\text{Na}_3\text{PO}_4 + 25\% \text{ IPA}$, pH 7
PMMA, nonporous	nRPLC, ADC	50 mM NH_4OAc , pH 7; 50 mM $\text{NH}_4\text{OAc} + 50\% \text{ IPA}$, pH 7

A Thermo Accela UHPLC system (Thermo-Scientific, Waltham, MA, United States) was used for the development of nRPLC separations at the Purdue lab. Lab-made nRPLC columns (2.1 \times 50 mm, 1.2 μm nonporous silica particles coated with various polyalkyl methacrylates were used as the analytical columns. A commercial column, MabPac HIC-Butyl (4.6 \times 100 mm, 5 μm nonporous), from Thermo Scientific (Waltham, MA) was used under both HIC and nRPLC conditions for comparison because both have polymeric surfaces. UV absorbance wavelength was set to 280 nm. The column temperature was 30 $^\circ\text{C}$, and the injection volume was 3 μL .

A TSKgel Butyl-NPR column (4.6 \times 35 mm, 2.5 μm , Tosoh, King of Prussia, PA) was used for HIC at the AbbVie site, with an Agilent 1200 HPLC (Agilent, Santa Clara, CA). The system is routinely used for HIC separations of ADCs to calculate DAR. With the mobile phase given in Table 1, the gradient started with 90% MPA, decreased to 75% MPA in 2 min followed by a gradient to 0% MPA in 10 min, and was held for 2 min before re-equilibrium. The flow rate was 0.8 mL/min, and column temperature was set to 25 $^\circ\text{C}$.

LC-MS. For RPLC-MS of the reduced ADC, this was generated in the Purdue lab by adding 1,4-dithiothreitol (DTT), a Thermo Accela UHPLC was used with a Thermo MabPac RP column (2.1 \times 50 mm, 4 μm , supermacroporous polymer particles) (Thermo-Scientific, Waltham, MA, United States), and the column was coupled to a Thermo LTQ Velos mass spectrometer (Thermo-Scientific, Waltham, MA, United States). With the mobile phase given in Table 1, the gradient started with 27% with MPB2, increased to 43% MPB2 in 15 min, and returned to 27% MPB2 for re-equilibrium. Flow rate was 0.2 mL/min, and column temperature was 80 $^\circ\text{C}$. Peak identities were assigned by matching deconvoluted masses with theoretical masses.

For RPLC-MS of the nonreduced ADC (no DTT), a Supelco Bioshell A400 Protein C4 column (2.1 \times 100 mm, 3.4 μm , Sigma-Aldrich, St. Louis, MO) was used in the AbbVie lab. With the mobile phase given in Table 1, the gradient started with 90% MPA3, ramped to 69% MPA3 in 1 min followed by a decrease to 52% MPA3 in 13 min and returned

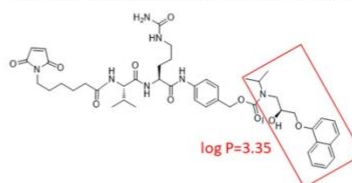
to original condition for re-equilibrium. Flow rate was 0.3 mL/min, and column temperature was 70 $^\circ\text{C}$. The ADC samples were analyzed using an Acquity UPLC H-Class coupled to a Synapt G2 Si mass spectrometer (Waters, Milford, MA). Peak identities were assigned by matching deconvoluted masses with theoretical masses.

For online nRPLC-MS analysis, the poly(methyl methacrylate) (PMMA) column made in the Purdue lab was used at AbbVie, where the LC-MS system was a Waters Acquity UPLC H-Class coupled to a Xevo G2 qTOF mass spectrometer (Waters, Milford, MA). With the mobile phase given in Table 1, the gradient started with 0% MPB4, held for 2 min, ramped to 15% MPB4 in 3 min followed by a gradient to 50% MPB4 in 15 min and held at 50% MPB4 for 6 min before re-equilibrium. Flow rate was reduced to 0.07 mL/min. Column temperature was 30 $^\circ\text{C}$. For MS condition, capillary voltage was 3.00 kV. Sample cone voltage was 85 V, trap collision energy was set to 60 V, source temperature was 140 $^\circ\text{C}$, and desolvation temperature was 500 $^\circ\text{C}$. The high sampling cone voltage was used to improve resolution and sensitivity in raw MS spectra, but this more prone to cause in-source fragmentation

RESULTS AND DISCUSSION

A model ADC was synthesized by AbbVie, with the chemical structure of the linker and drug portions depicted in Figure 1a.

a) linker+drug in AbbVie model ADC, Ab095-PZ, MW=857.99 Da



b) linker+drug in brentuximab vedotin, MW=1316.63 Da

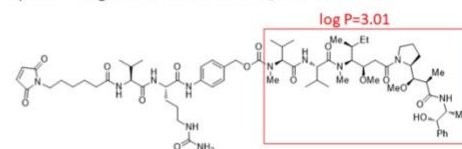


Figure 1. Chemical structures of linker-drug combination for (a) the AbbVie model ADC, Ab095-PZ and (b) brentuximab vedotin. Each drug or drug mimic part is in the red square, and its hydrophobicity is expressed by log P , where P represents the octanol/water partition coefficient.

The structure is similar to that of the commercial ADC, Brentuximab, also studied here, with its structure depicted in Figure 1b. These are both cysteine-conjugated ADCs using a similar, typical hydrophilic linker with coupling to the mAb cysteines via the maleimide group. The figure shows that the drug mimic for the AbbVie model ADC and the drug for brentuximab vedotin are quite hydrophobic, each with a log P in excess of 3, where P is the partition coefficient for octanol/water.

ADCs can be characterized with respect to their average DAR by fully reducing the ADCs with DTT and then separating the subunits by RPLC. Sketches to indicate labeling

for intact ADCs and the various subunits are given in Figure 2a. The RPLC chromatogram for the reduced AbbVie model

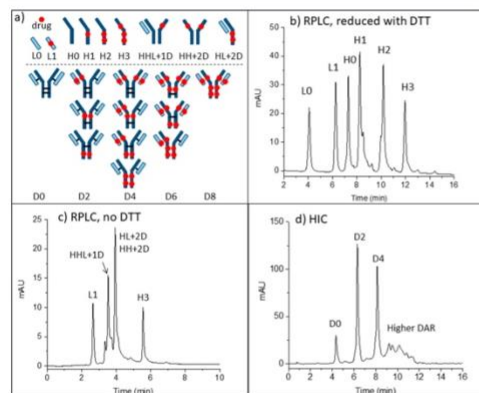


Figure 2. (a) Sketches explain abbreviations for peak assignments. (b) RPLC of the model ADC after reduction with DTT. (c) RPLC of the model ADC without DTT. (d) HIC of the intact ADC with tentative peak assignments. Condition are in the Supporting Information.

ADC Ab095-PZ is shown in Figure 2b. The mass spectrum of each peak (Supplementary Figure S1) was used to assign each of the six peaks to the subunit, as labeled in the chromatogram. The first two peaks are light chains without (L0) or with (L1) one drug+linker, and the latter four peaks are heavy chains with 0, 1, 2, and 3 drug+linker attachment(s). The average DAR calculated from the relative peak areas is 3.9. The RPLC chromatogram of Ab095-PZ without DTT reduction (i.e., nonreduced RPLC) is shown in Figure 2c. The peak assignments from MS were only partially reduced during the conjugation process, as expected. The results demonstrate that in conventional RPLC, without interchain disulfide bond linkages, the ADC dissociates into subunits. The value of this chromatogram is that it can be later compared to that for native RPLC with DTT absent. The HIC chromatogram of Ab095-PZ, using a commercial HIC-Butyl column and typical HIC salt gradient, is shown in Figure 2d. As is common practice, an isopropanol gradient was superimposed on the salt gradient to attain full elution of the ADC constituents. The species with higher drug loading gave multiple peaks, and this is shown later to be due to partial resolution of positional isomers. Mass spectrometry cannot be used to identify the peaks of Figure 2d because the conventional HIC salts suppress ionization and cause adduct formation, as discussed earlier. One can make tentative peak assignments based on typical drug loading profile for ADCs with an average DAR of 3.9, as indicated in Figure 2d.

The proposed strategy described earlier to enable native RPLC-MS is to use no more than 50 mM NH_4OAc . This amount of salt is normally reached at the end of a salt gradient for online HIC-MS;^{25,26,38} therefore, there is now little value in even running a salt gradient in RPLC mode. Despite this low level of salt, the same commercial HIC column as used for the HIC of Figure 2d (Thermo MabPac HIC-Butyl column) was found to give virtually no elution of the ADC, as shown in Supplemental Figure S2; the retention to the column is too strong for elution. This indicates that the lower kosmotropic

power of 50 mM NH_4OAc gives more retention than the higher kosmotropic power of 50 mM sodium phosphate of Figure 2d. The strong retention with 50 mM NH_4OAc is attributed to irreversible adsorption of the hydrophobic drug rather than to salting out of the intact ADC. The HIC stationary phase, which is said to be made of butyl groups, is thus too hydrophobic for use with isocratic 50 mM NH_4OAc , i.e., the hydrophobic interactions between ADC and bonded phase surface are stronger than the intramolecular hydrophobic interactions within the ADC. This inspires the proposed strategy to make the bonded phase less hydrophobic so that the free energy barrier for protein desorption is lower than the free energy barrier for protein denaturation.

Native RPLC chromatograms of model ADC Ab095-PZ using isocratic 50 mM NH_4OAc with a gradient of 0–50% isopropanol are shown in Figures 3a–d for a series of columns

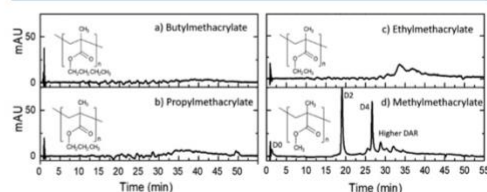


Figure 3. Native RPLC (nRPLC) of AbbVie model ADC with varying hydrophobicity of bonded phase, as denoted by the structures. Gradient conditions are A: 50 mM NH_4OAc , pH 7, B: 50 mM NH_4OAc , 50% IPA, pH 7, 0–100%B/40 min, 100%B/5 min, 100 $\mu\text{L}/\text{min}$, 30 $^\circ\text{C}$. The same tentative labels as for the HIC chromatogram of Figure 2d are made due to the similarity.

with decreasing bonded phase hydrophobicity, including polymethyl-, polyethyl-, polypropyl-, and poly(butyl methacrylate). The recovery and resolution are progressively higher with lower hydrophobicity, consistent with less denaturation of the ADCs lower mobile phase strength. Poly(methyl methacrylate), with the lowest hydrophobicity, gives a chromatogram similar to that of the native HIC chromatogram of Figure 2d, suggesting that intact ADCs are indeed eluted under mild organic phase content without dissociation. The chromatogram is quite different from that of the denaturing RPLC case of Figure 2c, again arguing that the ADCs are not dissociated.

The downside of the nRPLC separation of the ADCs in Figure 3 is that the native antibody, i.e., the species having no conjugated drug, D0, has low retention. This is an inherent outcome of the nRPLC strategy, where the designed retention mechanism is based on the hydrophobic interaction between the exposed/or partially exposed hydrophobic drug with the bonded phase. To increase the retention of D0 species, some mixed-mode copolymer could potentially be used with minimal effect on retention of the hydrophobic drug.

Mass spectrometry is used to test whether the constituents of the ADC peaks are intact vs dissociated under nRPLC conditions for the column with poly(methyl methacrylate) grown for 70 min. Figure 4a shows the nRPLC chromatogram for the AbbVie model ADC using the poly(methyl methacrylate) column, now with the gradient adjusted for faster elution. The peaks are labeled in detail based on the mass of the most prevalent protein for each peak. The raw mass spectral data are given in Figure 4b. By extracting high

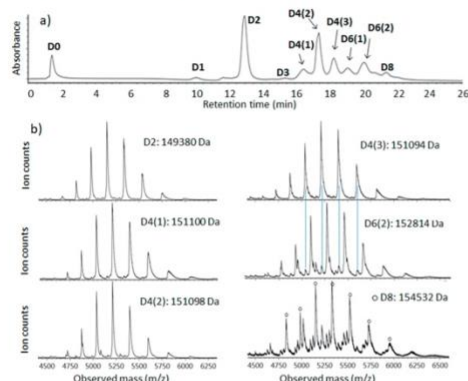


Figure 4. (a) nRPLC of the AbbVie model ADC Ab095-PZ, with peaks labeled based on the mass spectra. Gradient: 0 to 4.5% IPA/water over 3 min, then 4.5 to 50% IPA/water over 20 min. Detection at 280 nm. (b) Raw mass spectra for peaks as labeled, with the molecular weight based on deconvoluted mass spectra for peak ID. The blue lines show that extra peaks are from overlap.

mass range (extracted in chromatogram not shown), it was confirmed that the unconjugated species (D0), was barely retained and was nearly coeluting with the injection peak. The small peak in the chromatogram of Figure 4a eluting at 10 min was identified as D1. In Figure 4b, the first mass spectrum assigned the peak at 13 min as D2 based on deconvoluted mass, which gives the mass (149 380 Da) corresponding to that expected for D2 (theoretical mass: $147\,640 + 2 \times 859$). There are three peaks for D4, labeled as D4(1), D4(2), and D4(3) in the order of elution, and Figure 2a showed that there are theoretically four positional isomers for D4. Of note, the positional isomers of D4 that result from conjugation of the upper vs lower cysteine pairs in the hinge region likely coelute because they are only subtly different in structure. Similarly, D6 gives two peaks when there are expected to be three, but again, as illustrated in Figure 2a, two cases differ only by position on the heavy chain (upper hinge cysteine conjugation vs lower hinge cysteine conjugation). It is novel for a HIC column to resolve different D4 and D6 isoforms from one another, and the separation on this poly(methyl methacrylate) under nRPLC mode could be advantageous in process understanding and quality control. The mass spectrum of the larger of the two D6 peaks is given in Figure 4b. It shows some peak overlap with D4, as indicated by the light blue lines in Figure 4b. The mass spectrum of the peak labeled D8 indicates it to be mainly D8 with some overlap from D5, D6, and D7. No peaks due to fragments were observed. It is noteworthy that all ADC mass spectra demonstrated a native-like charge envelope distribution with charge state from 24 to 33, which further supports the conclusion of native RPLC.

Representative mass spectra of model ADC over a wider range of mass-to-charge ratio (m/z) are given in Figure 5a. All spectra show strong signals from a heretofore unexpected L1 fragment (light chain plus drug), despite the absence of corresponding species (ADC minus L1) in the higher mass range for intact ADC. This at first seems to contradict the claim of intact ADC elution during the discussion of Figure 4 for the higher mass range. Our conclusion is that this L1 signal

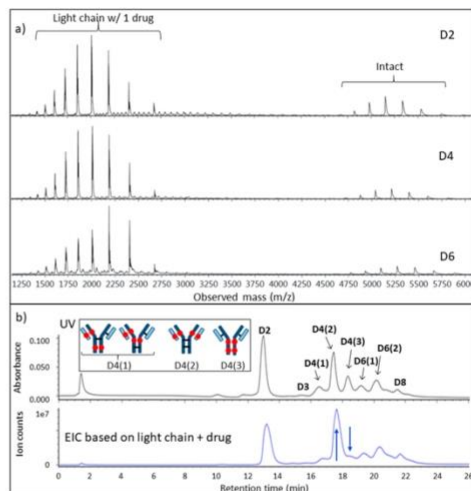


Figure 5. Evidence that light chain dissociates in MS source for AbbVie model ADC. (a) Full-range raw mass spectra show large signals for light chain+drug, but no significant signals for ADC minus light chain+drug. (b) Chromatogram with UV detection (top) and EIC based on light chain+drug (bottom). The blue arrows point to two peaks that changed intensities, and the inset depicts the structures for the isomers consistent with these intensity changes.

in Figure 5 arises from two circumstances: (1) in-source fragmentation of the ADC after elution due to the rather high sampling cone voltage and (2) a greater ionization efficiency of the L1 fragment to make its signal appear disproportionately strong compared to that of the intact ADC. If the signal strength were proportional to abundance, there would be a significant amount of ADC-L1 detectable in the higher range of m/z . Therefore, the large peaks for L1 must be due to greater ionization efficiency. In addition, if L1 dissociated from the ADC on the column, the EIC based on L1 would not be correlated with the UV chromatogram. The only reasonable way for the subunits of the ADC to travel together throughout the separation is for the ADC to be intact. An extracted ion chromatogram (EIC) for the L1 fragment is shown in Figure 5b, in comparison with the same chromatogram using UV detection. It is clear that the chromatograms closely track one another for the two different modes of detection. Further, the exceptions prove the rule: the blue arrows in Figure 5b show a D4 peak that is increased and a D4 peak that is decreased for EIC of L1. These are consistent with the expectation that one D4 should have two L1 species and one should have none. The inset images in Figure 5b depict the structures of the positional isomers. D4(2) has twice as many light chains with drug compared to D4(1), which would make its signal increase for EIC of L1. Likewise, D4(3) has no light chain with drug; hence, signal would decrease for EIC of L1. The EIC supports the conclusion that L1 dissociated postcolumn and all ADCs remained intact throughout the nRPLC separation. It is remarkable that D8, with fully reduced interchain disulfide bonds between subunits, eluted intact.

The native RPLC-MS strategy was also tested for a commercial ADC, brentuximab vedotin, which is a well-

characterized commercial ADC with an average DAR of 4.0, comparable to that of the AbbVie model ADC.³⁹ HIC was performed to compare DAR profiles of the two ADCs. The results are provided in Figure 6, confirming that the DAR

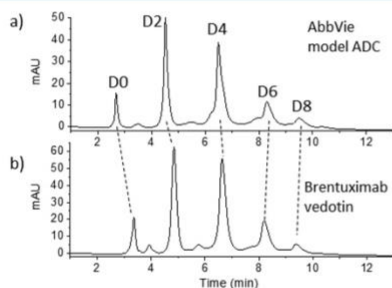


Figure 6. HIC separation of (a) model ADC and (b) commercial ADC Brentuximab vedotin. The dashed lines illustrate that the greater hydrophobicity of the mAb itself for Brentuximab vedotin. Tosoh TSKgel Butyl-NPR, 4.6 × 35 mm, 2.5 μm. MPA: 1.5 M ammonium sulfate, 25 mM sodium phosphate pH 7.0; MPB: 25 mM sodium phosphate pH 7.0 with 25% IPA; flow rate: 0.8 mL/min; column temp: 25 °C.

profiles of these two ADCs are qualitatively similar. The chromatograms show that the D0 peak elutes later for brentuximab vedotin, indicating that the brentuximab (mAb of brentuximab vedotin) sequence is more hydrophobic than that of the AbbVie model ADC. This is offset by the drug of brentuximab vedotin being less hydrophobic than the drug-linker of the AbbVie model ADC, with its lower octanol/water partition coefficient, $\log P = 3.01$, for MC-VC-MMAE compared to that of the AbbVie model drug, $\log P = 3.35$. The elution times of peaks with higher drug load in HIC are similar in both chromatograms: 10 min.

The nRPLC chromatogram for brentuximab vedotin, using the same poly(methyl methacrylate) column and separation conditions as for the AbbVie model ADC, is given in Figure 7a.

The chromatogram is similar to that for the AbbVie model ADC, with differences in relative peak heights and a small extra peak before D6. The D0 species is now slightly retained in nRPLC, owing to the greater hydrophobicity of the mAb that was noted using HIC. All ADC peaks elute somewhat earlier in nRPLC for brentuximab vedotin, consistent with the lower hydrophobicity of the drug. The mass spectra, detailed in Figure 7b, show that the D2 peak and the first D4 peak, D4(1), are intact, with no loss of L1. The other two D4 peaks, D4(2) and D4(3), show some loss of one or two light chains with drug (D4-L1 and D4-2xL1), in addition to the intact forms being observed. Overall, the results show that it is much easier to lose L1 from brentuximab vedotin than it is from the AbbVie model ADC.

As was done with the AbbVie model ADC to distinguish on-column vs in-source dissociation, Figure 8a shows representative mass spectra over wider range of m/z for brentuximab vedotin. The relative signals from the L1 fragment are much stronger than those of the AbbVie model ADC, again illustrating the greater ease of loss of L1 for brentuximab vedotin. To determine whether L1 dissociated on-column or in-source, the EIC for the L1 fragment is shown in Figure 8b, in comparison with the same chromatogram using UV

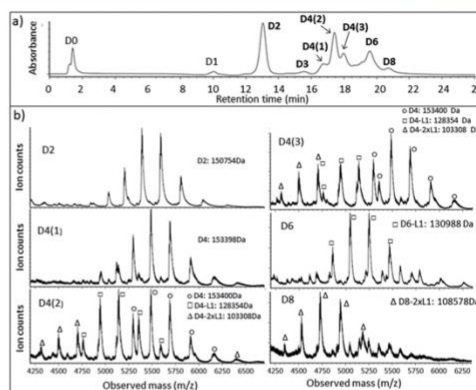


Figure 7. nRPLC and mass spectra for commercial ADC: brentuximab vedotin. (a) nRPLC with detection at 280 nm. Conditions same as those in Figure 4. (b) Raw mass spectra for D2, D4(1,2,3), D6, and D8, with the molecular weight based on deconvoluted mass spectra.

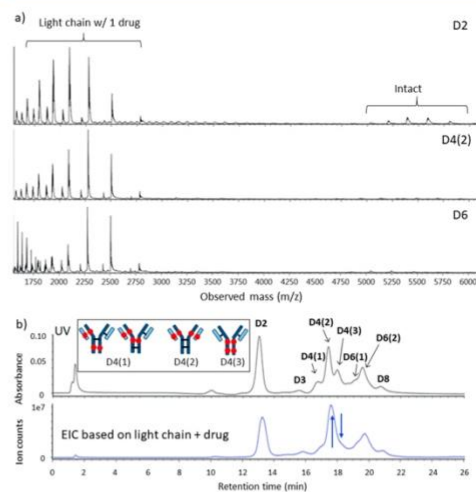


Figure 8. LCMS data for brentuximab vedotin, analogous to Figure 5. (a) Full-range raw mass spectra show even stronger signals for light chain+drug than observed for the AbbVie model ADC. (b) Chromatogram for UV detection (top) approximately tracks that of EIC for signal of light chain+drug, again indicating light chain+drug dissociated after separation. Again, the inset depicts the structures for the D4 isomers that are consistent with these changes.

detection. As with the case for the AbbVie model ADC, the UV and extracted ion chromatograms closely track one another. The lack of an L1 background across the chromatogram confirms that all of the ADCs remain intact throughout the course of the nRPLC separation. As with the AbbVie model ADC, the L1 fragment signal is more pronounced in the D4(2) position than the latter peak D4(3), indicated by the blue arrows. As with the case for the AbbVie model ADC, the

relative abundances of the L1 fragment peaks are likely associated with same two factors: (a) the L1 molar ratio in the positional isomer: 1, 2, and 0, for D4(1), D4(2), and D4(3), respectively; and (b) strength of the noncovalent interaction between L1 and heavy chain in the MS source. These two factors reflect on the L1 fragment peak abundance in the order of $D4(2) > D4(1) \gg D4(3)$. The comparison of EIC and UV chromatograms again supports the conclusion that nRPLC elutes intact brentuximab vedotin species. The greater loss of L1 in the source for brentuximab vedotin relative to the AbbVie model ADC indicates that the noncovalent interactions between light and heavy chains are weaker for brentuximab vedotin than that of the AbbVie model ADC Ab095-PZ.

CONCLUSIONS

A novel protein chromatography technique intersecting HIC and RPLC modes was developed, termed native reverse-phase liquid chromatography, nRPLC. nRPLC employs the solvent elution model and MS compatibility of RPLC while preserving the native form of protein and ADC as in HIC. This new nRPLC technique is an alternative to HIC for ADCs when in-line coupling of MS is desired by virtue of using only 50 mM NH_4OAc . The nRPLC method eluted intact ADCs for both a model ADC from AbbVie and a commercial ADC from Seattle Genetics. Key to this chromatographic advance was lower hydrophobicity of the bonded phase to make drug-surface hydrophobic interactions weaker than the intramolecular hydrophobic interactions that maintain the noncovalent complexes. Inherent to this strategy of designing retention only for interactions between the attached drug and chromatographic surface is that the D0 species has little retention at this stage in column development. The column gives partial resolution of positional isomers, thereby providing additional characterization beyond what is typically obtained using HIC. The lesser number of peaks in HIC permits full resolution of the ADC based on drug loading, which enables precise calculation of DAR. With its greater resolution of positional isomers that currently overlap, nRPLC will be a companion rather than a replacement for HIC until resolution is improved. Longer nRPLC columns, refinement of polymer growth conditions, and optimization of separation conditions could lead to sufficient resolution to determine DAR while also characterizing positional isomers. To our knowledge, this is the first time that intact ADCs made from reduced cysteines have been separated based on DAR using an MS-compatible mobile phase.

ASSOCIATED CONTENT

Supporting Information

The Supporting Information is available free of charge on the ACS Publications website at DOI: 10.1021/acs.analchem.8b04699.

Conditions for conventional chromatography in Figure 2; Figure S1a, RPLC chromatogram for AbbVie model ADC after reduction with DTT; Figure S1b, raw mass spectra and deconvoluted mass spectra for each peak in the chromatograms of part a; Figure S2, nRPLC of model ADC using a commercial HIC column (PDF)

AUTHOR INFORMATION

Corresponding Author

*E-mail: mwirth@purdue.edu; Phone: +1-765-494-5328.

ORCID

Mary J. Wirth: 0000-0003-2538-6985

Present Address

¹C.F.: Shire Pharmaceutical, Lexington, MA 02421, United States.

Notes

The authors declare the following competing financial interest(s): The corresponding author (M.J.W.) is part owner of a company, bioVidria, that has licensed the technology described in this paper.

ACKNOWLEDGMENTS

This work was supported by a grant from the National Institutes of Health, R01GM121910.

REFERENCES

- (1) Hughes, B. *Nat. Rev. Drug Discovery* **2010**, *9* (9), 665–7.
- (2) Thomas, A.; Teicher, B. A.; Hassan, R. *Lancet Oncol.* **2016**, *17* (6), e254–e262.
- (3) Beck, A.; Goetsch, L.; Dumontet, C.; Corvaia, N. *Nat. Rev. Drug Discovery* **2017**, *16* (5), 315–337.
- (4) Polakis, P. *Pharmacol. Rev.* **2016**, *68* (1), 3–19.
- (5) Lambert, J. M.; Berkenblit, A. *Annu. Rev. Med.* **2018**, *69*, 191–207.
- (6) Tsuchikama, K.; An, Z. *Protein Cell* **2018**, *9* (1), 33–46.
- (7) Flygare, J. A.; Pillow, T. H.; Aristoff, P. *Chem. Biol. Drug Des.* **2013**, *81* (1), 113–21.
- (8) Peters, C.; Brown, S. *Biosci. Rep.* **2015**, *35* (4), No. e00225.
- (9) Jain, N.; Smith, S. W.; Ghone, S.; Tomczuk, B. *Pharm. Res.* **2015**, *32* (11), 3526–3540.
- (10) Hamblett, K. J.; Senter, P. D.; Chace, D. F.; Sun, M. M. C.; Lenox, J.; Cerveny, C. G.; Kissler, K. M.; Bernhardt, S. X.; Kopcha, A. K.; Zabinski, R. F.; Meyer, D. L.; Francisco, J. A. *Clin. Cancer Res.* **2004**, *10* (20), 7063–7070.
- (11) Behrens, C. R.; Ha, E. H.; Chinn, L. L.; Bowers, S.; Probst, G.; Fitch-Bruhns, M.; Monteon, J.; Valdiosera, A.; Bermudez, A.; Liao-Chan, S.; Wong, T.; Melnick, J.; Theunissen, J. W.; Flory, M. R.; Houser, D.; Venstrom, K.; Levashova, Z.; Sauer, P.; Migone, T. S.; van der Horst, E. H.; Halcomb, R. L.; Jackson, D. Y. *Mol. Pharmaceutics* **2015**, *12* (11), 3986–98.
- (12) Sanderson, R. J.; Hering, M. A.; James, S. F.; Sun, M. M. C.; Doronina, S. O.; Siadak, A. W.; Senter, P. D.; Wahl, A. F. *Clin. Cancer Res.* **2005**, *11*, 843–852.
- (13) Sun, M. M. C.; Beam, K. S.; Cerveny, C. G.; Hamblett, K. J.; Blackmore, R. S.; Torgov, M. Y.; Handley, F. G. M.; Ihle, N. C.; Senter, P. D.; Alley, S. C. *Bioconjugate Chem.* **2005**, *16*, 1282–1290.
- (14) Ducry, L. *Antibody-Drug Conjugates*; Humana Press: New York City, NY, 2013; Vol. 1045.
- (15) Shen, B. Q.; Xu, K.; Liu, L.; Raab, H.; Bhakta, S.; Kenrick, M.; Parsons-Reponce, K. L.; Tien, J.; Yu, S. F.; Mai, E.; Li, D.; Tibbitts, J.; Baudys, J.; Saad, O. M.; Scales, S. J.; McDonald, P. J.; Hass, P. E.; Eigenbrot, C.; Nguyen, T.; Solis, W. A.; Fuji, R. N.; Flagella, K. M.; Patel, D.; Spencer, S. D.; Khawli, L. A.; Ebens, A.; Wong, W. L.; Vandlen, R.; Kaur, S.; Sliwkowski, M. X.; Scheller, R. H.; Polakis, P.; Junutula, J. R. *Nat. Biotechnol.* **2012**, *30* (2), 184–9.
- (16) Adem, Y. T.; Schwarz, K. A.; Duenas, E.; Patapoff, T. W.; Galush, W. J.; Esue, O. *Bioconjugate Chem.* **2014**, *25* (4), 656–64.
- (17) Boswell, C. A.; Mundo, E. E.; Zhang, C.; Bumbaca, D.; Valle, N. R.; Kozak, K. R.; Fourie, A.; Chuh, J.; Koppada, N.; Saad, O.; Gill, H.; Shen, B. Q.; Rubinfeld, B.; Tibbitts, J.; Kaur, S.; Theil, F. P.; Fielder, P. J.; Khawli, L. A.; Lin, K. *Bioconjugate Chem.* **2011**, *22* (10), 1994–2004.

- (18) Lyon, R. P.; Bovee, T. D.; Doronina, S. O.; Burke, P. J.; Hunter, J. H.; Neff-LaFord, H. D.; Jonas, M.; Anderson, M. E.; Setter, J. R.; Senter, P. D. *Nat. Biotechnol.* **2015**, *33* (7), 733–5.
- (19) Valliere-Douglass, J. F.; McFee, W. A.; Salas-Solano, O. *Anal. Chem.* **2012**, *84* (6), 2843–2849.
- (20) Firth, D.; Bell, L.; Squires, M.; Estdale, S.; McKee, C. *Anal. Biochem.* **2015**, *485*, 34–42.
- (21) Chen, J.; Yin, S.; Wu, Y. J.; Ouyang, J. *Anal. Chem.* **2013**, *85* (3), 1699–1704.
- (22) Wiggins, B.; Liu-Shin, L.; Yamaguchi, H.; Ratnaswamy, G. *J. Pharm. Sci.* **2015**, *104* (4), 1362–72.
- (23) Fekete, S.; Veuthey, J. L.; Beck, A.; Guillarme, D. *J. Pharm. Biomed. Anal.* **2016**, *130*, 3–18.
- (24) Alpert, A. J. *J. Chromatogr. A* **1986**, *359*, 85–97.
- (25) Xiu, L.; Valeja, S. G.; Alpert, A. J.; Jin, S.; Ge, Y. *Anal. Chem.* **2014**, *86* (15), 7899–906.
- (26) Chen, B.; Peng, Y.; Valeja, S. G.; Xiu, L.; Alpert, A. J.; Ge, Y. *Anal. Chem.* **2016**, *88* (3), 1885–91.
- (27) Wiggins, B.; Liu-Shin, L.; Yamaguchi, H.; Ratnaswamy, G. *J. Pharm. Sci.* **2015**, *104* (4), 1362–1372.
- (28) McCue, J. T. *Methods Enzymol.* **2009**, *463*, 405–414.
- (29) Queiroz, J. A.; Tomaz, C. T.; Cabral, J. M. S. *J. Biotechnol.* **2001**, *87*, 143–159.
- (30) Rippel, G.; Szepeszy, L. *J. Chromatogr. A* **1994**, *664*, 27–32.
- (31) Machold, C.; et al. *J. Chromatogr. A* **2002**, *972*, 3–19.
- (32) Xia, F.; Nagrath, D.; Garde, S.; Cramer, S. M. *Biotechnol. Bioeng.* **2004**, *87* (3), 354–63.
- (33) To, B. C.; Lenhoff, A. M. *J. Chromatogr. A* **2007**, *1141* (2), 235–43.
- (34) Baca, M.; De Vos, J.; Bruylants, G.; Bartik, K.; Liu, X.; Cook, K.; Eeltink, S. *J. Chromatogr. B: Anal. Technol. Biomed. Life Sci.* **2016**, *1032*, 182–188.
- (35) Chen, B. F.; Lin, Z. Q.; Alpert, A. J.; Fu, C. X.; Zhang, Q. Y.; Pritts, W. A.; Ge, Y. *Anal. Chem.* **2018**, *90* (12), 7135–7138.
- (36) Bobaly, B.; Beck, A.; Veuthey, J. L.; Guillarme, D.; Fekete, S. *J. Pharm. Biomed. Anal.* **2016**, *131*, 124–132.
- (37) Huang, X.; Wirth, M. J. *Anal. Chem.* **1997**, *69* (22), 4577–4580.
- (38) Valeja, S. G.; Xiu, L.; Gregorich, Z. R.; Guner, H.; Jin, S.; Ge, Y. *Anal. Chem.* **2015**, *87* (10), 5363–5371.
- (39) Janin-Bussat, M. C.; Dillenbourg, M.; Corvaia, N.; Beck, A.; Klinguer-Hamour, C. *J. Chromatogr. B: Anal. Technol. Biomed. Life Sci.* **2015**, *981*, 9–13.